THE EFFECTS OF MILL SPEED, FILLING AND PULP RHEOLOGY ON THE DYNAMIC BEHAVIOR OF THE LOAD IN A ROTARY GRINDING MILL

Keith Stuart Liddell.

A dissertation submitted to the Faculty of Engineering, University of the Witwatersrand, Johannesburg, in fulfilment of the requirements for the degree of Master of Science in Engineering

DECLARATION

I declare that this dissertation is my own unaided work. It is being submitted for the Degree of Master of Science in Engineering in the University of the Witwatersrand, Johannesburg. It has not been submitted before for any other degree or examination in any other University. I furthermore declare that the information used in this dissertation was obtained while I was employed by the Council for Mineral Technology, Randburg.

KLiddell

KEITH STUART LIDDELL

5th day of February 1986.

ABSTRACT

The effects of mill filling, rotational speed and pulp conditions on the dynamics of the load within a wet grinding mill are examined using measurements of torque and load position. The test equipment provided an accurate torque measurement, the toe and shoulder position of the load were measured using a conductivity probe mounted in the mill shell. The rheology of particulate pulps is examined at various solids concentrations, and the static angle of repose of the load is given for a number of pulp conditions. All the variables tested influence the load position, and hence the torque, with filling and speed having the greatest effects. The variables have interactive effects on both the torque and load position. Increasing mill speed and filling both cause an increase in torque to a maximum value, further increases in speed or filling cause a torque reduction. The effects of the variables on power and slip are shown. The position of the load toe is influenced only by the filling, up to speeds of approximately 80 per cent critical, whereas all the variables cause the load shoulder to rise as their magnitudes are increased. The dynamic motion of the load is examined by defining four areas where specific motion exists; a preliminary definition of these areas is proposed which is based on observation of cinematographic film and measured load positions. A comparison of power predicted by published equations and measured power is made, and a modified equation is proposed which can predict power for speeds up to 95 per cent of critical.

This dissertation is dedicated to my wife, Jane, and to my parents.

ACKNOWLEDGEMENTS

Sincere appreciation is expressed to:

Dr M.H. Moys for assistance with the setting-up of the experimental equipment and his encouragement and guidance during the evaluation of data and writing of the manuscript.

Dr P. Harris for the loan of the photographic equipment.

Dr I. Corrans and Mr R. Dunne for allowing the investigation to be conducted, and for their encouragement and support.

The Council for Mineral Technology for permission to conduct this investigation during their employ.

Mrs E. Schravesande for typing the manuscript.

LIST OF FIGURES

FIGURE

LIST OF TABLES

LIST OF SYMBOLS

C_m	Pulp solids concentration	mass per cent
C_v	Pulp solids concentration	volume per cent
D	Mill diameter	metre
J	Fractional mill filling	bulk vol./mil vol.
L	Mill length	metre
N	Mill speed	r/s
N_c	Critical speed	r/min
N_p	Per cent critical speed	
P	Power	kW
T	Time	seconds
W	Weight	Grams
d	Position of intersection of the Davis circle and mill	fraction of rev.
e	Position of the load shoulder	fraction of rev.
g	Acceleration due to gravity	m/s^2
j	Fractional volume below the equilibrium surface	vol/mill vol.
k_c	Consistency index	
k_s	Spiral constant	
ℓ	Polar length of equilibrium spiral	metre
m	Mass	g/kg
n	Flow index	
r_d	Radius of Davis Circle	metre
r_m	Radius of mill	metre

s, s'	Position of intersections of equilibrium surface and mill	fraction of rev.
t	Position of the load toe	fraction of rev.
u	Fraction of mill circumference covered by the load	
v_r	Initial tangential velocity of a parabolic trajectory	m/s
x, y	General coordinates	
T	Torque	
α	Angle of repose	degree
β	Angle that v_r makes with horizontal	degree
ε	Camera speed	frame/s
η	Viscosity	cP
θ	Angle subtended at the mill centre	degree
λ	Spiral constant	
μ	Coefficient of friction	
γ	Shear rate	1/s
ρ_b	Bulk density of the mill load	tonne/m^3
τ	Shear stress	dyne/cm^2
ϕ	Fraction of critical speed	
ψ	Polar angle of equilibrium spiral (anticlockwise from horizontal)	radians
ω	Angular velocity	rad/s

"Net power (of a grinding mill) is not capable of analytic determination because of present ignorance of the internal dynamics of the tumbling load"

A.F. Taggart, 1945

"Forty years later, few attempts have been made, and Taggart's forthright observation remains essentially valid"

C.C. Harris, 1985

1 INTRODUCTION

Most mineral processing operations involve a comminution stage in their circuits, the most common method used is the wet rotary mill in which the grinding media may be steel balls, pebbles produced during a crushing stage or the run-of-mine ore. It is estimated (1) that the power consumed by size reduction unit operations during the mid 1970s was fifty billion kWh per annum, and, based on theoretical surface-energy values, only 0,6 to 1,0 per cent of this power was used in effecting particle breakage and producing new surface area (2), although the actual efficiency achieved is in the order of 5 to 20 per cent (3).

Comminution processes, particularly those involving rotary mills have been the subject of a vast amount of theoretical and practical research and there is a plethora of books and technical papers dealing with most aspects. It is now generally accepted that the grinding process can be dealt with as a rate type process and can be adequately described by the so-called selection and breakage functions (3-5).

This method splits a particle-size distribution into discrete size fractions, usually in a $\sqrt{2}$ series. Each fraction has an individual selection function, which characterizes its rate of breakage into smaller size fractions. The breakage distribution function describes the distribution of smaller primary progeny particles produced by breakage of particles in each size fraction. The breakage function is generally normalized over the range of size fractions.

The selection and breakage functions can be calculated from batch grinding experiments and may be used to scale-up to industrial mills and predict their product size distribution. In the past, and probably still today, mill scale-up has been mostly performed using the Work Index method developed by Bond (6), which is a method based upon the power required to comminute an ore from a theoretically infinite feed size to a product with 80 per cent passing 100 microns, as determined in a standard laboratory batch mill.

It is now generally accepted that whilst the Bond method of sizing mills has worked well in the past, though not because of the reasons Bond claims (7), the more advanced methods available that treat the grinding mill as a reactor and use selection and breakage functions, residence time distributions and classifier parameters have reached a level of sophistication where they offer advantages.

Where it has been used to design large (> 5m diameter) mills the Bond method has predicted higher throughputs or a finer product than has been obtained, and has, for example, caused serious problems at the Bougainville Copper concentrator (8), due to under design of the capacity of the ball mill circuit. A detailed analysis of the behaviour of the load in the mill has clarified why this scale-up method is inadequate (9).

Whilst the grinding process itself is well understood and mills may be designed with some degree of confidence, very little practical information is available that describes the motion of the load inside a mill, and the influence that variables such as rotational speed, mill filling, and characteristics of the rock pulp have on the motion. It is the motion of the load that has the major influence on the power drawn by a mill. Examination of the literature shows that there are a number of equations that attempt to predict mill power from the load geometry; they generally are not based on observations of what happens inside the mill, but on assumptions that tend to be over-simplified. The motion of the load does not appear to have been studied under conditions that apply for wet milling.

The aims of this study are to run a ball mill under different conditions of filling, speed, and pulp solids content, and to examine the changes in torque and load position. In this way it is intended to increase the knowledge of the internal mechanics of wet-grinding mills and to provide data that is of a practical, rather than theoretical and assumed nature.

A discussion of the relevant literature is given in Chapter 2, the first section of which deals with the theories proposed to describe the motion of the load, which are generally based on force balances under ideal conditions. The development of various equations to predict mill power are discussed in Section

2.2 and the rheology of particulate rock pulps is briefly outlined in Section 2.3. The effects of pulp rheology on the milling process are presented in Section 2.4.

The experimental equipment and methods are presented in Chapter 3 which is divided into three sections that deal with milling, rheology and static angle of repose investigations; the accuracy of torque and load position measurements, and the primary processing of data is discussed.

In Chapter 4 the experimental results are discussed, the effects of the variables tested upon the torque and position of the toe and shoulder of the load are shown and interpreted.

The results from the investigation are used in Chapter 5 to provide an insight into the motion of the load, and a number of regions are identified within the load where specific types of motion exist. The basis for a mathematical definition of these areas is developed.

In Chapter 6 a comparison is made of a number of equations that predict mill power, and suggestions are put forward to improve a specific equation by taking into account the effects that filling and mill speed have upon the load motion.

2 LITERATURE REVIEW

2.1 The Motion of the Load

In order to calculate the power drawn by a mill, the position and motion of the load has to be described and, although this has been attempted from theory by Davis (10), Barth (11), and Rose and Sullivan (12), among others, a comparison of theory with reality in wet mills has not been done.

The point of projection of a particle from the body of the load, under conditions whereby there is no interference from other particles in the load, or any sticking effects due to the rock pulp, has been calculated by Davis and explained by Rose and Sullivan. For a particle to be ejected from the load, the initial radius of curvature of the parabolic trajectory has to be equal to or less than the radius of the circular path that the particle is travelling in. This is satisfied for all points in the mill by a circle which passes through the centre of the mill and has its centre $g/2\omega^2$ above the mill centre. This circle is known as the 'Davis Circle', as shown in Figure 2.1.

The radius of the Davis Circle is a function of the rotational speed of the mill and can be calculated from equation 2.1.

$$r_d = \frac{12,426 \times 10^{-3}}{N^2} \qquad (2.1)$$

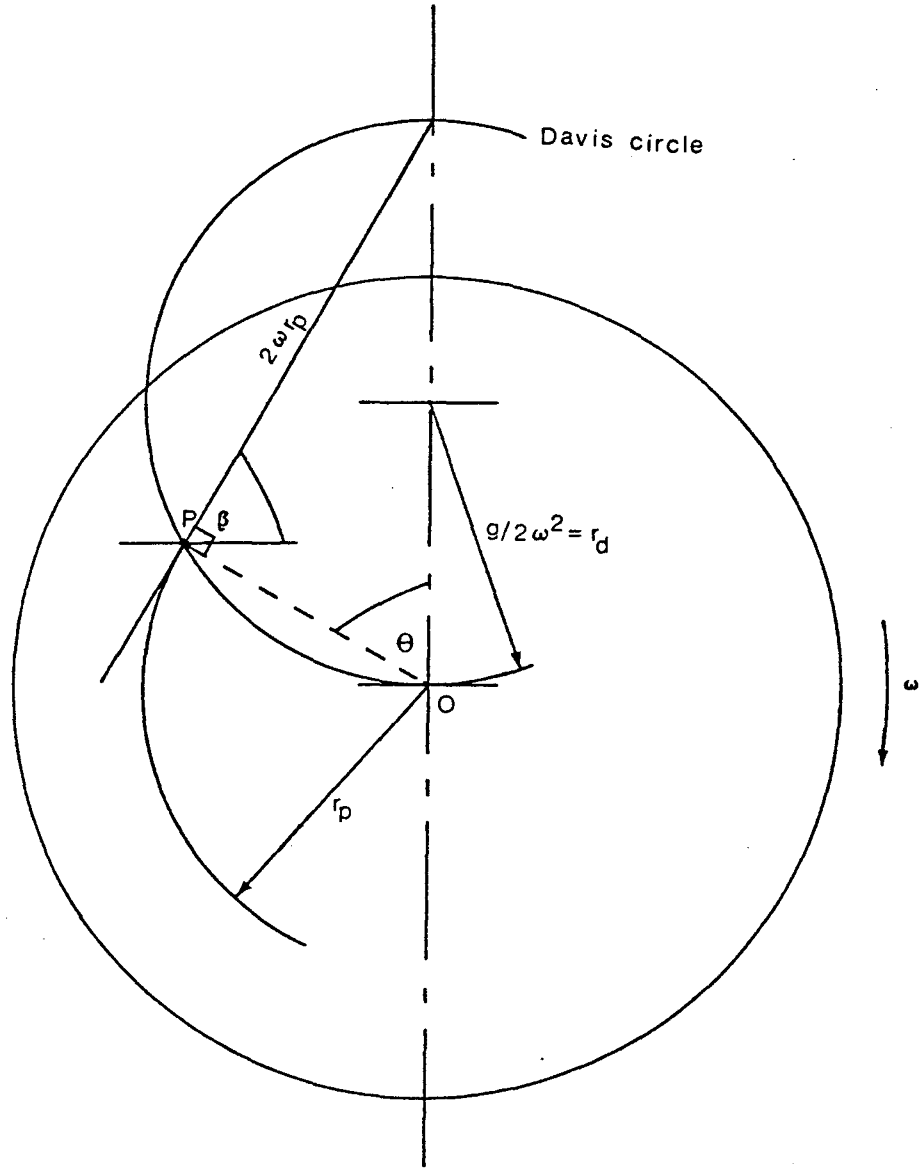

Note: A particle can commence a parabolic trajectory only when $\beta \leq \theta$

Figure 2.1 Co-ordinate system for the development of the Davis circle

After ejection from the load, the particles follow a parabolic trajectory and re-enter the load to follow a circular path at the same radius.

This implies that the paths of particles do not cross, and that there is no axial mixing of the load, which is clearly an over-simplification. This treatment also does not take into account interparticle friction and interference.

Barth and Hinsley and Fobelets (13) independently developed a theory based on a force balance on a particle which takes into account interparticle friction. This theory states that an equilibrium surface exists within the load, below which particles are subjected to the centrifugal and frictional forces and are thus locked into the rotation of the mill, and above which they may either roll down the load surface or follow a parabolic trajectory under the influence of gravity. At the equilibrium surface the particle is at equilibrium with respect to frictional, centrifugal, and gravitational forces.

Although slightly different approaches are used by Barth and Hinsley, they both concluded that the equilibrium surface has the form of a logarithmic spiral which has its origin g/ω^2 above the mill centre. Barth considered that a particle moving in a circular path, of radius r_p, around the mill axis is affected by its own weight, mg, in a vertical direction, and a centrifugal force $mr_p\omega^2$, in a radial direction (Figure 2.2). These forces can be resolved into a resultant which has the x and y components as shown below.

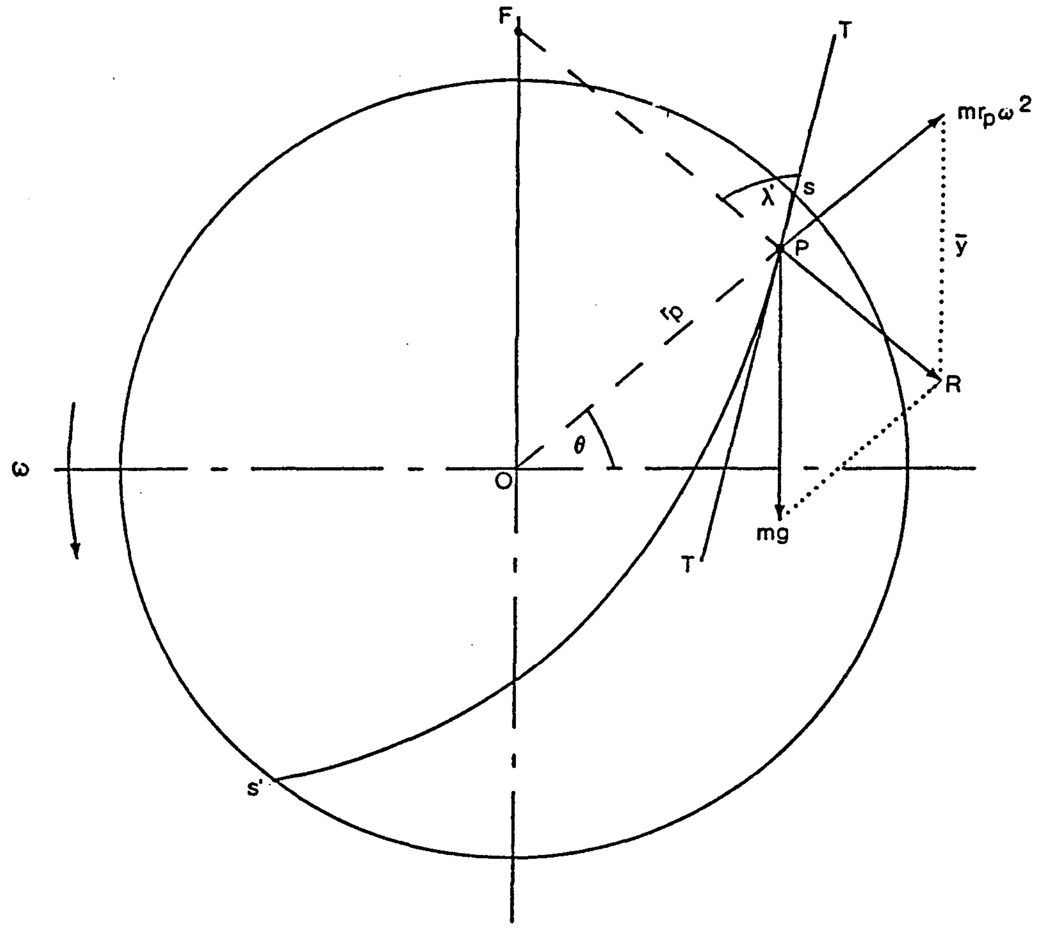

F - Pole of resultant forces

s-s' - Equilibrium surface

T-T - Tangent to s-s' at P

Figure 2.2 Co-ordinate system for a force balance on a particle on the equilibrium surface, after Barth

$$\bar{x} = mr_p\omega^2 \cos\theta \qquad (2.2.a)$$

$$\bar{y} = mg - mr_p\omega^2 \sin\theta \qquad (2.2.b)$$

If the resultants of the forces on particles on the equilibrium surface at various radii are extrapolated, they all pass through a point which lies g/ω^2 above the mill axis. As the mill is rotated, the charge will pile up until the angle, λ', between the tangent to the equilibrium surface and the force resultant, R, becomes greater than the angle of repose of the load (Figure 2.2). The curve that satisfies these requirements is a logarithmic spiral which has its origin at $x = 0$, $y = g/\omega^2$ (co-ordinates are expressed with the mill axis as the origin) and has the form:

$$\ell = e^{\lambda'\psi} \qquad (2.3)$$

where ℓ and ψ are polar co-ordinates, related to the spiral origin.

The treatment by Hinsley performs a force balance which includes the coefficient of friction derived from the static angle of repose of the load (Figure 2.3). A force balance tangential to the equilibrium surface gives:

$$\mu m\omega^2 \cos(\delta-\beta) + \mu mg \sin\beta + mr\omega^2 \sin(\beta-\delta) = mg \cos\beta \qquad (2.4)$$

Substitution, rearrangement, and integration gives:

$$\sqrt{(x^2 + z^2)} = C\, e^{\mu \tan^{-1}(z/x)} \qquad (2.5)$$

where $$z = (g/\omega^2 + y) \qquad (2.5.a)$$

This is the equation of a logarithmic spiral, expressed in rectangular co-ordinates. To convert to polar co-ordinates we use $x^2 + z^2 = \ell$

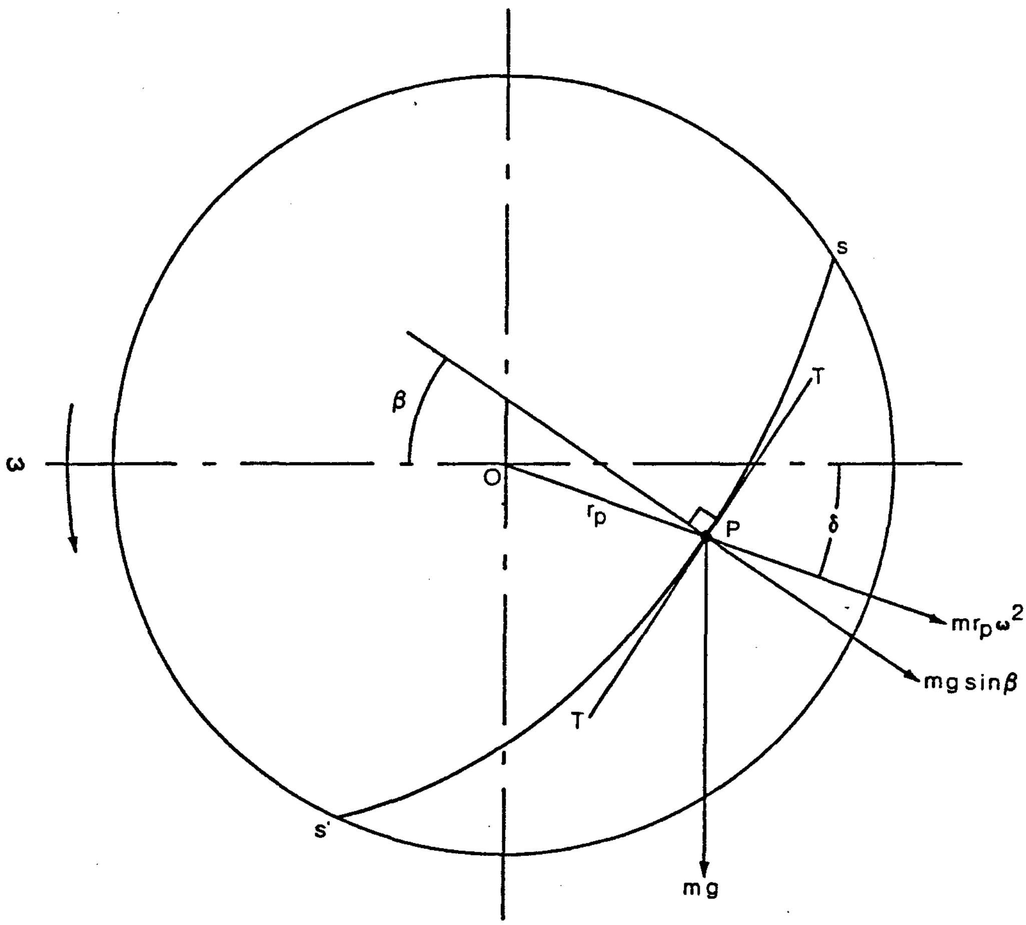

s–s' – Equilibrium surface

T–T – Tangent to s–s' at P

Figure 2.3 Co-ordinate system for a force balance on a particle on the equilibrium surface, after Hinsley and Fobelets and $\tan^{-1}(z/x) = \psi$, and equation 2.5 becomes:

$$\ell = k_s e^{\mu\psi} \qquad (2.6)$$

The origin of the spiral can be found when $\ell = 0$ and is at a point g/ω^2 above the mill centre, the same point calculated by Barth. The equation of the spiral developed by Barth does not have the constant introduced by Hinsley. This constant is related, but according to Rose and Sullivan not simply, to the degree of filling in the mill

After stating that k_s is a function of the mill filling, Rose and Sullivan do not attempt to relate k_s to the filling, but present diagrams of equilibrium surfaces at various mill fillings, J, that show the total load lying below the equilibrium surface at a speed of 70 per cent critical (Figure 2.4), which is obviously incorrect.

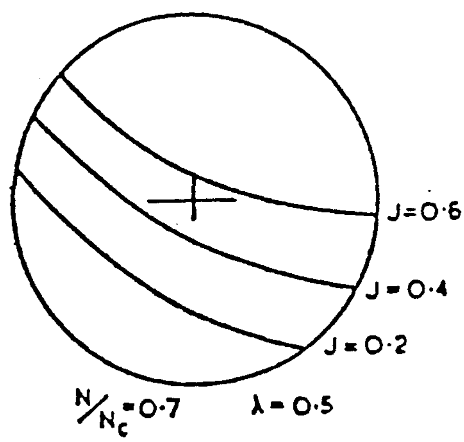

Figure 2.4. Equilibrium surfaces proposed by Rose and Sullivan

Barth also does not attempt to relate the position of the equilibrium surface directly to the mill filling or to the mill speed, but rotates the spiral to pass through different points on the x axis. The filling is then calculated as the sum of the volumes of material locked into the mill motion and in free motion under gravitational influence; but no allowance is made for any increase in porosity, thus decreasing the bulk density, of the freely-moving material, which means that the calculated fillings will be over-estimated.

In all the above treatments there has been no attempt to experimentally examine the load motion in wet grinding mills.

Vermeulen *et al.* (14) have physically examined the load action in a 4,88m diameter pebble mill by measuring impact and conduction with suitably instrumented liner bolts. Impact was measured with a piezo-electric sensor inserted into the bolt, and individual impacts onto the mill shell were measured in the first and second quadrants of the mill before the toe of the load was registered, as shown in Figure 2.5.

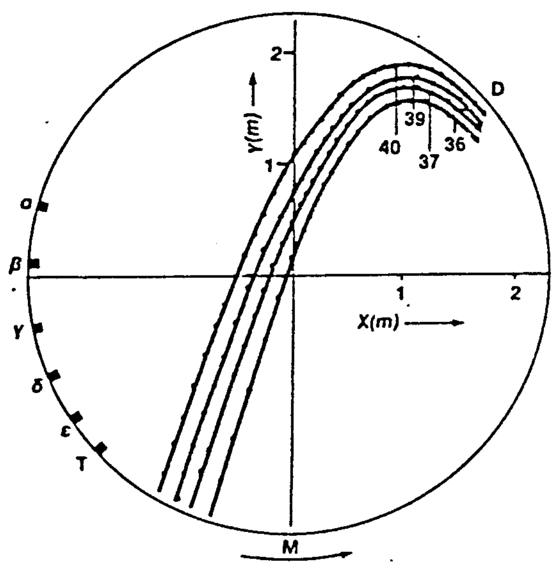

Figure 2.5. Individual impacts (Greek letters) measured by Vermeulen

When the theoretical parabolic trajectories were examined, they could not account for these measurements, and Vermeulen postulated that a combination of increased lift from the lifter bars and adhesion due to the pulp carried pebbles in contact with the lifter bars further than the general load. It is also likely that coarse particles in the pulp prevented the pebbles from rolling or sliding from the lifter bars and contributed to the increased lift. Results given by the conductivity bolt indicates that the position at which the bolt enters the toe of the load and exited from under the load at the shoulder, could be measured, and these positions were confirmed to some extent by the piezo-bolt.

It is suggested by Vermeulen that the dynamic angle of repose, as given by a line joining the toe and the shoulder, can be used to give an evaluation of the mill filling, but the use of this value will only give an approximation that becomes less accurate as the filling falls below 50 per cent.

2.2 Prediction of mill power

Most of the equations used to predict mill power are, considering the complex motion of the load, extremely simple, but some have nevertheless been used somewhat successfully in the design of industrial mills.

Davis, *op cit*, extended his treatment of load motion to calculate the power required at a calculated 'best operating speed', this is the speed at which, for a given mill filling, the particle impact velocities are maximized. The power is calculated from the change in kinetic energy possessed by the particles at the termination of their parabolic trajectories when they commence a circular path, and the number of load cycles per mill revolution. The power predicted by Davis' model when applied to industrial mills does not compare with the actual power (15).

The Davis power model was extended by Guerro and Arbiter (15), who stated that the power consumption was determined by two considerations: the rate at which potential energy is gained by the load as it is lifted, and the rate of change of momentum of particles as they terminate free motion and are taken back into the load by the mill rotation. This assumes that there is no slip between the load and mill shell and that energy is not lost whilst the particles are in free motion. A number of relationships derived by Davis are used in the formation of an equation to predict mill power, this results in their power equation only being applicable at Davis' best operating speed, which limits its applicability. The power equation is:

$$P \propto \rho_b D^{2,5} L \left| \frac{2(1-K^4)}{(1+K^2)^{3/4}} - \frac{1,775(1-K^6)}{(1+K^2)^{7/4}} + \frac{0,4432(1-K^8)}{(1+K^2)^{11/4}} \right| \qquad (2.7.a)$$

where $K = -0,026 + 0,39(7-10\ J)^{0,5}$ (2.7.b)

and the best operating speed is given by

$$N_{Bo} = \frac{48,95}{r_m^{0,5}\ (1+K^2)^{0,5}} \qquad (2.8)$$

This model has been criticized by Hogg and Fuerstenau (16), because the energy used to convert the particles from their free motion to a circular path is provided by their loss of the potential energy acquired by the lifting action of the mill shell. They then derive a model to predict mill power, based on the first consideration of Guerro's and also that the acquired potential energy is lost before the particles return to a circular path.

The equation derived by Hogg is, with reference to Figure 2.6:

$$P = \frac{2}{3} \rho_b g^{1,5} L \phi r_m^{2,5} \sin^3 \theta \sin\alpha \tag{2.9}$$

It is then assumed that the mill speed is low enough so that the load can be approximated by a straight line drawn from the toe to the shoulder (t-e), and that most of the load lies below this line. Then the mill filling can be related to angle θ by:

$$J = \frac{1}{\pi} (\theta - \sin\theta \cos\theta) \tag{2.10}$$

Equation 2.9 can be expressed in a more usable form by:

$$P = 3{,}627 \rho_b \phi L D^{2,5} \sin^3 \theta \sin\alpha \tag{2.11}$$

Guerro compared power predicted by equation 2.7 with the actual power for a number of ball mills operating at a speed similar to the best operating speed of Davis, and showed that it tends to overestimate the power, which supports Hogg's criticism. Hogg does not provide any comparison of predicted and actual power.

A method of calculating power that has been widely used is the torque-arm model. The model assumes that the load profile can be approximated by a straight line joining the toe and shoulder (t-e), the inclination of which (i.e. the dynamic angle of repose) gives the offset of the centre of gravity of the load from the vertical axis as shown in Figure 2.6.

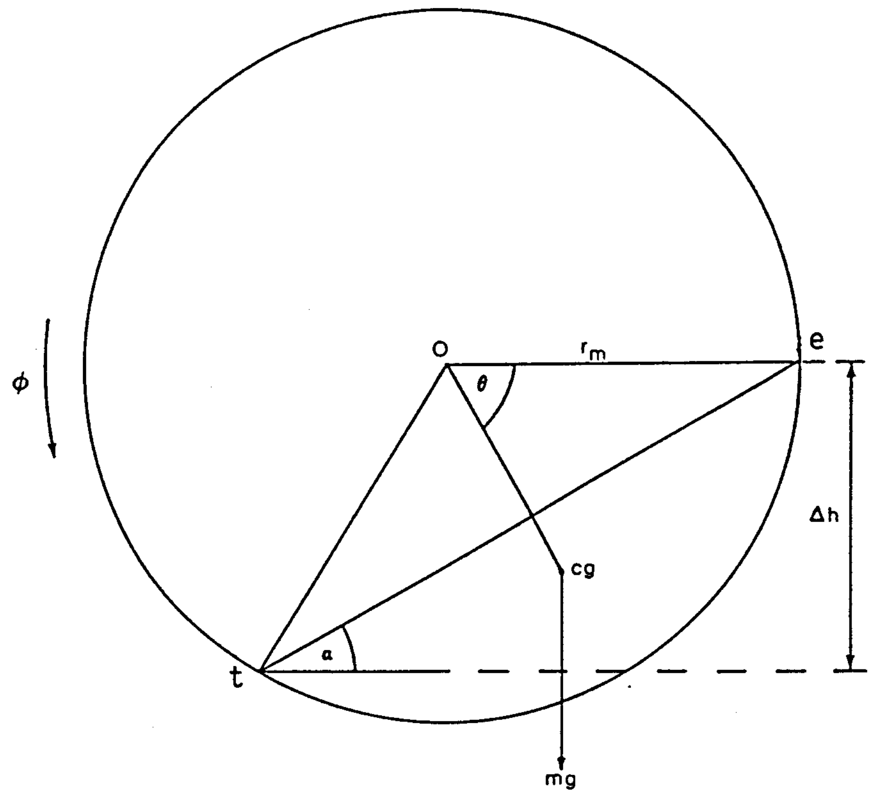

Figure 2.6 The load position assumed by models predicting mill power

The torque required to maintain the offset of the load centre of gravity is:

$$T = mgr_g \sin \alpha \qquad (2.12)$$

and the power required is:

$$P = 2\pi T N \tag{2.13}$$

Bond (17,18) has used the torque model as a basis for calculating mill power and has produced an equation to predict the power requirement for an overflow ball mill which is based on empirical data from industrial mills:

$$P = 12{,}262\ \rho_b\ L\phi D^{2,3} J(1-0{,}937J)(1-0{,}1/2^{9-10\phi}) \tag{2.14}$$

Equation 2.14 has the form:

$$P \propto \rho L D^{d} \tag{2.15}$$

where d can vary from 2,3 to 2,8 depending on conditions.

Rose and Sullivan, *op cit*, and Rose and Evans (19) have also derived equation 2.15 by the method of dimensional analysis of seventeen variables, and show that in theory d should be 2,5, but in practice it is 2,55 to 2,60. Austin (20) has stated that the deviation of d from the theoretical 2,5 to the actual 2,6 is due to the influence that mill diameter has upon specific rates of breakage.

A further power equation has been derived by Arbiter and Harris (9,21,22) using the torque method and the same assumptions about the load configuration (Figure 2.6). Their basic equation is:

$$P = (2DN\ m\ g\ \sin^3\theta\ \sin\alpha)/3J \qquad (2.16)$$

An approximation of $\sin^3\theta$ can be made by 4J(1-J), (comparative values are given (9)), and equation 2.16 becomes:

$$P = \frac{8}{3}\,mg\ ND(1-J)\ \sin\alpha \qquad (2.17)$$

and converting N(rps) to ϕ gives:

$$P = 1{,}880\ mg\ \phi\ D^{0,5}(1-J)\ \sin\alpha \qquad (2.17a)$$

A further simplification is to assume $\sin\alpha$ to be constant. A value of 17,5 has been calculated for $8/3\ g\ \sin\alpha$ (22), which implies an angle of repose of 42°; this value was calculated from 39 mills of various diameters. If this value is substituted in to equation 2.17a, and the load mass is calculated from

$$m = \frac{\pi}{4}\,\rho_b\ LD^2J \qquad (2.18)$$

we have

$$P = 9{,}690\ \rho_b\phi D^{2,5}LJ(1-J) \qquad (2.19)$$

Comparison of equations 2.9 - a potential energy model and 2.16 - a torque-arm model, shows that they have a similar form. This arises from them both having the same assumptions about the position of the mill load included in their derivations. As a result of the simplifying assumption made about the load motion in the derivations discussed, the power prediction equations are only truly applicable at low speeds, below 50 per cent critical, where the load has the form assumed. They will not predict the well-known observation of energy recovery (or torque reduction) at higher speeds, and that they can predict power up to speeds of 70 to 80 per cent critical is due to a fortunate change in the load motion rather than any predictive qualities of the models (16). These treatments also do not take into account the influence of characteristics of the rock pulp, such as viscosity, pulp density, and adhesion effects, and so may really only be applicable to dry milling. Rose and Evans, *op cit*, in their treatment of 17 variables, did not examine viscosity effects, which would have been possible by use of the Reynolds number.

An attempt to combine the more realistic features of the above treatments, together with the questionable hypothesis of increasing interparticle slip in the rising section of the load as the centre of the load is approached, has been made by Pauw (23), but this model is not based on any experimental work examining what motions occur in the load. Even so, this model can predict a reduction in power at higher speeds and fillings.

2.3 The rheology of particulate mineral-rock pulps

Fluids may be classified into a number of groups, depending on their rheological natures; the primary distinction is whether a fluid exhibits Newtonian or non-Newtonian behaviour. The viscosity of a Newtonian fluid is independent of the shear rate that it experiences, and is given by:

$$\eta = \frac{\tau}{\gamma} \tag{2.20}$$

A plot of shear stress, τ, versus shear rate, γ will, for a Newtonian fluid, give a straight line passing through the origin, the gradient of which is the viscosity.

The viscosity of a non-Newtonian fluid is dependent on the shear rate and cannot be described by equation 2.20. Non-Newtonian fluids can be devided into two general categories:'time-dependent' and 'time-independent' (24).

Generally, inert mineral and rock pulps will fall into one of the following categories, which are shown in Figure 2.7.

(a) Pseudoplastic - the viscosity of a pseudoplastic fluid decreases as the rate of shear it experiences increases. When shear stress is plotted versus shear rate, a pseudoplastic fluid will produce a curve that has a slope which decreases with increasing shear rate. These fluids are commonly called 'shear-thinning' and may exhibit a yield stress.

(b) Dilatant - a dilatant fluid has the opposite characteristics of a pseudoplastic; the viscosity increases with increasing shear rate. An example of this type of fluid is a maise flour and water mixture.

(c) Bingham plastic - this type of fluid will have a yield stress and show Newtonian flow when the yield stress is exceeded. This phenomenon is shown in some cases by ferrosilicon suspensions.

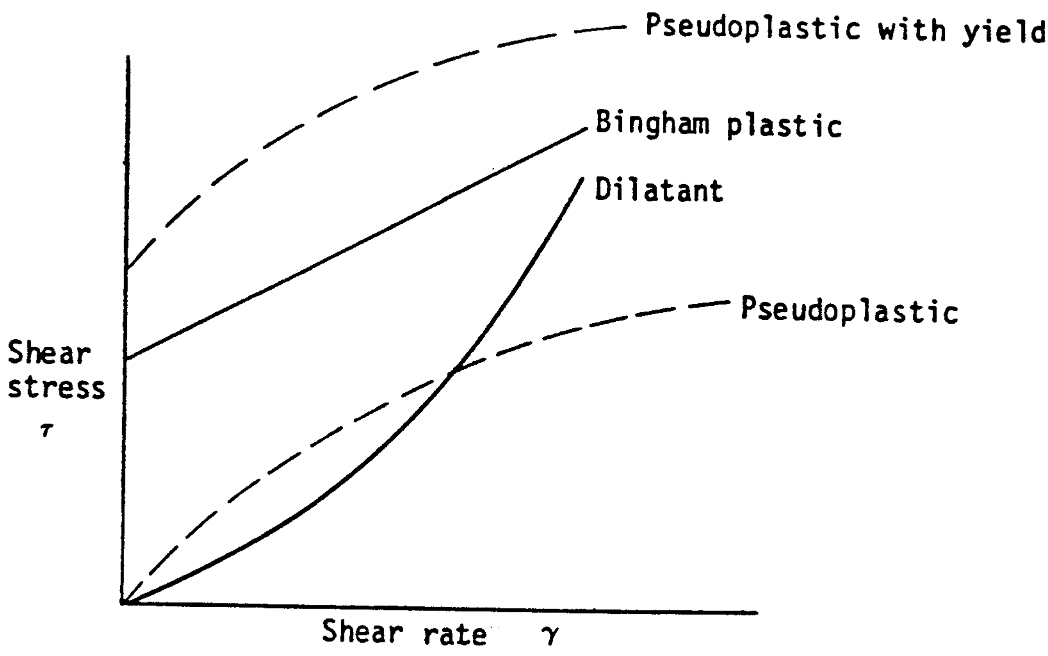

Figure 2.7 Characterization of non-Newtonian fluids

Particulate pulps generally exhibit pseudoplastic or dilatant behaviour, which can be described by a number of mathematical models. The Ostwald de Waele model is a useful method of characterising pulp rheology:

$$\tau = k_c \gamma^n \qquad (2.22)$$

The constants n and k_c may be used to characterize a pulp's rheological nature; the flow index, n, gives the degree of deviation from Newtonianism ($n = 1$); for $n > 1$ the pulp shows dilatant behaviour, and for $n < 1$ pseudoplastic behaviour. The constant k_c is called the consistency index and varies with the properties of the pulp.

The rheology of particulate pulps is affected by a number of properties, many of which may vary in a milling environment; for example, particle size distribution, particle shape, solids content, temperature, and surface charge. These effects have been placed into three main categories by Cheng (25):

(a) hydrodynamic action between the liquid and solid particles, which causes viscous dissipation of enrgy in the liquid (temperature, viscosity of liquid, particle shape and size, solid concentration),

(b) particle-particle contact, which results in frictional interactions (particle size and shape, solids concentrations, and

(c) interparticle attraction, which promotes flocculation or aggregation (zeta potential, shear rate).

The interaction of these effects can be seen in Figure 2.8.

The large number of equations that exist predicting shear rate-shear stress relationships, and which relate Newtonian viscosity to solids concentration, have been reviewed by Cheng and Levy (26). Cheng comments that he is aware of more than fifty equations that describe non-Newtonian rheology.

2.4 The effects of pulp rheology on the milling process

Investigations that have been performed to examine the influence of pulp rhelogy on the milling process have only examined how the breakage of the particles varies; and made passing comments about how the load motion has been altered by changes in rheology. As far as it is known, there has been no study of rheology effects on load motion.

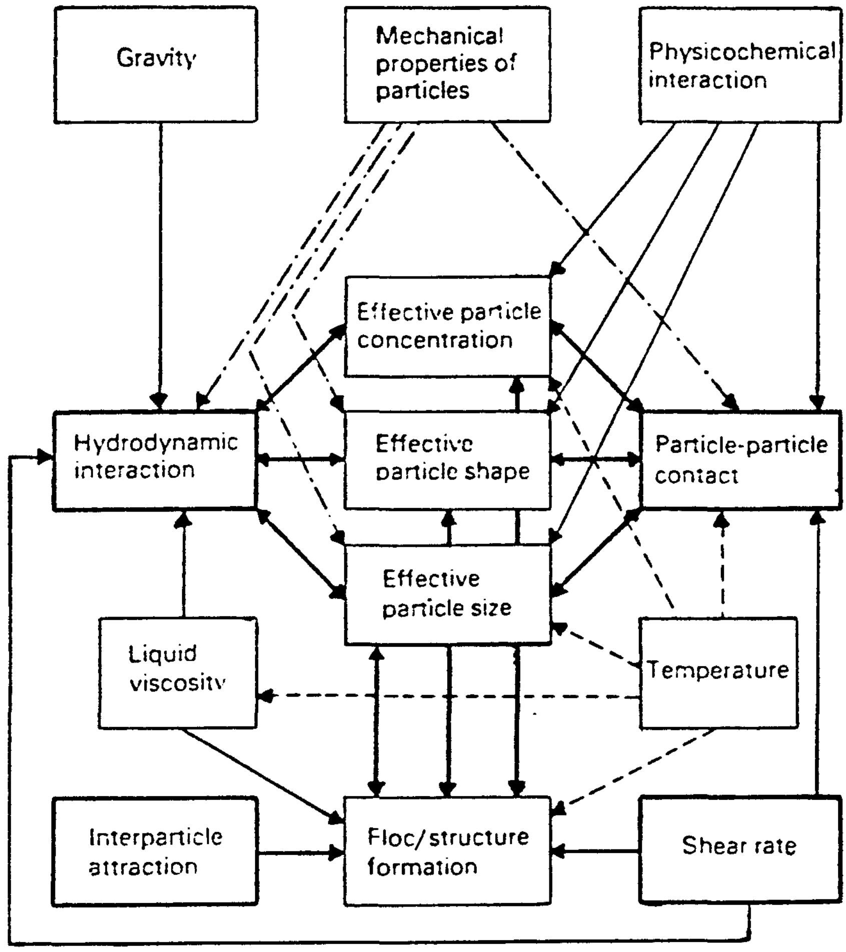

Figure 2.8 The interplay of factors affecting pulp viscosity (25)

The effects of pulp rheology on particle breakage are well documented. In an extensive study Meloy and Crabtree (27) examined the breakage of quartz which was gound in liquids of various viscosity, density, and surface tension. They concluded that liquid density had no effect; the grinding rate was constant up to approximately 100 centipoise, whereafter it tends to be reduced; up to 100 centipoise the surface tension of the liquid had an influence on breakage.

In a similar study, Hockings, Volin, and Mular (28) ground a closely-sized fraction of quartzite in a batch rod mill for short times using water-corn syrup mixtures to vary the viscosity; they obtained similar results as Meloy, as can be seen by comparison of Figures 2.9 and 2.10.

The pulp solids contents that produced maximum surface area of milled product were found to be 58 to 67 mass per cent for silica and 62 to 72 per cent for hematite by Yen and Salman (29). They concluded that new surface area produced increases with viscosity up to these solids contents, and thereafter it becomes independent of viscosity. Examination of their results shows that the new surface area produced is reduced at higher solids contents, probably due to the viscosity becoming so high that balls become coated with a layer of pulp that is so thick that the impacts are cushioned, which leads to reduced grinding rates.

Tucker (30,31) has also shown that as the solids content, and hence the viscosity, of a lead-zinc ore pulp is increased, grinding efficiency reaches a maximum and is then reduced. His results indicated that an increase in pulp solids content from 33 to

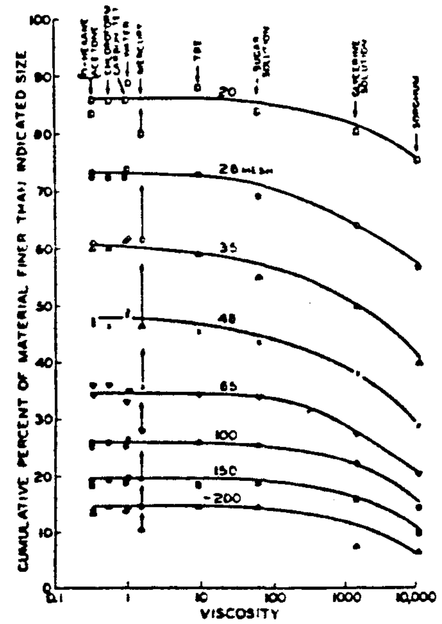

Figure 2.9 Lines of constant product size for quartz milled for two minutes in various liquids (27)

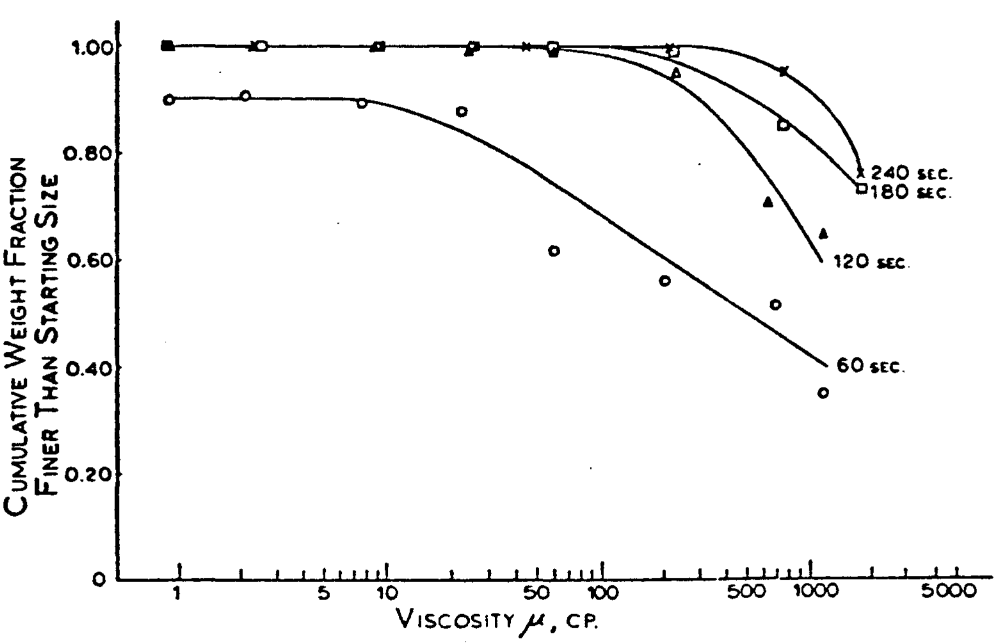

Figure 2.10 The effect of viscosity on the milling of closely-sized quartzite (28)

67 mass per cent solids causes an improvement in the grinding of particles of all sizes; at 80 per cent solids the breakage of fines (< 80μm) is further improved, while breakage of coarser particles is reduced; a further increase to 88 per cent solids causes a large reduction in breakage, espeically of coarse particles. Tucker's results are shown in Figure 2.11.

With the use of selection and breakage functions to describe the grinding process, a number of workers have examined the influences of pulp characteristics on these functions. Tangsathitkulchai and Austin (32) have found that for coal, quartz and a copper ore, the rate of breakage is at a maximum when the pulp contains approximately 45 volume per cent solids, Figure 2.12. They examined the variation with solids content (i.e. viscosity) of the characteristic rate of breakage parameter, a, in the rate of breakage equation:

$$S_i = a(X_i/X_o)^{\alpha} \qquad (2.22)$$

The parameter, a, was found to be at a maximum at 45 volume per cent solids for the three mineral types.

An extensive research effort into the effect of pulp rheology in milling has been performed by Klimpel and his co-workers, with the emphasis on the influence of viscosity reducing chemicals, and is reviewed by Klimpel (33). Essentially, they concluded that the rheological nature of the pulp has an effect on the magnitude of the rate of breakage and also on the order of the breakage rate.

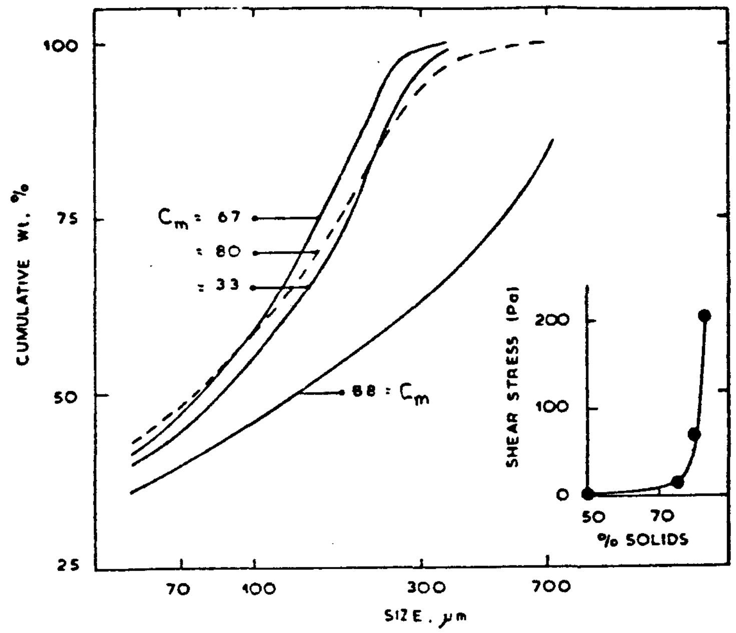

Figure 2.11 Size distributions of products from 5 minute batch grinds of a lead-zinc ore of various pulp solids concentrations (31)

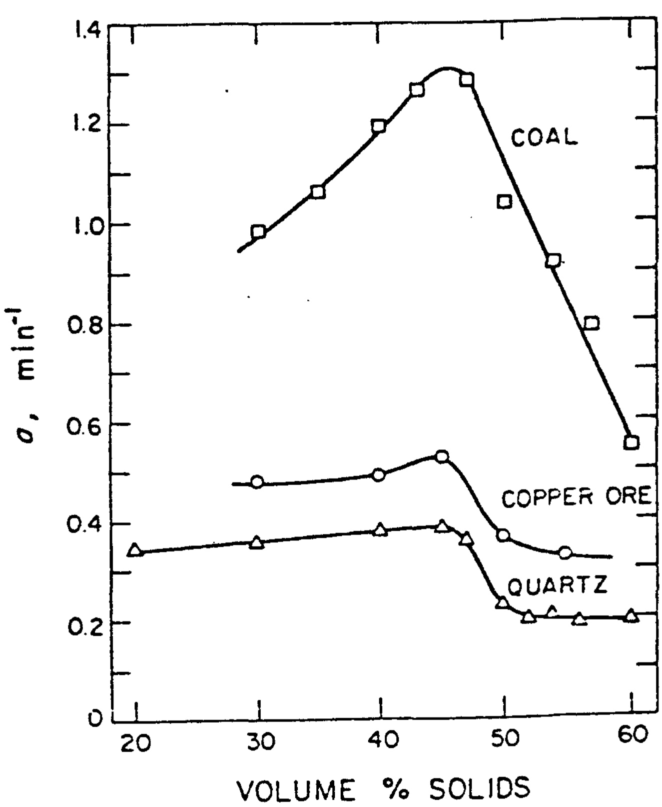

Figure 2.12 Variation of the breakage parameter, a, with pulp solids content (8)

The rheological natures of rock pulps at various solids content were examined and correlated to parameters that characterize the selection and breakage functions (e.g. a and α in equation 2.22). It was found that dilatant pulps show first-order breakage rates; pseudoplastic pulps also have first-order breakage with faster rates, but pseudoplastic pulps with a yield stress demonstrate slower, non-first-order rates (33-35). It was also shown that the addition of a viscosity modifying agent to a high solids content pulp showing non-first-order breakage can cause it to exhibit first-order breakage; these phenomena can be seen in Figure 2.13. The pulp rheology was shown to have little or no influence on the breakage distribution (35). Contrary to the results of Tucker, no changes in the preferential grinding of various particle sizes were observed by Klimpel, who commented that the preferential grinding of particles in a batch mill is due to the viscosity increase of the pulp as the batch grind time increased.

The influence of pulp viscosity and magnitude of viscosity increase will increase with pulp solids content. An industrial copper milling circuit has been examined by Klimpel (33), and Klimpel and Manfroy (36), where it was stressed that for a viscosity modifying agent to be effective, the pulp rheology should be such that non-first-order breakage rates occur. Increases of 8 to 15 per cent in the mass throughput of the grinding circuit, in open and closed circuit, were realized by using the viscosity modifier. The product size could also be reduced if the feed rate was kept constant, as shown in Figure 2.14. It is of importance to note that the viscosity modifier had an effect on the performance of the hydrocyclone

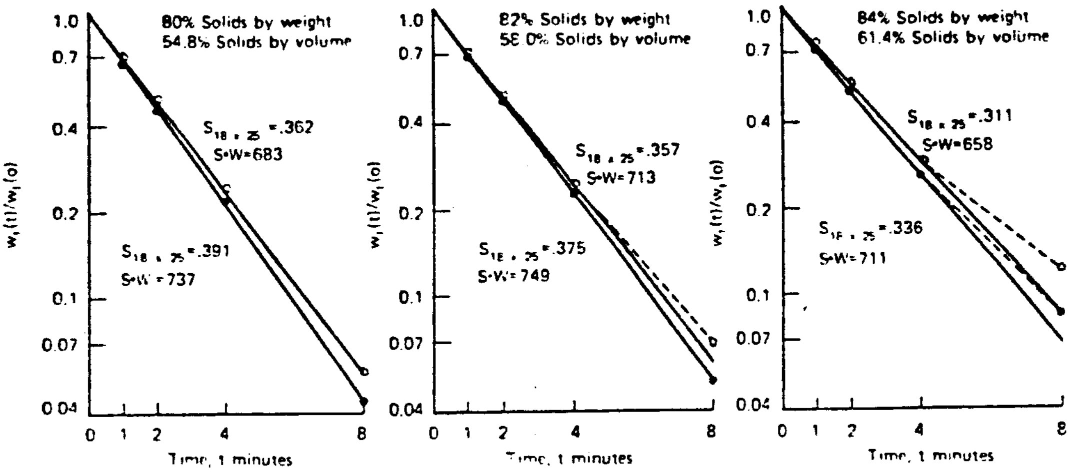

O without grinding and ● with 1 lb/t grinding aid

Figure 2.13 First order decay plots for batch grinding of closely-sized taconite at various pulp solids content (34)

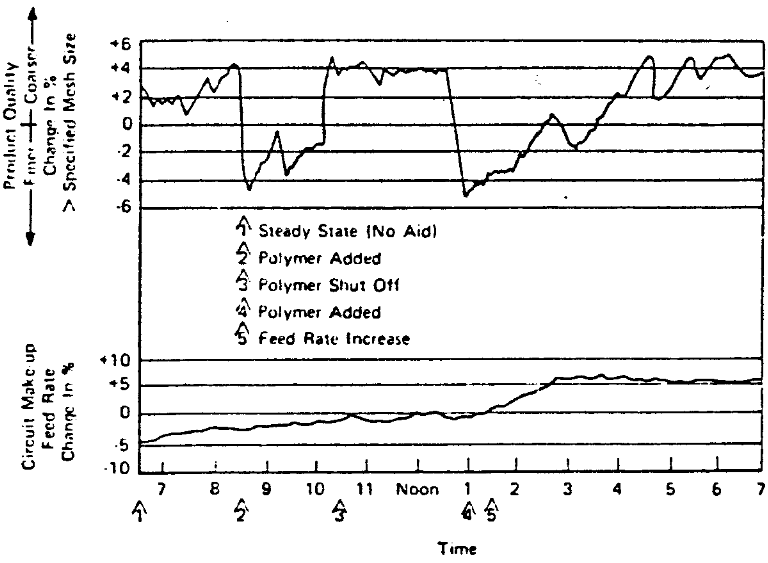

Figure 2.14 The response of a copper grinding circuit to the addition of a polymer viscosity modifying grinding aid (34)

classifier used in the closed circuit test (37).

The pulp rheology will also have an effect upon the flow of pulp through the mill, which will alter the relationship of residence time distributions of the various particle sizes, the radial mixing of the pulp, and, possibly, the dynamics of the charge motion. In their recent study on the scale-up problems of large mills, Arbiter and Harris (22,38) state that the use of power intensity alone (e.g. kW.h/t) is insufficient for scale-up, especially to large mills. They suggest that the ratio of ball flow rate (the mass rate of ball circulation) to feed rate, which scales up breakage kinetics, should also be used, and that another dominant factor in scale-up is pulp flow velocity and radial ball-pulp mixing; it is likely that changes in the pulp rheology will affect the ball flow and pulp flow.

3 EXPERIMENTAL EQUIPMENT AND METHODS

3.1 Milling Investiations

The aim of the milling investigations was to examine the torque and position of the load under different conditions of mill rotational speed, mill filling, and pulp solids content. The measurement of torque is described in the next section. The position of the load was measured by two methods.

(a) by a conductivity probe mounted in the mill shell which showed increased conductivity when contact was made with a steel ball, and

(b) by still and moving photography.

3.1.1 Description of the milling installation

The milling installation used was designed by Moys (39) and is probably the most versatile and sophisticated of its kind. It can be used for continuous pilot-scale tests, in open or closed circuit, and the mill shell is removable so that various mill sizes can be used. All the important flow streams are measured and controlled as necessary, and data is logged by an H.P. 9816 computer (for these tests an H.P. 85c was used) via an H.P. 2240 Measurement and Control Processor. In addition, the torque on the mill axle is measured to an accuracy of 0,5 per cent of the value, and the mass of pulp in the mill is measured to an accuracy of 1kg by load beams.

For the series of tests discussed in this dissertation the mill was operated in a batch manner, and a special mill shell was designed and constructed. In order that the load could be observed and photographed, the mill had a polycarbonate front and a bulkhead at the back, also of polycarbonate, behind which was a circular fluorescent lamp to provide backlighting. The mill was 0,545m diameter inside the liners, which were 13mm steel mesh, the effective length was 0,308m.

The mill was rotated by a 2,5kW variable speed D.C. motor, with an associated tachogenerator and speed control unit. Mill speed was controlled by the computer at the required set point, and measured by a switch activated by a cam on the axle. The accuracy of measurement of the speed was 0,5 per cent of the set point, and all speeds quoted will be the set point speeds with this accuracy implied. The motor was slung in a cage mounted on and supported by the axle so that friction losses in the gearbox and drive chain are included in the torque measurement, the only friction not accounted for is in the two axle bearings, and this is negligible. The torque was measured by a load beam connected to a projection from the motor cage of known distance from the centre of mill rotation, the equipment is shown in Figures 3.1 and 3.2.

The conductivity probe and associated electronic circuitry was designed by Moys and built by the Central Electronics Unit of the University of the Witwatersrand. The probe is shown in Figure 3.3. The sensitivity of the probe was sufficient for it to indicate whether or not it was covered by the load of steel balls. As the periodic signal produced was quite complex, it was converted to a simple on-off square wave by means of a threshold that was manually adjusted while examining the signal on an oscilloscope.

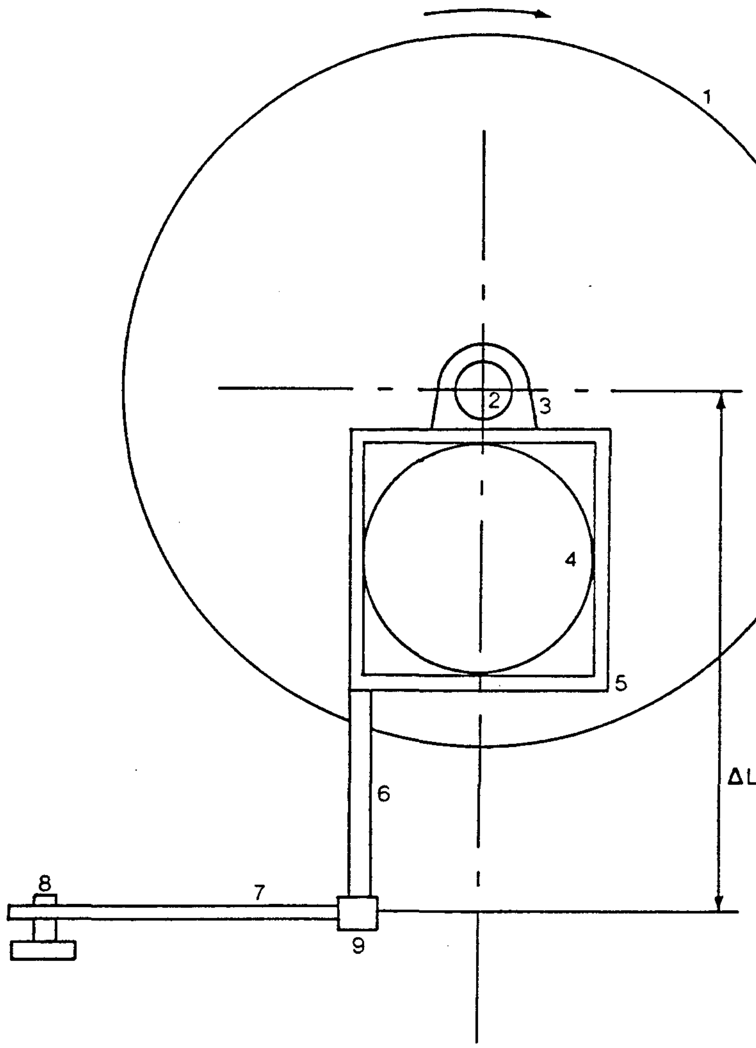

1. Mill
2. Drive shaft
3. Bearings from which motor cage is slung
4. Motor
5. Motor cage
6. Torque arm
7. Connecting arm
8. Load cell
9. Flexible coupling

Figure 3.1 Arrangement for the measurement of torque

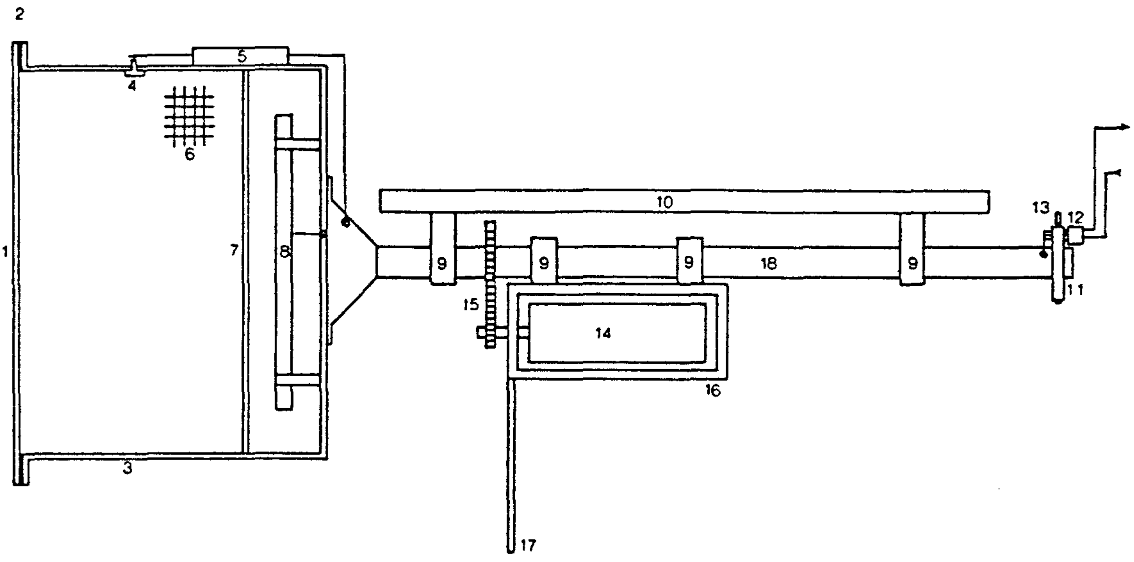

1. Polycarbonate end-plate
2. Rubber gasket
3. Mill shell
4. Conductivity probe
5. Signal processor
6. 13mm grid lining
7. Polycarbonate bulkhead
8. Fluorescent light
9. Bearings
10. Support beam (hung on load beams which are not shown)
11. Slip ring
12. Carbon brush pick-ups
13. Switch monitoring mill speed (activated by a rise on slip ring)
14. Motor and gearbox
15. Chain drive
16. Motor cage
17. Torque arm
18. Axle

Figure 3.2 Essential features of the milling equipment

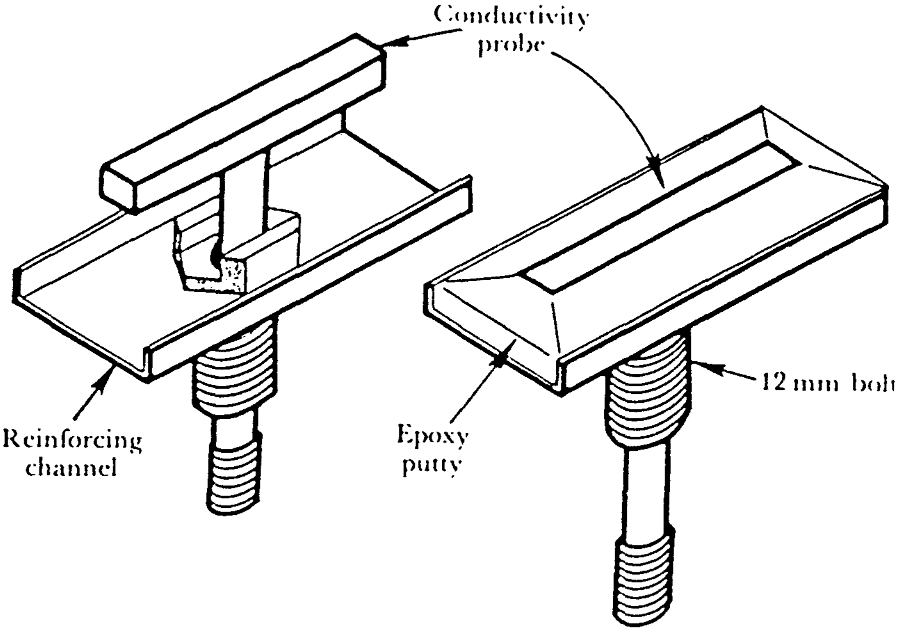

Figure 3.3 Conductivity probe (39)

It was found that once the threshold had been set on start-up of the installation, it had to be reset infrequently; when it had to be reset, it was positioned to cut at a characteristic point of the signal. A generalized pattern of the signal, with its major features, is shown in Figure 3.4. For each revolution a timer in the computer was reset by a reference marker switch, of known position, on the axle. The relative times of the on and off signals from the probe were taken and converted to periodic positions using the time for one revolution (taken from the mill speed) and the reference position.

The torque and position data were taken every mill revolution,

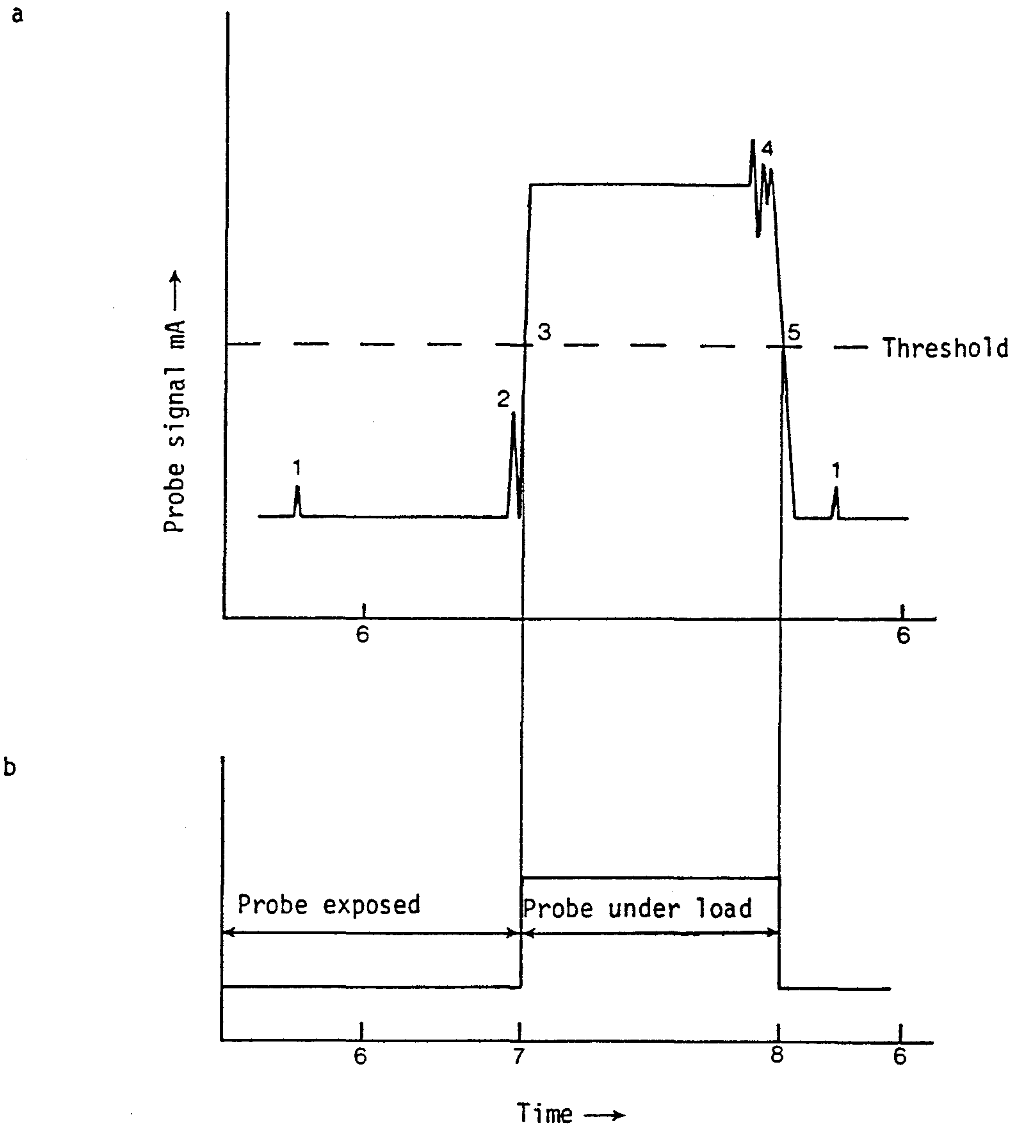

1. Small peak when probe is in the 12 o'clock position, probably due to drainage of pulp
2. Small peaks before probe enters the load toe, due to splashes and rebounding balls
3. Threshold indicating toe position, t.
4. Peaks near shoulder position, indicating some load movement
5. Threshold indicating shoulder position, s
6. Marker signal
7. Toe position read by the computer, relative to the marker
8. Shoulder position read by the computer, relative to the marker

Figure 3.4 General features of the probe signal
(a) Probe output
(b) Synthesized output seen by the computer

stored, then processed and printed out every ten revolutions.

The output signal from the probe, and the power for the fluorescent light, were transferred by means of carbon brushes contacting with slip-rings mounted on the axle.

For the purpose of photographing the load, the mill was illuminated from the front by two lamps of 0,5 and 1,0kW, as well as being backlit by the fluorescent lamp. Still photographs were taken using a 35mm Rolleiflex camera at a speed of 1/500 sec., which froze the motion of the load at all speeds. Moving film was taken with an Eumig Movie camera on Super 8mm film at 40 frames per second; examination of the film was done with a variable speed Eumig projector with single-frame examination facility.

3.1.2. Experimental conditions

The experimental conditions were chosen to correspond to the variations found in industrial practice as far as possible, so that the results can be considered to be more representative of what occurs in industrial mills. The conditions that were varied in the tests were: mill speed, mill filling, and pulp conditions. The variations are shown in Table 3.1.

The load motion could not be examined photographically using steel balls and rock pulp, as the transparent end-plate became smeared with the pulp and it was impossible to see inside. Instead, white ceramic balls and glycerine-water solutions were used.

Table 3.1 The variations of mill speed, filling, and pulp solids content used in the tests

Variable	Symbol	Unit	Values tested
Mill speed	N_p	Per cent of critical speed	50, 60, 70, 75, 80, 90, 95
Ball filling	J	Fraction of mill volume occupied by ball bulk volume	0,3, 0,4, 0,5
Pulp solids content	C_v	Volume per cent solids	35,4, 46,0, 52,2
(equivalent to)	C_m	Mass per cent solids (S.G. = 2,743)	60,0, 70,0, 75,0

So that the movements observed for the ceramic-glycerine system would at least be similar to those of the steel-pulp system, and could be correlated to the conductivity probe measurements, the size distribution of the ceramic balls was similar to that of the steel balls and the glycerine solutions where chosen to have viscosities that were similar to those of the various pulps used with the steel media. The pulp rheology determinations are described in section 3.2.

The tests were also performed using steel media and glycerine solutions as a comparison to the rock pulp, the load position was measured with the conductivity probe.

The 13mm mesh lining was chosen in preference to lifter bars as it was thought that the lifting effect the lifters have on the outer layer of balls, referred to by Vermeulen, *op cit*, would cause misleading readings of the load toe and shoulder to be indicated by the probe. The individual balls impacting on the mill shell as a result of the lifters would also cause the probe signal to be more complex. The mesh was chosen in preference to a smooth mill as slip between the load and mill would occur in a smooth mill causing unrealistic results; the mesh provided sufficient friction between the load and mill without influencing the charge motion.

A range of ball sizes was chosen in preference to a single ball size because the media loads of industrial mills contain varying ball or pebble sizes as a result of wear. Three ball sizes were used: -40 +25mm, -25 +15mm and -15mm. Ideally each size range should contain the same number of balls, but insufficient small balls were available. The ball load was made up of 35,4, 47,8, and 16,8 per cent (by number) of the large, medium, and small balls, respectively. This distribution had a voidage of 40,4 per cent.

The pulp volumes were chosen so that 85 per cent of the voids in the ball load were filled. Previous investigations (8,40) have shown that throughput and breakage rates are at a maximum between voidage fillings of 80 and 100 per cent.

Although the viscosity determinations were performed on a relatively coarse pebble mill discharge product, it was decided to use a somewhat finer gold mine tailings sand as feed for the tests. This decision was made because, as the tests were of a batch-type, the size distribution would become progressively finer, causing a rheology change; although the viscosity increase, due to a finer particle size distribution, would be offset somewhat by the temperature rise of the pulp. The use of a finer feedstock, which has a lower rate of breakage, would result in less of a difference in the size distributions, and hence rheology, of the feed and product. The size distribution of the feed material is shown in Table 3.2.

Table 3.2 Particle size distribution of the sand feed

Size interval µm	Individual mass %	Cumulative % finer
+850	1,2	-
-850 +425	0,7	98,8
-425 +300	1,7	98,1
-300 +212	8,5	96,4
-212 +150	24,8	87,9
-150 +106	31,7	63,1
-106 + 75	17,2	31,4
- 75 + 53	6,9	14,2
- 53 + 38	2,3	7,3
- 38	5,1	5,1

3.1.3 Experimental procedure

The procedures followed for tests using steel and ceramic media will be described separately.

(a) Steel media

The correct weight of balls to give the required filling was loaded into the mill (ball bulk density = 4,81 tonne/m^3) through a port in the shell, followed by sand and water in the proportions necessary to produce the desired solids content and void filling.

The mill was rotated at 75 per cent critical speed for approximately 40 revolutions to mix the charge and examine the probe signal and threshold point. The speed was reduced to 50 per cent critical, and after the speed and torque had stabilized, readings of torque and position were taken for approximately 120 revolutions. The speed was then increased to 60 per cent critical and the procedure repeated until a run at 95 per cent critical had been completed. The mill was then stopped and the pulp temperature was taken (ambient temperature was approximately 20^{o}C). The mill was re-started at 95 per cent critical and the procedure was repeated for reducing speeds; the total milling time was approximately 35 minutes. After the test was completed the pulp temperature was taken. The mill was then well flushed with water to remove the solids and reduce the temperature back to ambient; the conditions of load filling and pulp solids content were then adjusted as required for the next test.

The procedure of increasing and then decreasing the speed over the range tested was adopted so that the average of the two sets of data obtained for each speed could be taken and the average would correspond to conditions after approximately 850 revolutions.

The same range of tests was also performed using glycerine solutions of three viscosities in place of sand pulp, and it was apparent from the results that a large amount of slip was occurring under these conditions.

(b) Ceramic media

The procedure followed here was essentially the same as for the steel media apart from the variation in load measurement. The glycerine solutions used had viscosities (at 25°C) of 10,7, 63, and 275 centipoise (1 cP = 10^{-3} Pa.S). The speeds were progressively increased and reduced as before, so that the average torque at 850 revolutions could be calculated, but photographs were only taken for each speed while the speed was being increased.

After a change in speed, the torque and speed were monitored and when they had become constant (generally within 10 to 15 revolutions after a speed change), the load was photographed. Two still shots were taken for each condition and cinematographic film was taken for approximately 8 seconds.

At the end of a test, the mill shell was flushed with water while slowly rotating so that the mill, balls, and glycerine would be cooled. When the temperature of the glycerine had reached approximately 25°C, the conditions were changed for the next test.

3.1.4. Accuracy and preliminary processing of results

Some primary processing and filtering of the results was performed by the computer controlling the mill; the fractional deviation (standard deviation ÷ average) of the accepted information was also computed every ten revolutions. The computer programme was developed by Moys.

The fractional deviation of the torque for speeds up to 90 per cent critical generally varied between 0,004 and 0,006; over 90 per cent critical the deviation increased to up to 0,009. A fractional deviation of 0,006 on a torque of 14,5 kg.m (approximately the maximum recorded) represents a standard deviation of 0,09 kg.m which is 0,6 per cent of the value. The error in the torque measurement is very small due to the method of using a load beam and is approximately 0,5 per cent of the value. Therefore, the maximum total error associated with a torque measurement is approximately 1 per cent of the value. This error includes the error in the measurement and the error due to variance from the average; all quoted values of torque will have this error implied.

The torque measurement was periodically tested for zero during the tests by running the mill empty at the various speeds, and corrections were made to the measured torque values.

The measurements of the position of the toe and shoulder of the load obtained from the conductivity probe are subject to a larger variance, due to the surging motion of the load. Examination of the fractional deviation of the period spent by the probe under the load, u, showed that it did not vary with load filling, pulp solids content, or speed up to 95 per cent critical, and had an average value of 0,03. For 95 per cent critical the average fractional deviation was 0,04, which indicates increased load instability at this speed.

The load position data was assessed by the computer on acquisition for spurious readings, which were rejected. The data had to pass three tests to be accepted. These were:

(a) the calculated angle of repose had to be greater than zero and less than eighty degrees,

(b) the period of rotation had to be within the limit defined by:

$$\left(\frac{\text{Set point - actual}}{\text{Actual}}\right)^2 < 0{,}02, \qquad (3.1)$$

(c) the time taken for the probe to travel from the toe to the shoulder had to be greater than zero.

3.2 Rheological Investigations

As glycerine solutions were used so that the load motion could be photographed, it was necessary to examine the rheology of a pulp having a particle size distribution that is representative of those found in practice, so that viscosities corresponding to different solids contents could be specified. The viscosities of the pulps varied with shear rate, and as the shear rate in a mill varies with position, pulp solids content and mill filling, and is difficult or impossible to calculate, viscosities were calculated at a shear rate of 100 sec^{-1}. It was not intended that the viscosities should be highly accurate, but rather that the differences in magnitude between them should correspond to those of the pulp of three different solids contents.

3.2.1 Description of the viscometer

A Stormer viscometer was used, which is a rotating spindle type, that had been modified to maintain the pulp in suspension and provide vertical flow past the spindle. The modification, described by Walt and Fourie (41), consists of a four-bladed paddle at the base of the test vessel, which is contained in a water jacket, driven by a variable speed D.C. motor. Vertical baffles prevent rotation of the pulp and ensure that a vertical downwards flow passes the spindle. The vessel and spindle geometry are shown in Figure 3.5.

The viscometer is operated by placing a weight on the end of a non-elastic string which falls due to gravity, as it falls the weight rotates the spindle via a set of gears. Resistance to rotation of the spindle is due to the fluid viscosity. By using a range of weights, the shear stress may be varied. The readings obtained from the viscometer are times for 100 revolutions of the spindle, measured by a tachometer, which can be related to the viscosity from previously determined calibration equations.

3.2.2 Calibration of the viscometer

Before any rheology determinations could be performed, the viscometer had to be calibrated for torque and viscosity. The torque is a function of the driving weight (W, grams) and the function was found to be linear.

$$T = 199{,}55W + 95{,}05 \text{ dyne.cm} \qquad (3.2)$$

This enabled the shear stress to be defined for each weight used.

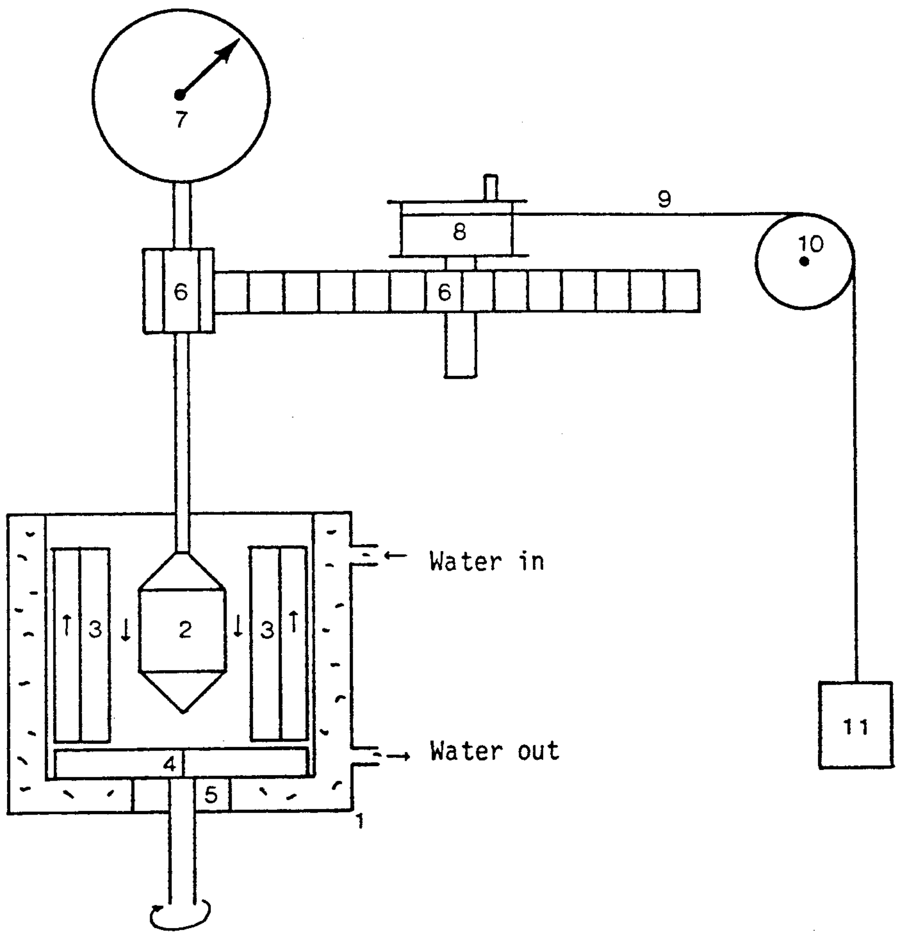

1. Vessel, with water jacket
2. Spindle
3. Baffles giving vertical pulp flow
4. Paddle
5. Seal
6. Gears
7. Tachometer
8. Winding drum
9. Non-elastic cotton
10. Pulley
11. Driving weight

Figure 3.5 Essential operating features of the Stormer viscometer

The viscometer was calibrated for viscosity using a range of seven glycerine-water solutions, the maximum and minimum viscosities being 17 and 366 cP. The weights used had masses of 12, 18, 24, 30, 45, 60, 80, and 100 grams, and a calibration equation, with viscosity a linear function of the time for 100 revolutions, was produced for each weight. The calibrations are given in Appendix A, and were performed with the paddle rotating at 50 r/min.

3.2.3 Experimental conditions

A sample of pebble mill discharge pulp was obtained from East Driefontein Gold Mine, the size distribution of which is given in Table A2 in Appendix A, and has 28,9 per cent passing 75μm and a Schumann slope of 0,78. The sample was dried and repulped for the tests at four solids contents of 35,4, 40,4, 46,0, and 52,2 volume per cent (solids S.G. = 2,743).

3.2.4 Experimental procedure

The required volume of water and solids mass were calculated to give the correct solids content and a pulp volume of 0,343 litre. The water was placed into the vessel, the stirrer turned on, and the solids added slowly to ensure mixing. The baffles were inserted, the spindle fixed into position, the pulp temperature was measured (all tests were conducted at 25°C), and, if necessary, was allowed to reach 25°C.

The tachometer indicator was positioned 25 revolutions before zero to ensure that the spindle had reached its terminal angular velocity when timing commenced, and a weight was hung on the string.

The brake was released and timing started when the tachometer indicator passed through zero and finished when the indicator again passed zero, i.e. 100 revolutions. This was repeated four times, and the average time used to calculate the viscosity from the calibration equation for the weight used.

The procedure was repeated for each weight, with the constraint that the time for 100 revolutions should not be less than 10 sec or greater than two minutes, and in this manner a range of viscosities at known shear stresses could be produced for each pulp.

3.2.5. Results

The results will be briefly mentioned here, as they were used to calculate the viscosities of the glycerine solutions used in the milling tests.

By using the viscometer to find a range of viscosities at known shear stresses for a particular pulp, the shear rate at which each viscosity is measured is calculated from the quotient of the shear stress and the viscosity. Thus a number of points can be generated for the shear rate/shear stress curves, then fitted to the De Waele equation (equation 2.21) and the constants n and k_c found; the viscosity at a given shear rate can then be calculated. This treatment is shown graphically in Figure A1, in Appendix A. The viscosities of glycerine used in the milling tests were unfortunately determined from the pulp rheology using an incorrect torque calibration which was only discovered after the tests were completed, and resulted in their values being somewhat lower.

The erroneous and correct values are compared in Table 3.3, and it can be seen that the differences are not sufficient to change the magnitude of the differences between the viscosities used.

Table 3.3 Comparison of erroneous and correct viscosities (at $\dot{\gamma}$ = 100 sec^{-1})

Volume solids %	Correct viscosity cP	Erroneous viscosity cP
35,4	15,6	10,7
46,0	89,6	63,0
52,2	325,4	275,0

The viscosities and shear rates were calculated at a number of shear stresses for each of the four pulp sands contents. The viscosity, shear rate, and shear stress data is given in Table A3 of Appendix A, and the rate-stress diagrams in Figure A2. The data was fitted to the De Waele equation (equation 2.21) and the rheological constants n and k_c determined, these are given in Table A4. The viscosity (calculated at a shear rate of 100 sec^{-1}) rises exponentially with pulp solids content, this is shown in Figure 3.6.

3.3 Investigation into the static angle of repose of the load

As the static angle of repose is required in the calculation of the spiral that defines the equilibrium surface, it was necessary to calculate it for the conditions used in the tests described.

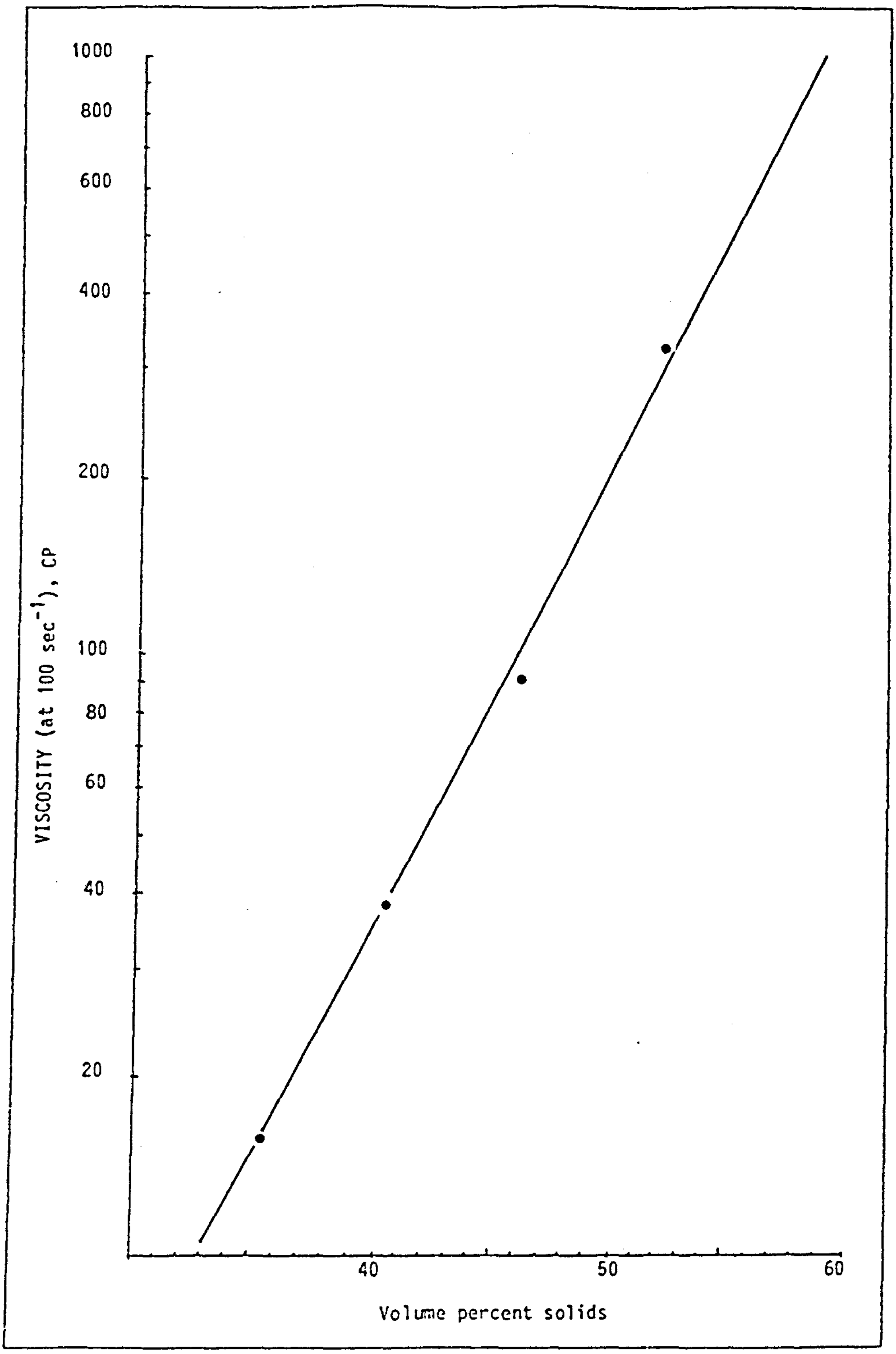

Figure 3.6 The influence of pulp solids content on viscosity

Consideration of a pile of balls placed on a flat surface indicates that it will have little or no angle of repose as the balls will roll away, and that the angle of repose experienced in a mill is rather a 'confined static angle of repose' where the balls are supported to some extent by the mill shell and cannot roll away as on a plane surface.

3.3.1 Experimental conditions

Determinations were performed using both the steel and ceramic media that were used in the milling tests. The angles were measured for each media with feedstock sand and milled product that was sampled at the end of a number of tests, with the pulp solids content varying to match those used in the tests. Angles were also measured for both media types with glycerine solutions of the same viscosities as those used in the tests. The angle was also measured for dry conditions.

3.3.2 Experimental procedure

A clear perspex box was constructed 0,40m long 0,20m wide, and 0,20m high to contain the balls. The box was placed on a horizontal surface, half-filled with balls and the appropriate pulp or glycerine solution was added and thoroughly mixed. One end of the box was lifted slowly until the mass of the balls was seen to shift, and the height of the edge of the box was measured. The angle of inclination, and thus the angle of repose, was then calculated. The balls and fluid were then remixed and the procedure repeated; the averages of five determinations were taken for each test.

3.3.3 Results

The angles of repose that were determined for the various conditions are shown in Table 3.4 and it can be seen that the static angle of repose increases with pulp solids content and particle coarseness. This is seen for the steel and ceramic balls. When glycerine solutions are added to steel or ceramic balls the angle of repose is almost unchanged from that of the dry balls, even by the 275 cP solution. For steel balls the addition of a small amount of feed sand to a 10,7 cP solution gives an angle of repose equivalent to a feed sand pulp containing 35,4 per cent solids.

Table 3.4 Measured static angles of repose (α)

Media	Dry	Feed sand, vol. %			Milled sand, vol. %			Glycerine solution cP		
		35,4	46,0	52,2	35,4	46,0	52,2	10,7	63,0	275
Steel	34,7	38,2	41,8	47,2	35,9	39,9	42,0	34,4 38,2*	35,0	35,9
Ceramic	35,2	36,9	42,7	46,9	36,4	38,6	41,8	35,3	35,5	36,5

*10,7 cP glycerine + feed sand

Note: Coefficient of friction (μ) = tan (α)

4 DISCUSSION OF RESULTS

The results obtained from three series of tests will be referred to; viz

(a) Steel media and sand pulps.

(b) Ceramic media and glycerine solutions.

(c) Steel media and glycerine solutions.

The torque and load position measurements for the steel media and sand pulp series are the most applicable to real conditions and conclusions will generally be based on these results. The torque results from the ceramic media tests show the same trends as for the steel and sand pulp series, although the actual values and results are influenced somewhat by the lower angles of repose measured. The load position will be discussed using the results obtained from the conductivity probe, which are the averages of 80 to 100 revolutions. The load positions quoted for the ceramic-glycerine system are calculated from the two still photographs taken for each condition (i.e. two revolutions), and as they are subject to much more error, may be used for comparison purposes only. The steel media and glycerine solution series of tests provide a good indication of the effects of slip within the load. The results for each test (where pulp conditions and fillings are constant and the speed varied) are presented in tabular and graphic form in Appendices B, C, and D, where Appendix B contains results from series (a),

Appendix C contains results from series (b), and Appendix D contains results from series (c).

When the locations of the toe and shoulder (t and e) are discussed, the positions are expressed as fractions of the mill circumference (inside liners) with the 12 O'clock position being the datum.

The influence of the variables upon energy will be discussed primarily in terms of torque rather than power. This is because power contains a component of mill speed, and as mill speed is one of the variables, discussion of results in terms of power means that speed cannot be isolated. Where necessary, the effect of variables upon power will be discussed.

4.1 The influence of pulp conditions on torque and load position

The pulp within a mill has two characteristics which can influence the load motion and hence the torque. These characteristics are the viscosity of the pulp which provides both adhesion and viscous resistance to flow, and the presence of solid particles that cause friction within the load, and between the load and liner. Increasing the solids content of the pulp causes both the viscosity and the internal friction of the load, (as measured by the static angle of repose), to rise; as demonstrated in chapter 3. Using the results from all three media-pulp systems, it is possible to infer the individual effects of the two characteristics.

4.1.1 Viscosity

The effect of viscosity alone can be seen from the tests where glycerine solutions were used in place of a particulate pulp with the steel media.

The combination of glycerine and steel balls gave rise to a large amount of slip occurring within the load. This is indicated by the fact that at fillings of 30 and 40 per cent no torque reduction is seen at higher speeds, and at 50 per cent filling a torque reduction is only achieved at speeds greater than 90 per cent critical. Measurements from the conductivity probe show that the dynamic angle of repose is lower than for the steel-sand system, indicating that the load is slumped.

The slip is caused by a combination of the smooth surfaces of the steel balls and the glycerine solution acting as a lubricant.

The torque measurements for the ceramic-glycerine system are similar to those for the steel-sand system in that they show a reduction at higher mill speeds. This indicates that much less slip occurs. This is due to the rough surfaces of the ceramic balls. Examination of the cinematographic films confirmed the lack of slip at higher fillings, and measurements showed the angular velocities of rising balls to be equivalent to that of the mill.

The effect of viscosity on torque is demonstrated at various speeds in Figure 4.1, the data refers to a ceramic ball load at a bulk filling of 40 per cent of the mill volume. The mill was run under dry conditions, with water (η = 0,890 cP at 25^{o}C) and

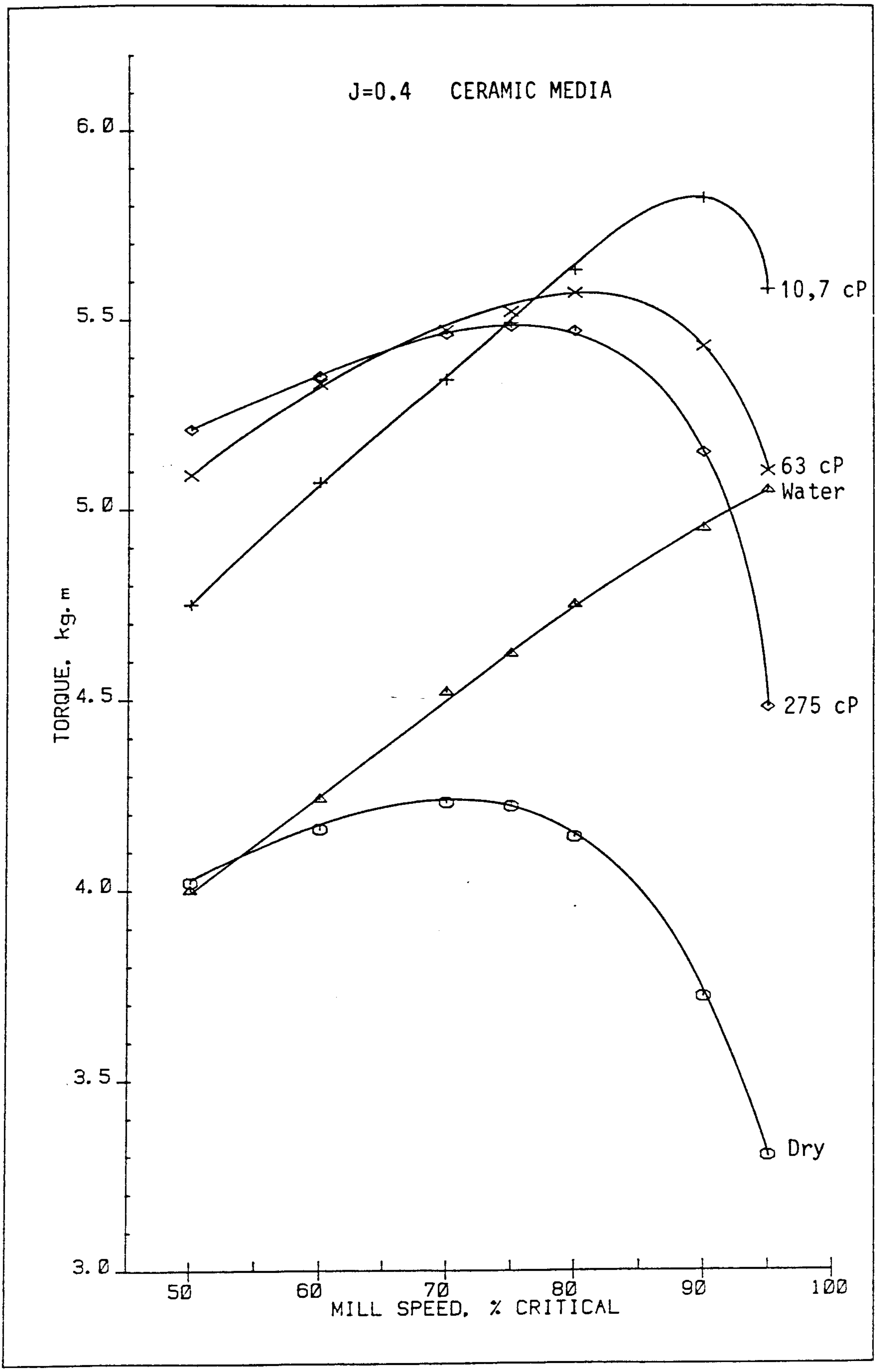

Figure 4.1 The influence of pulp viscosity on torque

with glycerine solutions having viscosities of 10,7, 63 and 275 cP. For dry conditions the torque shows a maximum value of 4,24 kg.m at 71 per cent critical speed. The addition of water to the mill causes a linear increase in torque with speed, with no maximum observed; at 50 per cent critical speed the torque is equivalent to that of the dry load. Further increases in the viscosity restore the occurrence of a maximum torque, with increasing viscosity causing a reduction in the value of the maximum torque, and the speed at which the maximum occurs; this is shown in Table 4.1

TABLE 4.1 Maximum torques, and the speeds at which they occur, for various pulp viscosities

Conditions	$Torque_{max}$ kg.m	$Speed_{max}$ % critical
Dry	4,24	71
Water	5,12	95*
10,7 cP	5,74	87
63 cP	5,56	79
275 cP	5,53	76

*No maximum in the range 50 to 95 per cent critical

The liquid distribution has a greater effect on the torque with ceramic media than for steel media. Due to the lower density of the ceramic media, the liquid represents a larger fraction of the total mass of the load. Therefore, the results of these data have to be interpreted with this in mind.

The addition of liquid into the mill results in an increase in the mass of the load and, depending upon how the liquid distributes itself, this increase in mass has an effect on the torque in terms of equation 2.12. Changes in the measured torque are, when compared with dry conditions, therefore due to a combination of the increase in mass upon addition of the liquid, the distribution of the liquid and any modification to the load motion resulting from the liquid addition.

The distribution of the liquid within the load varies with viscosity and mill speed. Two extremes can be considered, and represented by modifications of equation 2.12:

(a) the liquid is well mixed with the load, and the centre of gravity of the load, for the purposes of equation 2.12, can also be considered to be the centre of gravity of the liquid. This situation can be seen to occur at the higher viscosities (i.e. 63 and 275 cP), and can be represented by equation 4.1 and Figure 4.2a.

$$T = (m_m + m_p) g\, r_g \sin \alpha \qquad (4.1)$$

where m_m is the media mass and m_p is the pulp mass.

(b) the liquid is not uniformly distributed within the ball load, and can be considered to have a different centre of gravity than the solids. This situation can be represented by equation 4.2 and Figure 4.2b.

$$T = m_m \, g \, r_{gm} \sin \alpha_m + m_p g \, r_{gp} \sin \alpha_p \qquad (4.2)$$

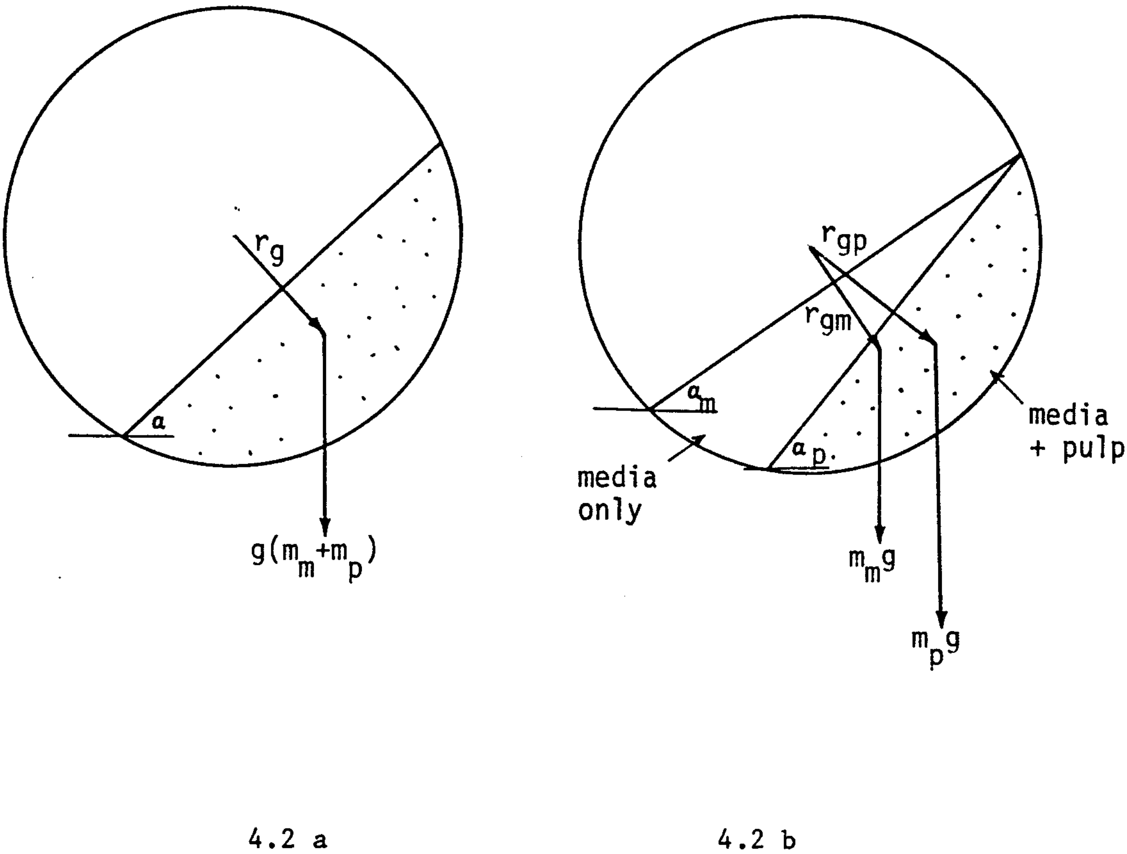

Figure 4.2 Torque-arm configurations for (a) well-mixed pulp and media, (b) poorly mixed pulp and media

When water was added to the mill, the charge mass increased by 25 per cent, compared to the dry load, yet at low mill speeds the torque increases by much less than this amount, and at 50 per cent critical speed there is no difference in torque. Visual observation showed that at the low speeds, the water tended to remain in the toe area as its viscosity was not high enough to ensure that it was retained within the voids of the balls. The distribution is that described by equation 4.2, with the liquid having a low angle of repose and therefore causing only a small increase in torque. This increase is offset by the lubricating action of the water which causes a lower angle of repose of the balls, and hence a lower torque due to their position. This lubricating effect is also shown by the torque for the ceramic-water system not showing a maximum, up to 95 per cent critical speed.

A viscosity of 10,7 cP is sufficient for the liquid to be retained within the ball voids, but the lubricating effect still outweighs the adhesion effect. This is demonstrated by the percentage increase in torque, between dry conditions and 10,7 cP liquid addition, at 50 per cent critical, being less than the percentage increase in mass due to the liquid addition. If the lubrication effect was not present, a torque increase greater than that predicted by a proportional mass increase would be expected, because the liquid distribution is such that the centre of gravity of the liquid is more offset than that of the load. This is demonstrated in Figure 4.3, which is a still photograph for the conditions $J = 0{,}4$ $\phi = 0{,}5$, $\eta = 10{,}7$ cP, and it can be seen that the rising portion of the load is moving at a faster velocity than the liquid can flow downwards through the voids of the balls. At higher mill speeds this effect tends to disappear as a result of a more efficient mixing action.

The higher viscosity liquids of 63 and 275 cP cause maximum torques to occur at 79 and 76 per cent critical speed respectively. The rate of reduction in torque, as the speed is increased beyond that which results in maximum torque, increases as the viscosity increases.

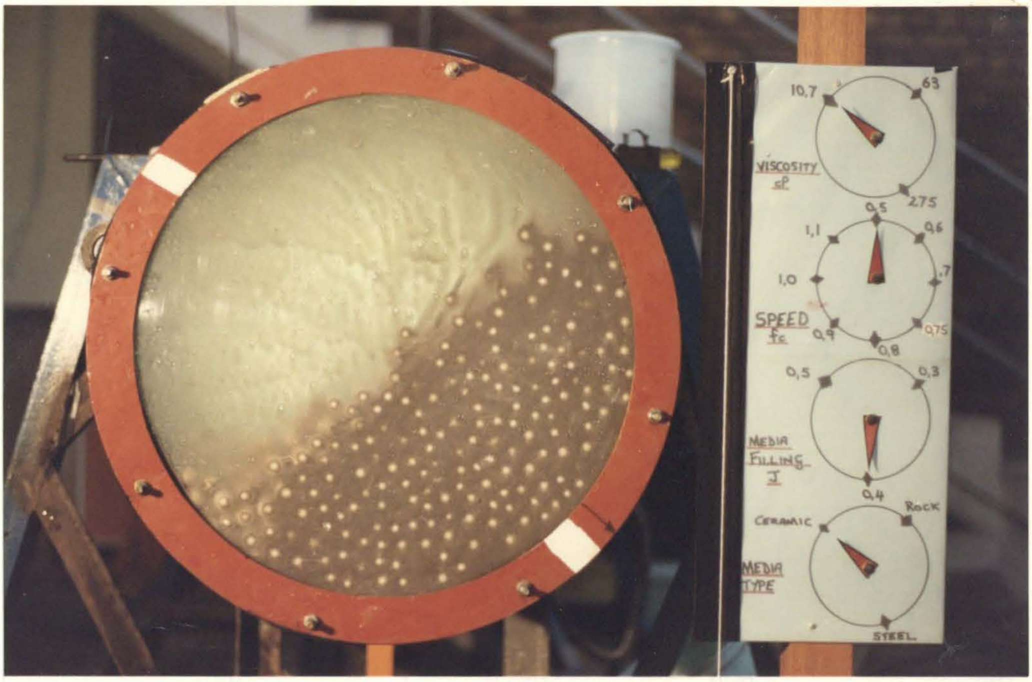

Figure 4.3 Photograph showing the absence of 10,7 cP glycerine solution at the load toe

The conductivity probe does not efficiently measure the position of ceramic media, so accurate positional data is not available for this set of tests. Values of the shoulder position, e, for conditions of 10,7, 63 and 275 cP, determined from photographs of the load are given in Table 4.2. These values indicate that an increase in viscosity results in the load rising further, due to adhesion within the load, and between the load and liners.

TABLE 4.2 Values of the shoulder position, e, for various mill speeds and glycerine solution viscosities

Mill speed	Viscosity, cP		
% critical	10,7	63	275
50	0,824	0,828	0,855
60	0,844	0,843	0,861
70	0,851	0,870	0,879
75	0,863	0,875	n.d.
80	0,881	0,886	0,891
90	0,902	n.d.	0,940

Conditions, J = 0,4, ceramic media

n.d. = not determined

4.1.2 Friction

As demonstrated in the previous section, the addition of a liquid to the load can cause a lubricating effect which predominates at low viscosities; this effect is negated to a large extent by the addition of particles, and is demonstrated in Figure 4.4. The data is for steel media, it can be seen that with a 10,7 cP glycerine solution the torque increases almost linearly with mill speed, and no reduction in torque is experienced over the range of speeds tested, indicating that slip is occurring, especially at higher mill speeds. The addition of 2 kg of sand to the 10,7 cP liquid results in a maximum torque being obtained at 78 per cent of critical speed. Data from the test where a

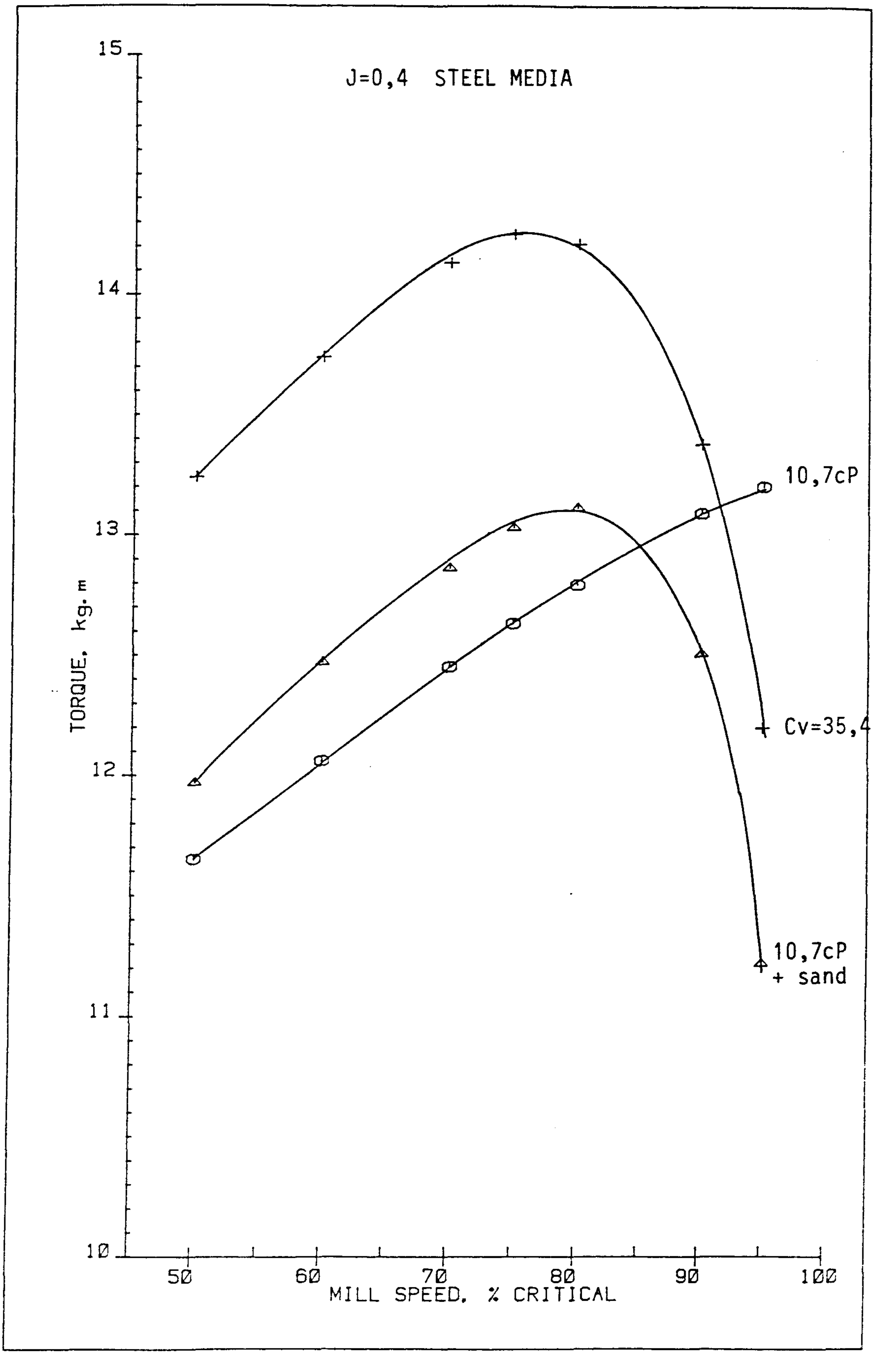

Figure 4.4 The influence of friction on torque

35,4 per cent solids pulp was used is also shown, the torque curve is of a similar shape to that of the 10,7 cP liquid plus sand, and the maximum occurs at 78 per cent critical speed.

The load position is influenced by the addition of solids to the glycerine solution, as shown in Figure 4.5. For glycerine only the toe position ,t, is almost invariant with changes in mill speed, whereas the addition of solids to the glycerine increases the values of t, indicating that the toe lies lower; in fact, the toe positions for glycerine plus solids corresponds to those for the 35,4 per cent solids pulp. This indicates that, for all mill speeds tested, the position of the load toe is influcenced by friction rather than viscosity.

The interaction of friction and viscosity (adhesion) in the region of the load shoulder appears to be more complex. At the lower speeds of 50 and 60 per cent critical the shoulder positions of all three fluid types are equivalent, as seen in Figure 4.5. Only when the mill speed is further increased does a difference become apparent, with the shoulder lying highest for the 35,4 per cent solids pulp, and lowest for the 10,7 cP glycerine solution. This indicates that at the lower speeds the shoulder position is primarily a function of viscosity, but as the speed is increased, the shoulder position becomes dependent upon a combination of viscosity and friction. This is because at higher speeds, the tendency for the load to slip, both within itself and between the liners, increases and the viscous adhesion effects alone are not sufficient to prevent this slip at the higher speeds.

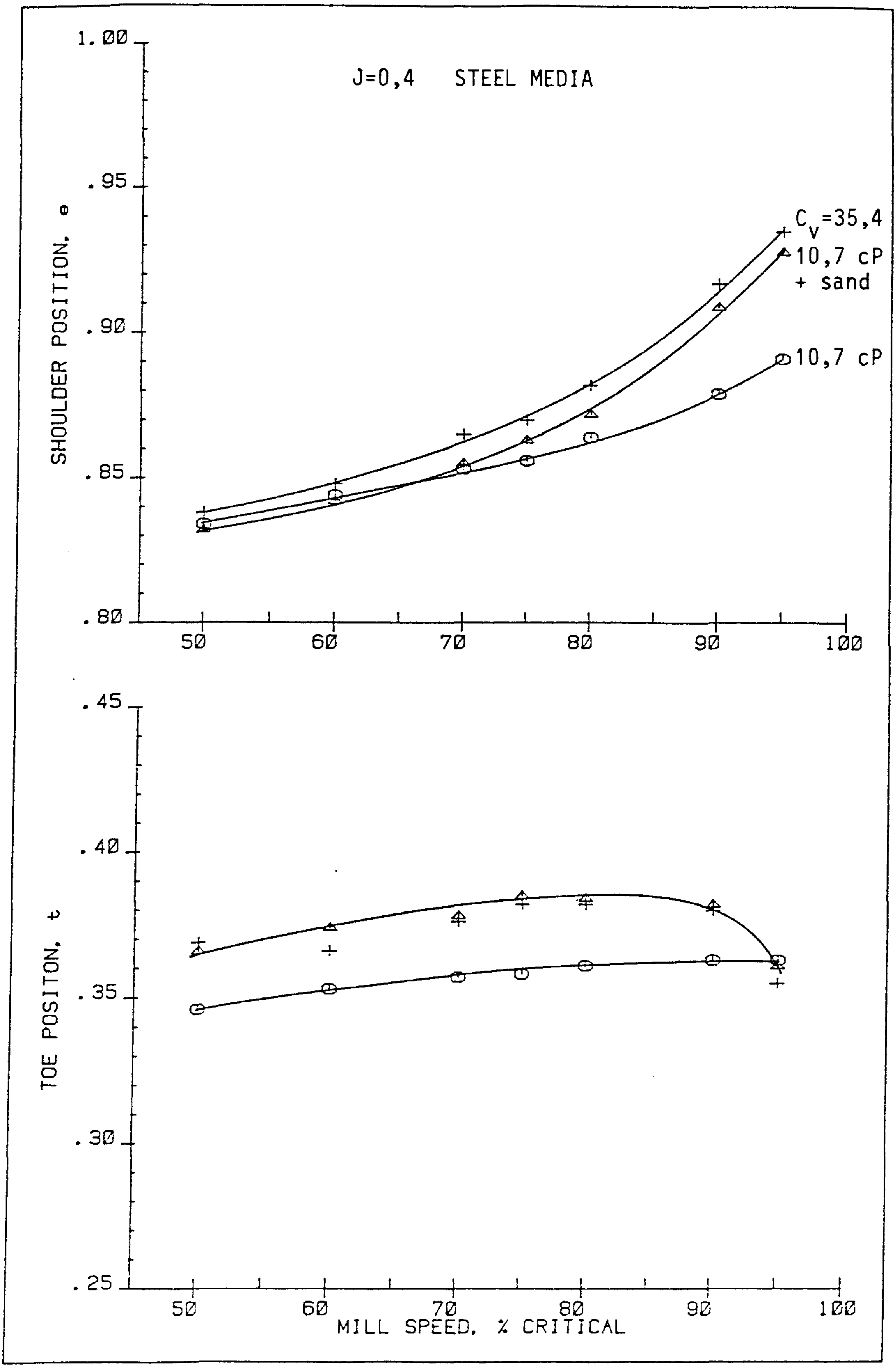

Figure 4.5 The influence of friction on toe and shoulder positions

4.1.3 Combined effects of viscosity and friction as observed with particulate pulps

The results presented in the previous two sections have demonstrated the individual effects of pulp viscosity and friction due to the ore particles present in the pulp. The combined effects will be examined using data obtained with steel media, at a bulk filling of 40 per cent of the mill volume, and particulate rock pulps of 35,4, 46,0, and 52,2 volume per cent solids. The torque and load position data are shown as a function of speed in Figure 4.6.

At mill speeds of 50, 60 and 70 per cent critical, there is little difference between the torques obtained with the three pulps. At speeds greater than 70 per cent, a difference becomes apparent, with the torque at a given speed decreasing as the pulp solids content increases. The value of the maximum torque, and the speed at which it occurs, are only weakly influenced by a change in solids content, as shown by Table 4.3, although the difference becomes greater when the filling is increased to 50 per cent.

TABLE 4.3 Maximum torques, and the speed at which they occur, for various pulp solids contents and mill fillings

Pulp solids content	J = 0,4		J = 0.5	
vol., %	$Torque_{max}$ kg.m	$Speed_{max}$ % critical	$Torque_{max}$ kg.m	$Speed_{max}$ % critical
35,4	14,29	76	14,77	75
46,0	14,26	74	14,37	72
52,2	14,18	73	14,23	71

Conditions: Steel media, sand pulp

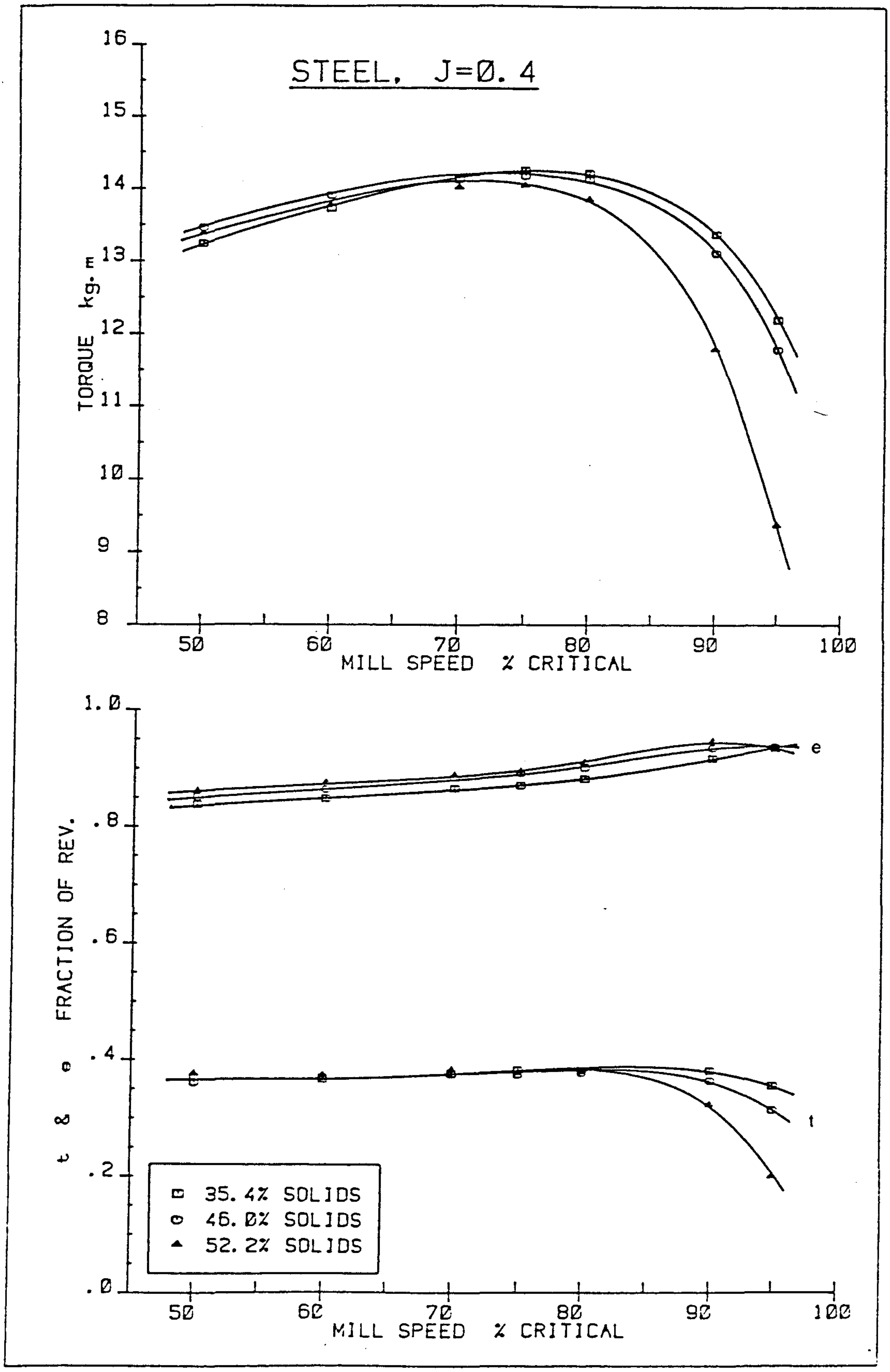

Figure 4.6 Torque and load position for various pulp solids contents

Although the trend is slight, it can be stated that an increase in the pulp solids content causes a reduction in the value of the maximum torque, and a reduction in the speed at which the maximum is attained.

At speeds up to 80 per cent critical, the toe position is not influenced by the pulp conditions, over the range of solids contents tested. At speeds greater than 80 per cent critical the value of t decreases as the pulp solids content increases, indicating that the toe is at a higher position in the mill. At these speeds the downcoming balls are impacting upon the mill liners rather than into the bulk of the toe.

The position of the load shoulder is influenced by the pulp solids content at all speeds, with a rise in solids content causing the shoulder to rise higher up the mill side. At lower speeds the difference is primarily due to changes in viscosity, whereas at higher speeds the difference is due more to the increased friction as a result of the presence of more solids in the mill causing a reduction in the susceptibility of the load to slip.

The torque is influenced by a change in pulp conditions because the load motion is affected, and it is the load motion that determines the characteristics of the torque curve. Increasing the solids content causes the shoulder to rise, which changes the motion of the downward moving balls. A rise in the shoulder causes the impact points of the falling balls to move across the toe towards the intersection of the mill liner and the toe. This results in a greater amount of energy being recovered, which assists the mill in rotating, and thus reduces the energy required to maintain the mill rotating at the set speed. The shift of impact points due to increasing solids content causing the shoulder to rise can be seen in Figure 4.6 at speeds of 90 and 95 per cent critical. This is further illustrated in Figure 4.7, which shows the parabolic paths that balls have to follow to leave the measured shoulder points and impact at the measured toe points, for 90 per cent critical speed and the three pulp solids contents. The rise in the shoulder position due to increasing solids content caused by increased viscosity and friction results in the impact points of the balls rising further up the downcoming side of the mill.

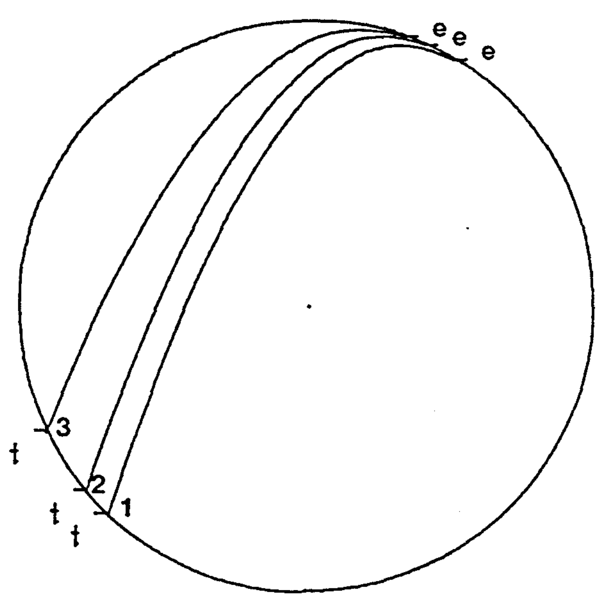

Conditions: J = 0,4, ϕ = 0,90, steel media

1: C_v = 35,4, 2: C_v = 46,0, 3: C_v = 52,2

Figure 4.7 The influence of pulp solids content on the shoulder position and parabolic trajectories of falling media

4.1.4 Summary of the effects of pulp conditions

Variation of the pulp solids content has two effects which can alter the load motion and hence the torque. The change in the amount of solids present results in a change in the friction within the load and between the load and liners, and thus causes a variation of the slip. A rise in the solids content causes an exponential increase in the viscosity. The pulp viscosity promotes adhesion within the load, and between the load and liners especially in the region of the shoulder.

At speeds where the downcoming balls are not impacting upon the liners, the toe position is insensitive to changes in pulp conditions, within the range of conditions used in practice, whereas the shoulder position is influenced by pulp solids content; an increase in solids content causes a rise in the shoulder position. The interactive influence of viscosity and friction on the shoulder position appears to vary with speed. At low speeds (i.e. less than 60 to 70 per cent critical) the viscosity has the major influence on the shoulder position, whereas at the higher speeds a combined influence is seen. The change in shoulder position due to changes in pulp conditions has a small effect on torque at speeds lower than the speed where the maximum torque is obtained, whereas at speeds higher than this the effect is greater due to increased energy recovery from the load.

The large variation in pulp solids content from 35.4 to 52,2 per cent resulted in a small change in the value of the maximum torque and the speed at which it occurs, with the trend being that increasing solids content reduces the maximum torque and its speed of occurrence.

4.2 Slip

The occurrence of slip within a grinding mill results in wasted power, increased wear of liners, and increased and unnecessary wear of the grinding media. Slip can be thought of in two forms: slippage of the *en-masse* load over the liners and slippage within the body of the load.

Slip between the load and liner has been examined by Manz (42), albeit for dry conditions; he concluded that the slip is much reduced as the load volume is increased above 30 per cent, and the slip is increased as the mill speed is increased. Vermeulen and Howat (43) have derived an expression that relates slip between the liner and load of a smooth mill to the pressure on the liner. The pressure is a function of the load mass, and therefore increasing the load mass would increase the pressure and reduce the slip. These investigations have not made an assessment of the slip that occurs within the load, and have been concerned with mills operated under dry conditions.

4.2.1 The effect of filling on slip

The position at which the Davis circle cuts the mill shell can be regarded as the lowest point that a particle can theoretically leave the mill shell and fall under gravity. The Davis circle calculation is based on the assumption that no slip occurs between the load and the liner.

The shoulder positions for the steel-pulp system are shown in Figures 4.8 and 4.9 for the various conditions of pulp solids content and mill filling; also shown are the theoretical Davis points calculated for each speed.

For fillings of 40 and 50 per cent, the shoulder positions lie above the Davis points, whereas for a filling of 30 per cent the shoulder lies below the Davis point at some conditions of speed and pulp solids content. This implies that at these conditions the load is moving at angular velocity less than that of the mill, due to slippage between the load and liner. These results show that the calculations that the slip is reduced as the load is increased, made by Manz and Vermeulen, hold true under wet milling conditions.

4.2.2 The effect of mill speed on slip

The results shown in Figures 4.8 and 4.9 show that, for a filling of 30 per cent, increasing the mill speed causes the shoulder position to fall below the Davis point. This shows that, when the filling is low enough for slippage to occur, the amount of slip is increased by increasing the speed.

4.2.3 The effect of pulp solids content on slip

The results shown in Figure 4.9, for the 30 per cent filling, indicate that increasing the amount of solids in the pulp decreases the slip. For a pulp of 35,4 per cent solids the shoulder position falls below the Davis point at speeds greater than 70 per cent critical, whereas for the 46 per cent solids pulp the shoulder

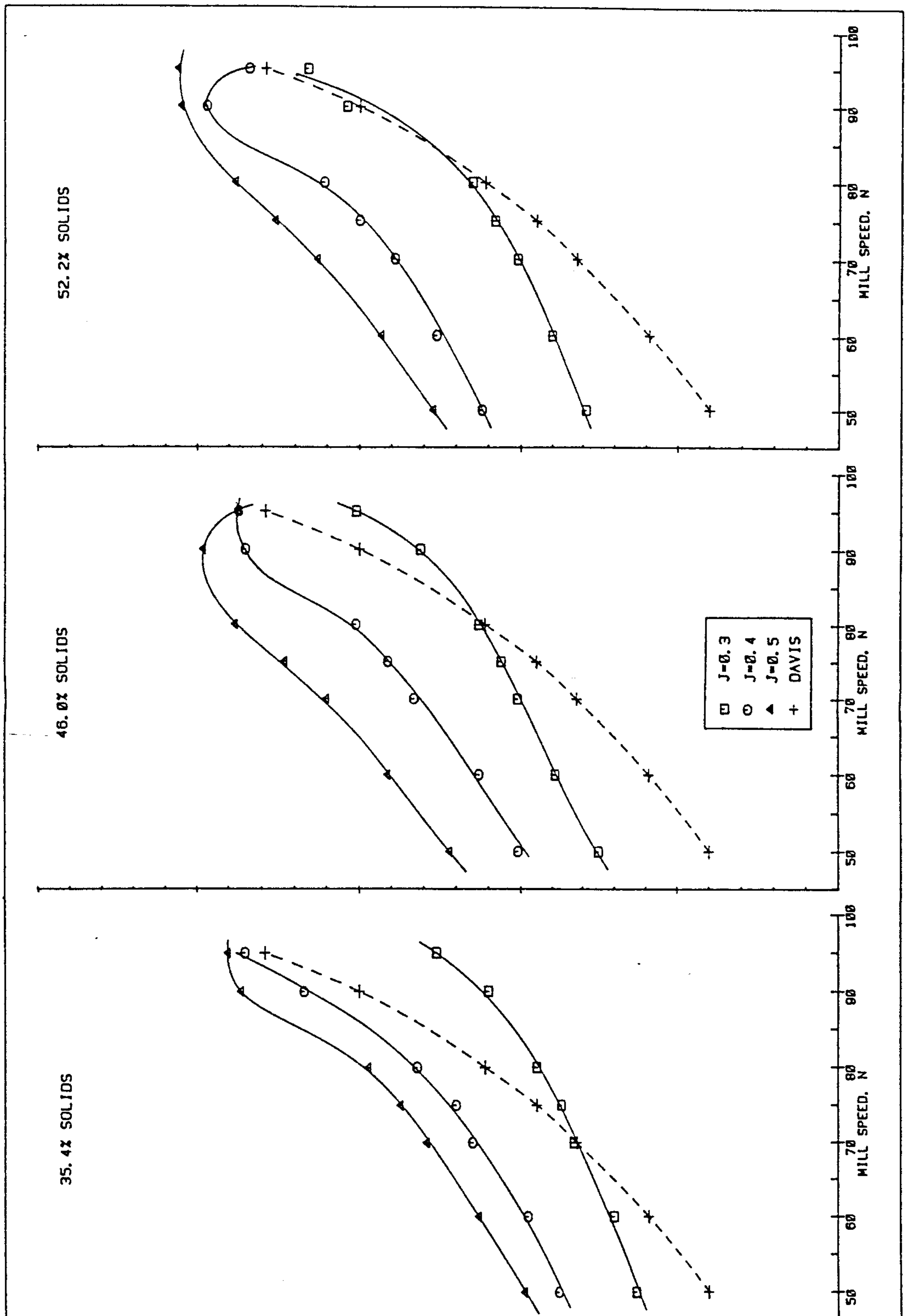

Figure 4.8 Variation of the shoulder position with mill filling

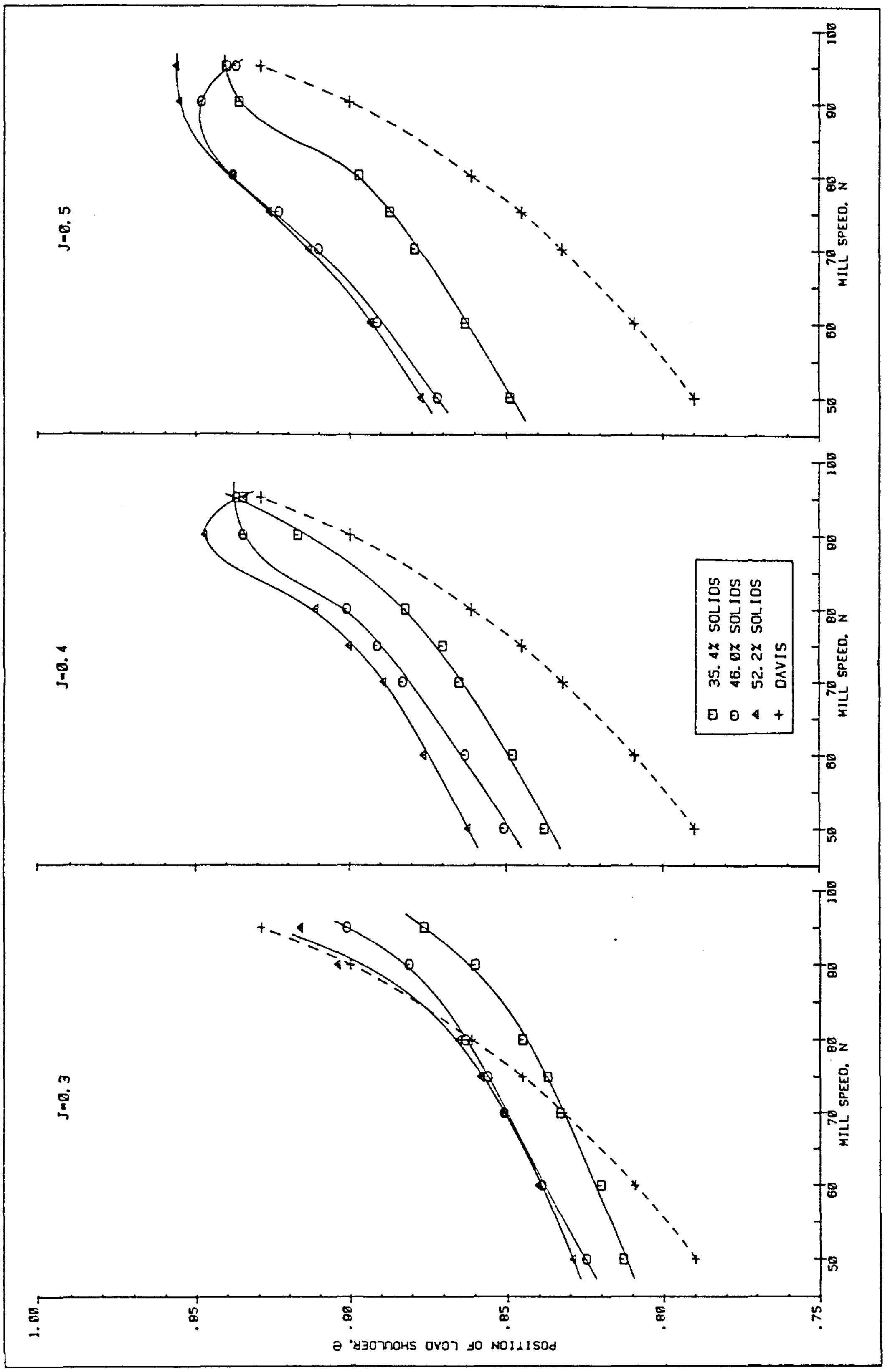

Figure 4.9 Variation of the shoulder position with pulp solids content

position falls below the theoretical at speeds above 80 per cent. For the 52,2 per cent solids pulp the shoulder position lies above the Davis point at speeds up to 90 per cent critical, and conforms to it at higher speeds.

4.3 The effect of mill filling and speed on torque

In order to simplify the discussion, the effect of mill milling will be examined at a pulp solids content of 46 per cent. The nature of the effects of the filling and speed are not changed by variation of the pulp solids content, over the range tested, only the magnitudes of the measured values are altered.

4.3.1 Mill filling

It is well-known that power increases parabolically with filling (12,20,44), the maximum power draw occurs at a filling of approximately 50 per cent. At constant mill speed, power is directly proportional to torque, and torque characteristics therefore parallel the power characteristics.

The variation of torque with filling at constant mill speed for the steel-pulp system can be seen in Figure 4.10. The data has been fitted to parabolas, which are drawn for each speed; the fillings at which the maximum torques occur, and the values of the maxima are shown in Table 4.4.

At mill speeds up to between 75 and 80 per cent critical, the maximum torque occurs at fillings of approximately 45 per cent, and as the speed is further increased the filling required to

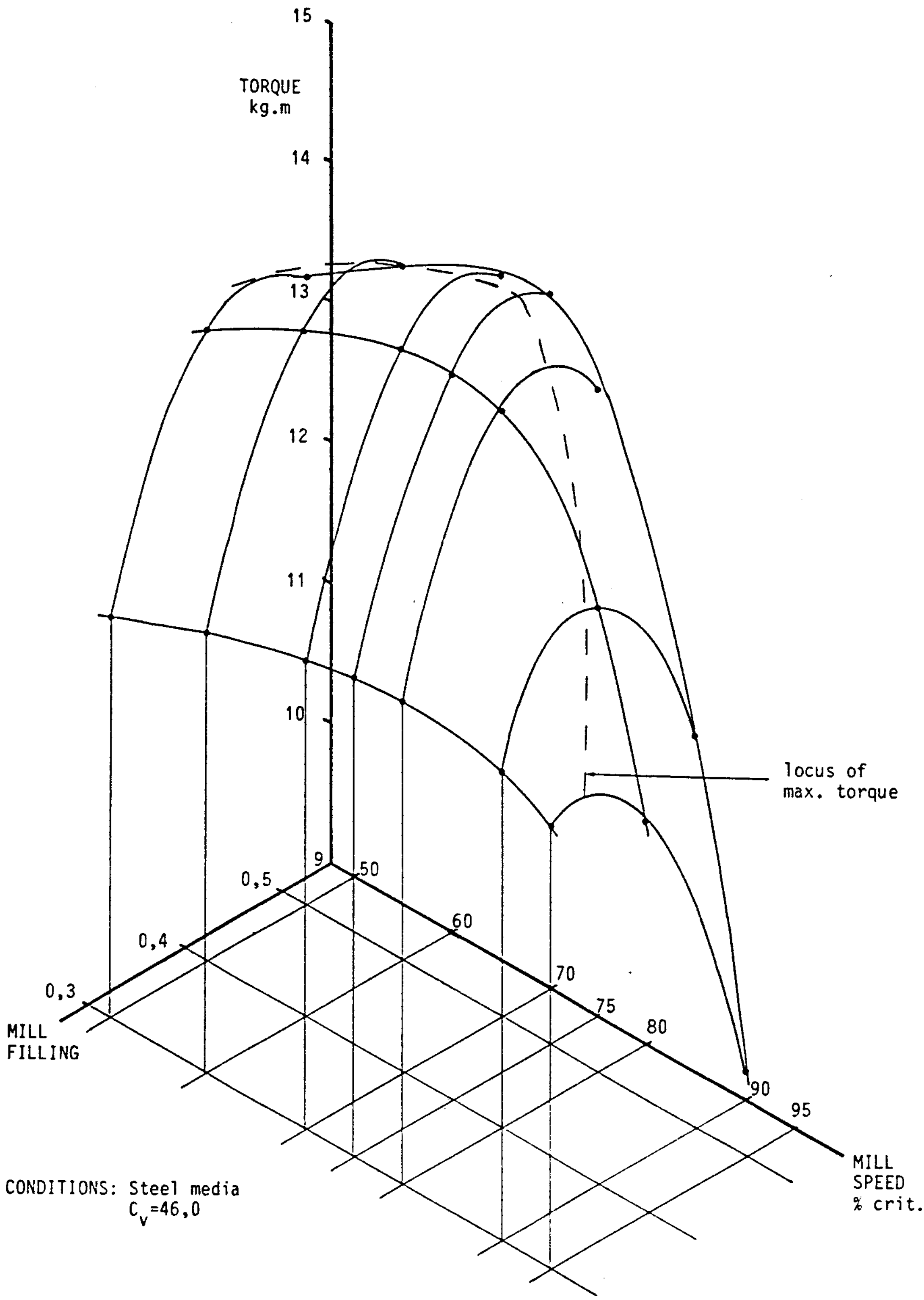

Figure 4.10 Variation of torque with mill filling and mill speed

TABLE 4.4 Maximum calculated torques, at various speeds, and the fillings at which they occur

Mill speed % critical	Max. torque T_m, kg.m	Filling at max. torque, J_{max}
50	13,65	0,448
60	14,16	0,454
70	14,42	0,455
75	14,49	0,463
80	14,25	0,436
90	13,14	0,386
95	12,25	0,328

Conditions: Steel media, C_v = 46,0

produce the maximum torque decreases. It is of interest that, at industrial operating speeds, the filling required to produce the maximum torque is in the region of 45 to 47 per cent. In most mills this is the maximum level to which a mill can be charged. For an overflow discharge mill filling beyond 45 per cent causes ejection of grinding media into the mill discharge, and although grate discharge mills do not have these problems, over filling can cause excessive wear of the mill feed arrangement. Austin has shown (20) that the rate of particle breakage is at a maximum when the filling is approximately 45 per cent.

It is accepted in industry that throughput is maximized when power is at a maximum, and this is a major control feature of multivariable milling control systems used for autogenous milling circuits. The power is controlled around the maximum by varying the feedrate; in effect the mill filling is determining the power, and is the controlled variable, with the power being an indirect measurement of the filling.

When the mill speed rises above 75 per cent critical the optimum filling becomes increasingly dependent upon speed, and the filling that results in the maximum torque is reduced. This is because increasing filling and speed both result in increased cateracting of the load, which causes a rise in the amount of energy recovered from the falling mass.

4.3.2 Mill speed

The torque varies considerably with changes in the mill speed, which indicates that the load position and movement is being affected. The variation of torque with speed can be seen at various fillings for a 46 per cent solids pulp and steel media in Figure 4.10.

At a low filling of 30 per cent the torque profile is a shallow curve with a relatively indistinct maximum occurring. At fillings of 40 and 50 per cent a more distinct maximum is seen, with a rapid reduction in torque at higher speeds. The rate of torque reduction at higher speeds is made greater by increasing the filling or the pulp solids content, showing that both actions have a similar effect upon the load motion. The rate of torque increase with speed up to the maximum torque is approximately the same for each filling.

The torque can be fitted as a function of speed to a cubic polynomial to give good regression coefficients (i.e. $r^2 > 0,96$), the speed at which the maximum torque occurs can be calculated for each filling. The values are shown in Table 4.5 for the 46 per cent solids pulp. The maximum torque for each filling occurs at a different speed, which means that the values of the maximum torque are not directly relevant to industrial mills which run at a constant speed. To overcome this the power has been calculated for each speed at the various fillings and then fitted to a cubic polynomial.

TABLE 4.5 Maximum calculated torques and power, at various fillings, and the speeds at which they occur

Mill filling	Torque		Power	
J	Max. kg.m	$Speed_{max}$ % crit.	Max. kW	$Speed_{max}$ % crit.
0,3	12,44	81	*	*
0,4	14,26	74	0,688	88
0,5	14,37	72	0,658	82

Conditions: Steel media, $C_v = 46,0$

*No maximum obtained in the range 50 to 95 per cent critical speed.

The maximum calculated powers and their speeds of occurrence are also shown in Table 4.5. For a 30 per cent filling, no maximum power is obtained in the range 50 to 95 per cent critical speed, whereas a maximum torque occurs at 81 per cent critical speed. This demonstrates that power can be a misleading indicator of load dynamics, and that its use can disguise features that are seen when torque characteristics are examined. For fillings of 40 and 50 per cent maximum power occurs at 88 and 82 per cent critical speed respectively, which are higher than the speeds at which maximum torques occur, which is expected since $P \propto NT$.

As previously stated, it is generally accepted that maximum grinding efficiency, either expressed as throughput rate at a constant grind, or product fineness at a constant feed rate, occurs at maximum power draw. This is because maximum power is a compromise between the speed at which the load is in a position that results in maximum torque and the rate of circulation of the load. The rate of load circulation increases with speed, and increasing the circulation increases the number of impact events per unit time, which in turn increases the grinding rate. Thus, although the speed that corresponds to maximum power results in a reduction in torque from the maximum value, this is offset by an increased number of impact events causing a faster grinding rate.

Therefore, when designing a mill, care should be taken when specifying the operating speed, because once the mill is installed the speed cannot be varied without costly changes to the drive train.

4.4 The effects of mill filling and speed on load position

The position of the load in the mill is important because it determines the energy drawn from the motor (which is a balance between the energy required to maintain the load in an offset position and the energy recovered from the falling mass), and the type of breakage (i.e. impact, abrasion, attrition) that is dominant. As was done in the previous section, the results will be discussed in detail using data from the steel media - 46 per cent solids pulp tests. To summarize the results discussed in section 4.1, the toe position is not affected by a change in pulp solids content from 35,4 to 52,2 per cent, whereas increasing solids content causes a rise in the position of the load shoulder. The toe and shoulder positions, as measured by the conductivity probe, are shown in Figure 4.11.

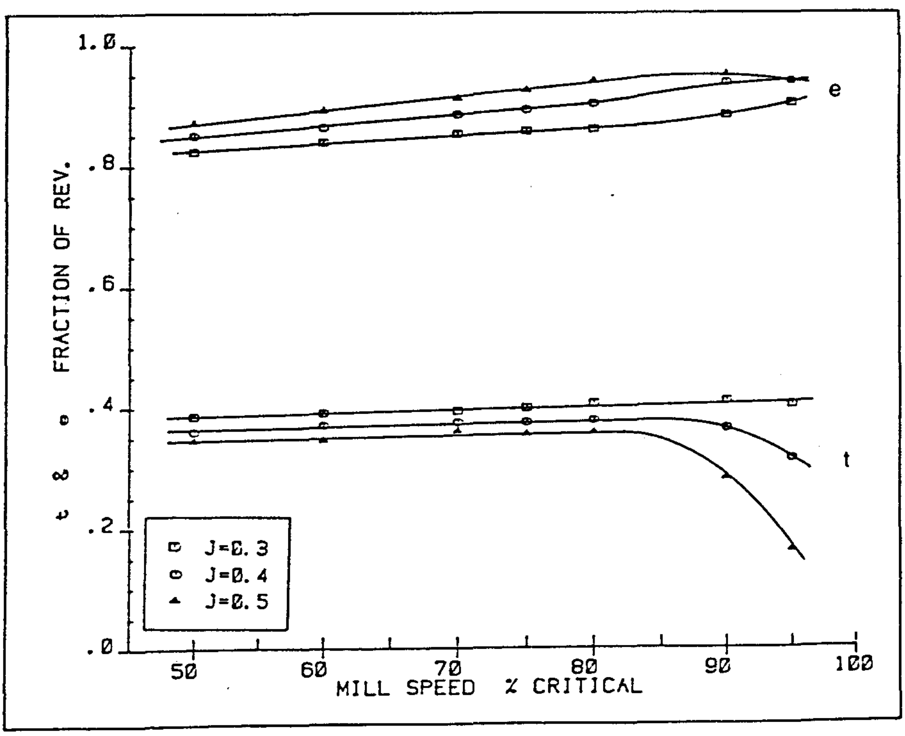

Figure 4.11 Toe and shoulder positions at various speeds and mill fillings

4.4.1 Toe position

The results show that the toe position is almost independent of mill speed between 50 and 80 per cent critical, and that t increases very slightly over this range. At speeds above 80 per cent critical, t decreases rapidly indicating that the load is impacting onto the mill shell. The filling and pulp solids content both determine the rate of decrease of t at higher speeds, with increases in both causing the reduction in t to occur at lower speeds, although the filling has a greater effect than the pulp solids content.

The variation of t with speed for each filling, at speeds up to 80 per cent critical can be fitted to straight line equations. The gradient of these equations is very low, typically 5×10^{-4} t per % critical. This gradient indicates that if t has the value of 0,400 at 50 per cent critical, increasing the speed to 80 per cent critical will cause a value of t = 0,406, which is within the experimental error. The position of the toe of the load is therefore not affected by variations of the mill speed or pulp solids content, within the range of speed and solids content encountered in industrial milling.

The position of the toe is influenced by the mill filling. An increase in the filling causes a decrease in t which indicates that the toe lies higher up in the mill, this is presumably due to a crowding effect of having a larger volume of material within the mill. The average value of t calculated for speeds of 50 to 80 per cent critical is shown for the various fillings and pulp solids contents in Table 4.6. The averages are also plotted in Figure 4.12, and a linear relationship is evident between t and J.

TABLE 4.6 Average values of t for 50 to 80 per cent critical speed

Mill filling	Pulp solids content, vol. %		
J	35,4	46,0	52,2
0,3	0,400 (0,009)	0,395 (0,007)	0,395 (0,005)
0,4	0,375 (0,007)	0,374 (0,006)	0,378 (0,003)
0,5	0,354 (0,008)	0,353 (0,006)	0,350 (0,004)

Values in parentheses are standard deviations

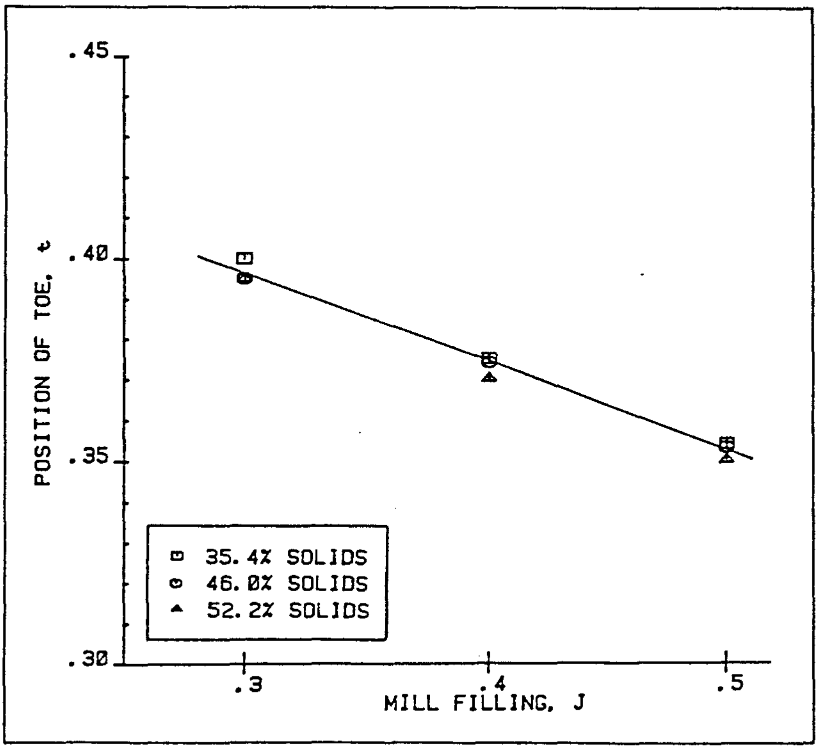

Figure 4.12 The effect of mill filling on the load toe position

Values are averages of t at speeds of 50 to 80 per cent critical

This result implies that a measurement of the toe position will provide an estimation of the volume of the load within a mill.

4.4.2 Shoulder position

The change in position of the shoulder with speed and filling can be seen in Figure 4.11. Increasing the speed and filling, as well as the pulp solids content, causes the load shoulder to rise, with changes in the filling having the greatest effect.

As with the toe position, the shoulder position can be given as a linear function of speed between 50 and 80 per cent critical, with each combination of filling and pulp solids content having an individual linear equation. At speeds of 90 and 95 per cent critical the values of e become scattered, due to a possible combination of slip causing surging of the load, and increased error in the measurement of e.

The coefficients of the linear equations relating e to per cent critical speed are given in Table 4.7. Increasing the filling increases the rate at which the shoulder rises with speed, whereas increasing the pulp solids content has little effect.

4.5 Examination of results at constant mill speed

Since mills are generally run at constant speed, a discussion of the effects of filling and pulp conditions at one speed will show how changes in either variable will affect an industrial mill. A speed of 75 per cent of critical speed has been chosen because this is a typical operating speed. A summary of the data is given in Table 4.8, and is shown graphically in Figure 4.13.

TABLE 4.7 Linear constants for the shoulder position, e, at speeds of 50 to 80 per cent critical

Mill filling J	Pulp solids content, vol. %					
	35,4		46,0		52,2	
	a	$bx10^4$	a	$bx10^4$	a	$bx10^4$
0,3	0,765	9,55	0,769	11,55	0,769	11,88
0,4	0,764	14,47	0,764	16,93	0,784	15,38
0,5	0,769	15,86	0,768	20,88	0,773	20,36

Equation has the form e = ax + b, where x = % critical speed

TABLE 4.8 Data for the steel-sand system at 75 per cent critical speed

Vol. % solids in pulp	J = 0,3			J = 0,4			J = 0,5		
	Torque kg.m	t	e	Torque kg.m	t	e	Torque kg.m	t	e
35,4	12,635	0,405	0,837	14,252	0,382	0,870	14,722	0,359	0,887
46,0	12,398	0,398	0,856	14,175	0,374	0,891	14,385	0,355	0,923
52,2	12,352	0,399	0,858	14,051	0,381	0,900	14,095	0,355	0,926

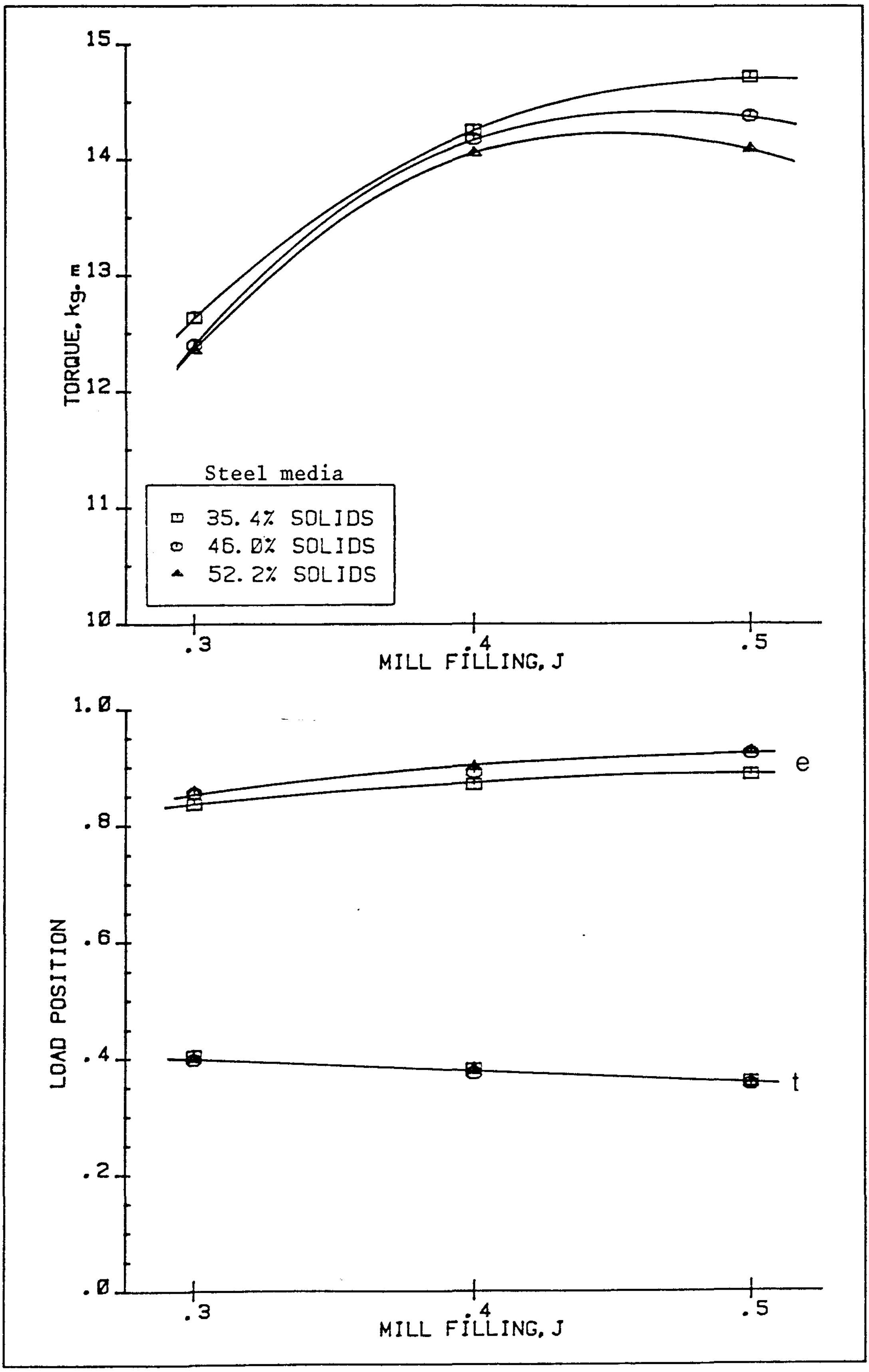

Figure 4.13 The influence of mill filling on torque and load position at 75 per cent critical speed

4.5.1 Torque

The variation of torque (and therefore power) with filling is shown in Figure 4.13, and the usual parabolic curves are seen. The filling at which the maximum torque occurs is reduced by increasing the pulp solids content. For pulps of 35,4, 46,0, and 52,2 per cent solids the fillings at which the maximum torques occur are J = 0,49, 0,46, and 0,45 respectively.

An increase in pulp solids content reduces the torque, as shown in Figure 4.14. This effect is also demonstrated by a reduction in the maximum torques calculated for the parabolas shown in Figure 4.13. The maximum torque values are 14,7, 14,5, and 14,3 kg.m for pulps of 35,4, 46,0 and 52,2 per cent solids respectively.

4.5.2 Toe Position

The toe position is not influenced by the pulp conditions, as shown by the superimposition of the points in Figure 4.13. The toe position is, however, affected by the filling, and the relationship between J and t is linear.

4.5.3 Shoulder Position

The shoulder position is influenced by both the filling and the pulp conditions, with the filling having the greater effect. By increasing the filling the balls are forced to rise further up the mill shell before leaving it due to a crowding effect. An increase in pulp solids content increases both the adhesion of the balls to the mill shell and the friction between the balls and liners, thus causing them to leave the shell at a higher position.

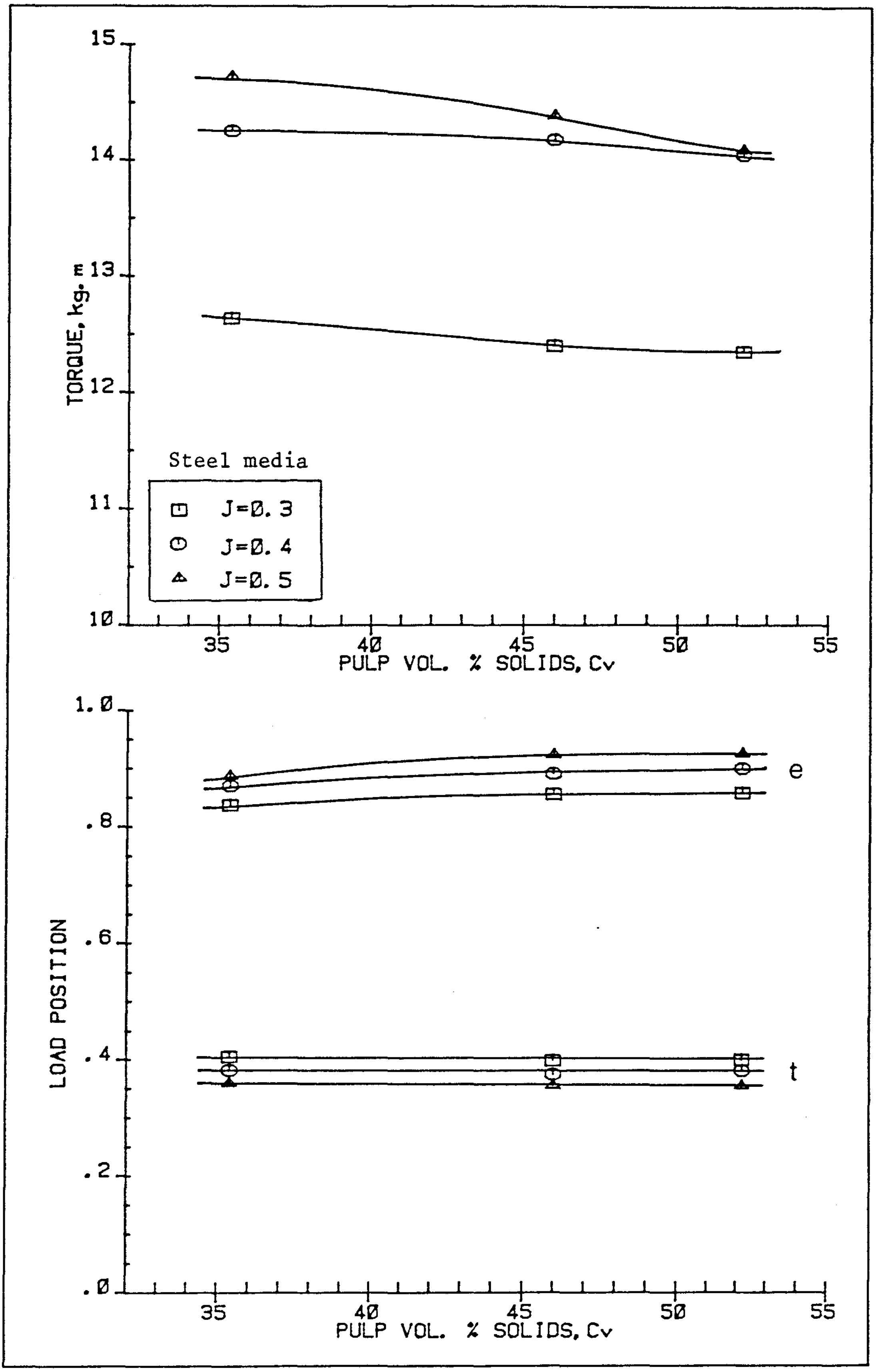

Figure 4.14 The influence of pulp solids content on torque and load position at 75 per cent critical speed

4.6 Interactive effects of filling and pulp conditions on power

The parabolic relationship between filling and mill power has been demonstrated previously, but the interactive effects of filling and pulp conditions on power were not clearly shown. This interaction is an important effect in autogenous milling where both parameters may change, either as a result of varying ore hardness or due to process control actions. The power calculated from the torque measurement is shown, for the various conditions of filling and pulp solids content, in Figure 4.15.

At load fillings of 30 and 40 per cent of the mill volume, the pulp solids content has no effect upon the power at mill speeds up to 70 per cent critical, and at a filling of 50 per cent an increase in pulp solids content causes a small reduction in power. It is at speeds higher than 70 per cent critical that the pulp conditions influence the mill power, and this influence becomes greater as the filling increases, as seen in Figure 4.15.

As the mill speed rises above 80 per cent of critical the power tends to decrease, the only conditions where this does not occur is at a load filling of 30 per cent and pulp solid contents of 35,4 and 46,0 per cent. The power does not decrease for these conditions because there is slip between the liner and load, and therefore the load is not lifted into a position whereby the falling balls can contribute some energy to the mill rotation. For the remaining conditions where the power does decrease with increasing mill speed, the reduction becomes more marked as the pulp solids content increases. A concomitant increase in the value of the shoulder point, e, is also noted.

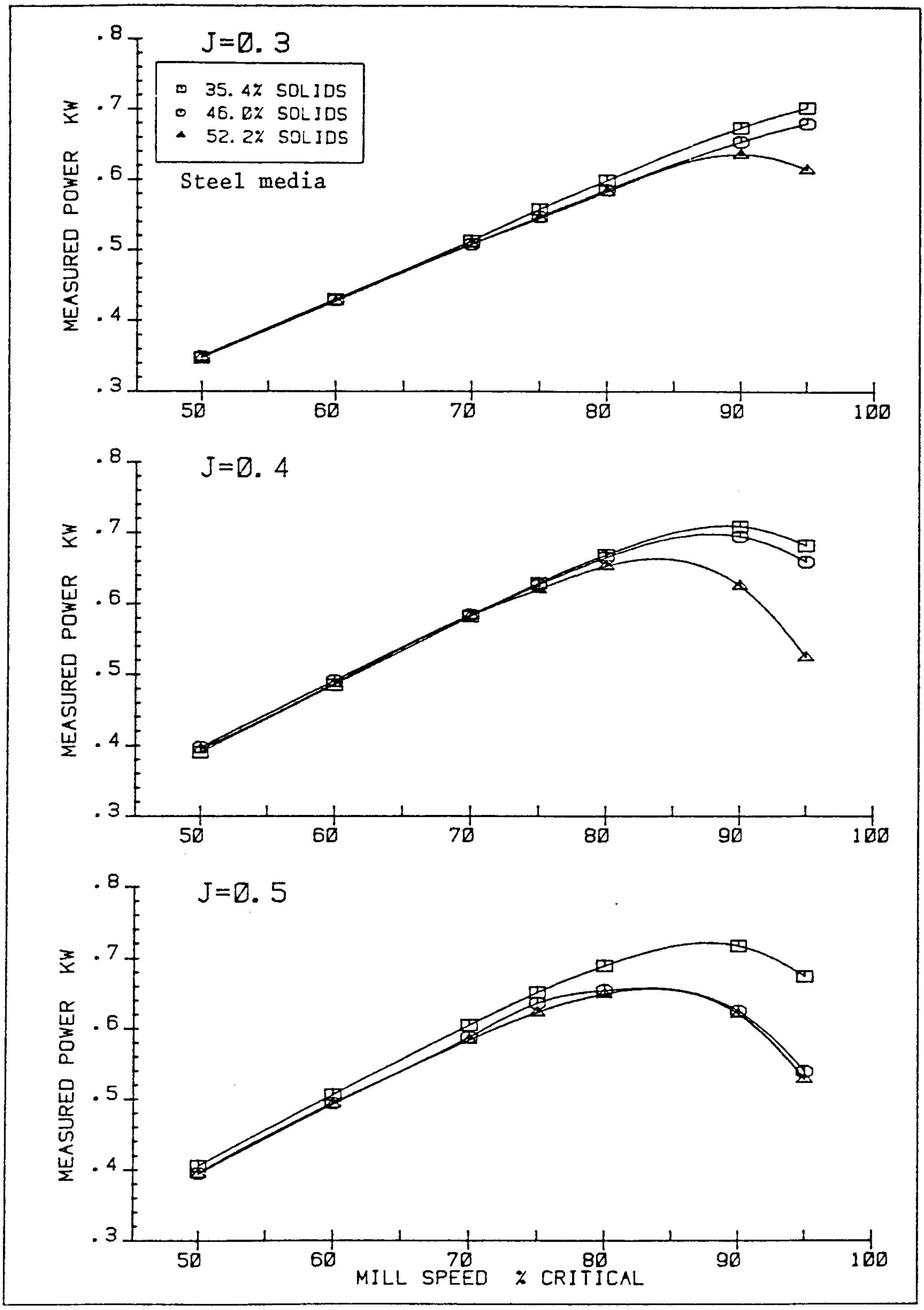

Figure 4.15 The influence of mill filling, pulp conditions and mill speed on power

4.7 General discussion

The torque required to rotate the mill at a given speed is dependent on the four variables examined. It is influenced strongly by the mill speed, mill filling, and the internal load friction, and weakly by the pulp viscosity. In comparison with steel media, the pulp viscosity has a greater influence on the torque when ceramic media is used. This is due to the difference in densities of the media types; the adhesion effect of the pulp is greater for the ceramic balls because they are of an equivalent size to the steel balls and therefore weigh less. Although the media in autogenous mills is of a similar density to the ceramic media used in this investigation, the autogenous media tends to be of a larger size in compensation, and the weights of autogenous media particles and steel balls are approximately equivalent. This means that in an autogenous mill the effects of viscosity will be similar to the results discussed here for the steel-sand system. The mill speed affects the torque by changing the load motion; at low speeds the falling balls do not contribute much energy to the mill rotation, and this is probably due to them rolling down the load surface and dissipating their energy by inter-ball contacts. At higher speeds (above 80 per cent critical speed) the torque is dramatically reduced by balls contributing some of their acquired potential energy in assisting the mill to rotate. At these speeds the balls are moving in free and hindered parabolic trajectories and do not lose so much energy in inter-ball contacts. They also have greater energy than at low speeds, as they have been lifted higher. The maximum torque for a given set of conditions occurs at a speed lower than the speed at which the balls are seen to strike the mill shell, the torque has generally reduced substantially at the speed where the balls start striking the decending liners, as measured by a reduction in t. This indicates that,at the speed at which the maximum torque occurs,the majority of the falling balls are landing in a manner such that they are not contributing energy to the rotation of the mill. At higher speeds increased cateracting occurs, which reduces the effective mass of the charge being lifted at any point in time, and increases recovery of energy by the mill from the cateracting balls.

The mill filling has a similar effect on the torque which, as the filling increases, rises to a maximum between approximately J = 0,46 to 0,50, and then decreases. The initial decrease in torque is due to a crowding effect at higher fillings causing the balls to impact further towards the mill shell and thus contributing some energy to the mill rotation. As well as affecting the torque by altering the charge motion, increasing the filling has a direct effect by increasing the mass of balls in the mill; but once the filling exceeds 50 per cent of the mill volume, the energy recovery becomes a larger influence than the charge mass. As the filling approaches 100 per cent the load would act as a flywheel, reducing the torque to zero. Thus the parabolic dependency of torque upon filling is a result of a combination of the load mass, energy recovery and freedom of motion of the load.

The internal friction of the load also has a major effect on the torque; it affects the magnitude of the maximum torque and the speed at which the maximum torque occurs. If the internal friction is very low, the maximum torque may only occur at speeds greater than critical speed. It would be expected that wet industrial mills, both ball and pebble type, operate at a sufficiently high pulp solids content and feed size that provides adequate friction within the load.

The pulp viscosity has an effect on the torque. An increase in viscosity causes the torque to be reduced slightly for a given set of conditions because the load motion is altered. The value of e increases with viscosity, indicating that the pulp gives an adhering effect between the balls,and between the balls and mill liner,which causes them to be carried higher, and thus projected further across the mill. As the load is lifted higher by this action, it would be expected that an increase in torque would be obtained. Instead, a net decrease occurs due to the load motion being affected in a manner which causes a larger amount of energy to be recovered, because the falling balls move further towards the liner and exert a greater turning moment on the mill. The adhesion effect can also be seen at speeds that are high enough to cause the balls to strike the mill shell. At these speeds the toe position is dependent on the pulp solids content (i.e. viscosity and friction).

The position of the toe of the load is strongly influenced by the mill filling only, at speeds and pulp viscosities that do not cause the balls to continually impact onto the mill shell. This has great significance for the control of autogenous mills in which the load volume varies continuously with time, and it is desirable to control the feedrate to keep the filling constant at the level which constitutes maximum power draw. The technology to measure the load position has been developed, as discussed by Moys and Vermeulen, and is presently being improved and installed in a 2,4 MW run-of-mine mill at Deelkraal Gold Mine, and in other run-of-mine mills at Randfontein Estates Gold Mine, and Vaal Reefs Gold Mine (43).

The position of the shoulder of the load is influenced by all four variables tested, although in an industrial mill the speed is invariant. An increase in pulp solids content has the combined effect of increasing the adhesion effect and the internal friction of the load, both effects causing a rise in the position of the shoulder; an increase in the filling also causes a rise in the shoulder position.

5 ANALYSIS OF THE LOAD MOTION

The results discussed in chapter 4 have shown that the load position and motion is influenced by the mill speed, filling, pulp viscosity, and the internal friction of the load (as indicated by the static angle of repose). The position and motion of the load in turn influences the torque that needs to be applied, and hence the power to be supplied by the motor. The available literature does not seem to contain a complete description of the load motion, and all theory proposed is more applicable to dry milling conditions. From the results obtained by these investigations a qualitative assessment of the load motion can be obtained, which can provide a basis for the design of further experiments to answer some of the questions raised here.

An attempt was made to use positional data of the balls in the load from the cinematographic films of the ceramic media-glycerine pulp tests, but due to surging of the load occurring, a large number of revolutions would have to be examined in order to obtain statistically significant data. Even then, the relevance of this data to actual conditions would be questionable. This chapter may therefore be regarded as a qualitative examination of the motion of the load and the influence of the operating variables examined.

5.1 Description of the motion seen on film

Examination of the cinematograph films taken of the ceramic-glycerine system show that the load motion is complex and cannot be adequately described by any of the treatments discussed in chapter 2. The films were examined at a low film speed where the relative motions of the balls could be observed, and also by taking the film frame-by-frame and markingthe position of individual balls, in this way the paths of selected balls were found.

The rising balls that are locked into the rotation of the mill, and therefore lie below the equilibrium surface proposed by Barth and Hinsley, follow circular paths about the mill axis at various radii from the mill centre. In this region there is no movement of the balls relative to each other or to the mill and their angular velocity is that of the mill. As they rise towards the shoulder region, the balls start to show relative movement to each other, and while still having an upward motion, their paths are no longer circular about the mill centre and tend to have a curved shape which moves closer to the mill centre as the balls are lifted further up. This is shown in Figure 5.1.

The region of rising balls with inter-ball movement ends when the balls commence parabolic trajectories or start to roll down the surface of the rising mass. The balls that lie near the centre of gravity of the load do not follow parabolic trajectories due to interference from balls above; they roll down on top of underlying balls and generally do not pass into the toe of the load, but re-enter the rising mass at a similar radius to that followed previously. Only the outermost balls that are close to the mill shell follow discrete parabolic trajectories, and only if the mill

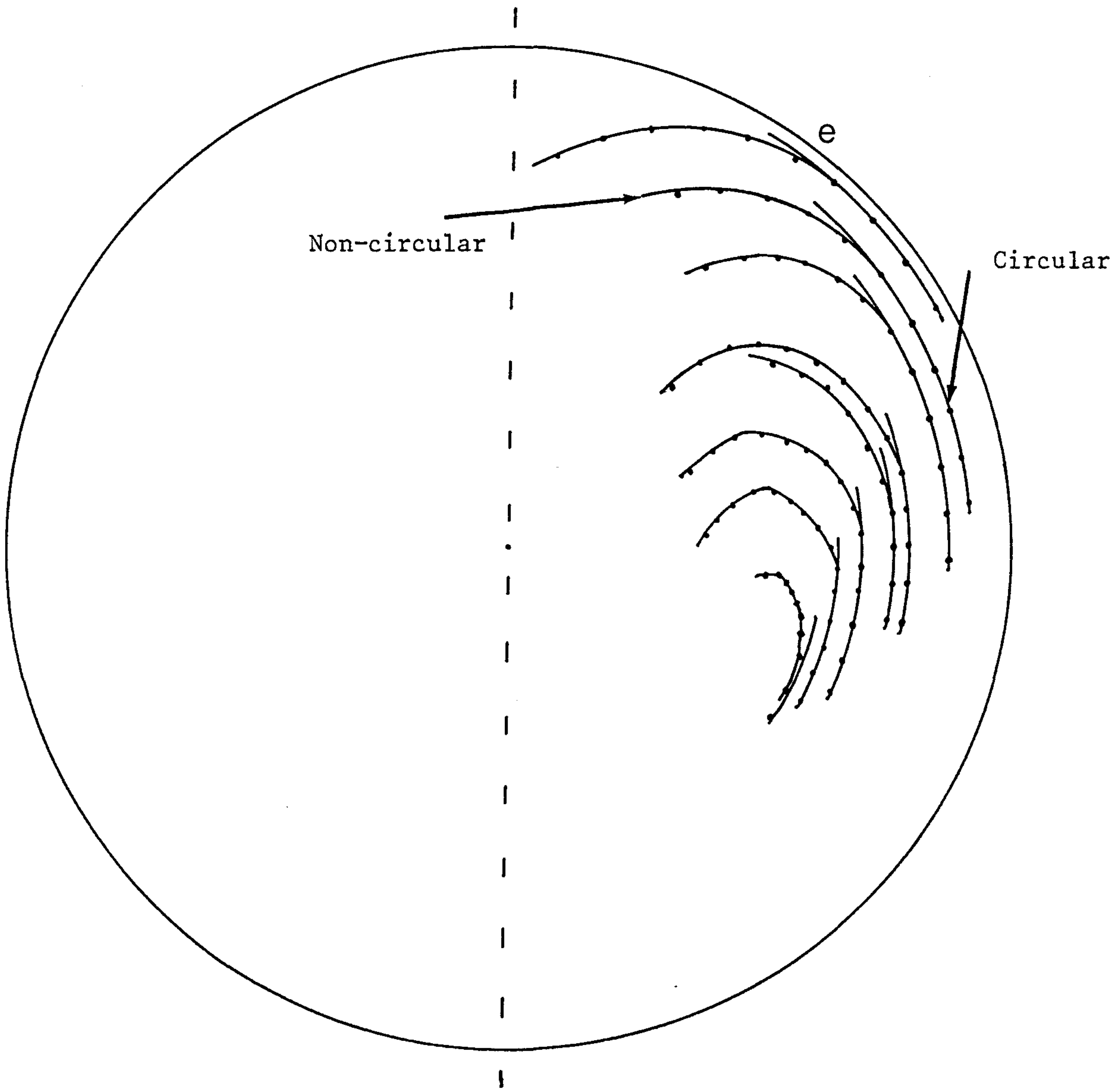

Figure 5.1 Ball paths measured from cinematographic film
Conditions: Ceramic media, J = 0,4 ϕ = 0,80 η = 275 cP

speed is high enough. If the mill speed is low they roll down the load surface. Between the regions of balls having forced rolling motion and those of free parabolic trajectories is one where hindered parabolic trajectories occur, here the paths of individual balls across each other, and there is occasional contact between the balls.

The trajectories of the falling balls terminate at the toe of the load, which is an area where random and turbulent motion of the balls exists, they spend some time in this area before they are taken back into the rising mass. In this area it is impossible to follow a ball frame-by-frame as the balls move axially as well as laterally. The unvarying position of the toe, as seen by the conductivity probe for the steel-sand system is also seen on the films, at lower speeds the balls impact onto the toe and as the speed increases the points of impact gradually move across the toe to the mill shell.

A centre of motion exists for the rising balls with circular paths and the falling balls that have a rolling motion, and it lies upon the boundary between these two areas; at times a ball was observed to remain almost motionless at this point.

The various regions of the load are shown in Figure 5.2.

To summarize, there are four distinct regions within the load where different motion is occurring:

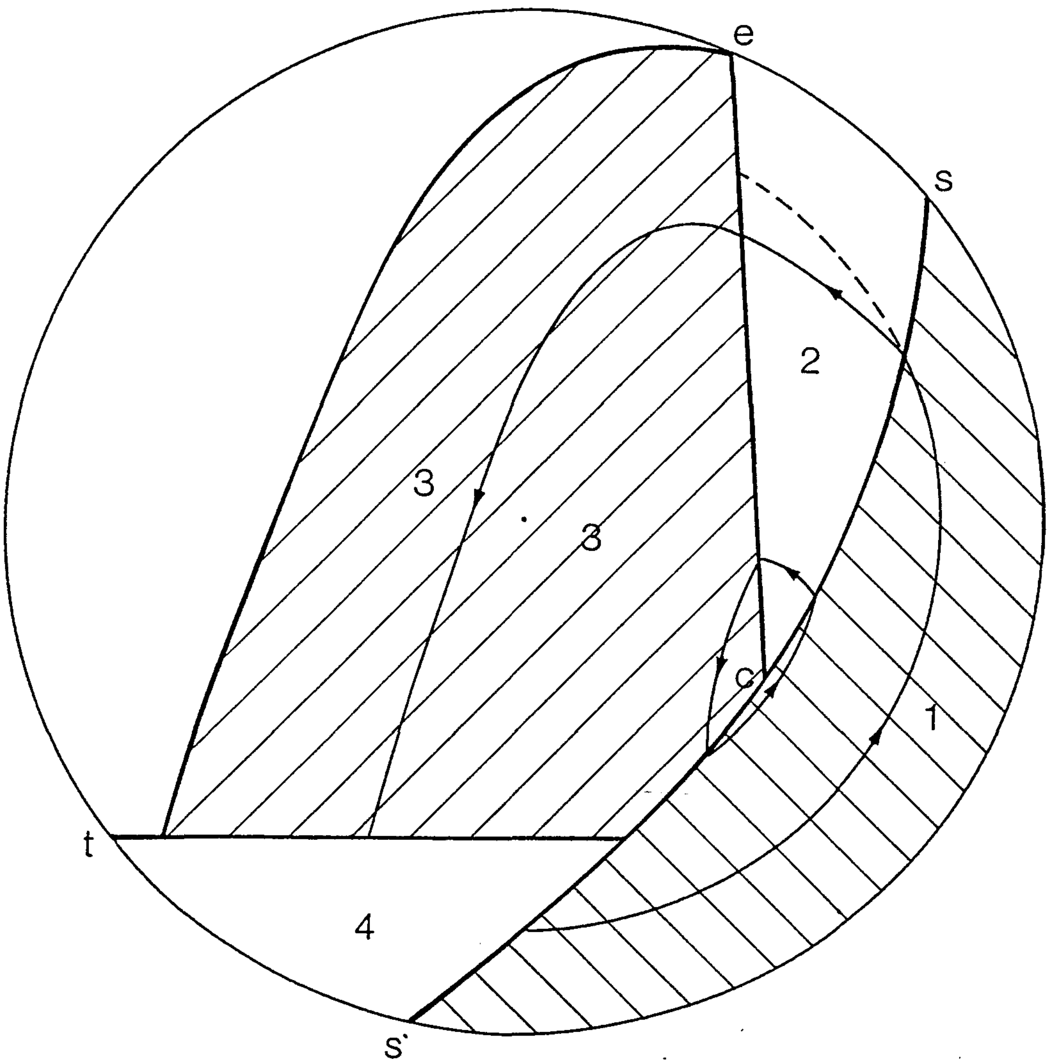

Region 1 - Balls rising in circular paths

Region 2 - Balls rising, but not in circular paths, and having relative motion to each other and the mill

Region 3 - Balls falling in either parabolic or rolling paths

Region 4 - Random and turbulent motion at the toe

Figure 5.2 The various regions within the load

Region 1: the balls are rising in circular paths and have the same angular velocity as the mill. This region is bounded by the equilibrium surface and the mill shell.

Region 2: the balls have passed through the equilibrium surface but no longer have circular paths, their motion is still in an upward direction.

Region 3: the balls are falling under the influence of gravity, whether they fall in a free or hindered parabolic trajectory or roll down the upper surface of the load, depends on their velocity and the radius of the point of ejection.

Region 4: this is the toe area where random and turbulent motion of the balls is seen.

5.2. Formulation of a Preliminary Mathematical Description of the Regions within the Load

5.2.1. Region 1

The positions of the toe and shoulder of the load have been given by the conductivity probe, but these positions do not define the positions of the four regions. It is apparent from the cinematographic films that region 1 does exist within the load, and that its upper boundary has a curved shape. It is therefore not unreasonable that the boundary of this region can be given by some form of the equiangular spiral proposed by Barth (11) and Hinsley (13). The equation of the spiral incorporates the static angle of repose of the load, and its pole is given by the angular velocity of the load (i.e. the mill speed if there is no slip between the load and liners).

The spiral is derived from a force balance on a particle which has the radial, gravitational and frictional forces that are acting on it under equilibrium (see chapter 2). This treatment does not account for the pressure that also acts on the particle, which is a result of the balls in the load that lie above the equilibrium surface. It would be expected that the pressure will not be equal along the equilibrium surface.

The equation of the spiral is:

$$\ell = k_s e^{\lambda(\pi-\psi)} \tag{5.1}$$

where ℓ and ψ are polar co-ordinates that can be expressed in cartesian form by:

$$\ell = (x^2 + (2r_d-y)^2) \tag{5.2a}$$

$$\psi = 1{,}5\pi + \cot\left\{\frac{x}{2r_d-y}\right\} \tag{5.2b}$$

In this case the mill rotates anticlockwise and the mill centre is the origin of the co-ordinate system.

If it is considered that all material below the equilibrium surface is consolidated by the radial force and locked into the motion of the mill, then the equilibrium surface does not pass through the toe that is measured by the conductivity probe. The conductivity probe measures the intersection of the mass of randomly moving balls and the mill shell, and cannot give an indication of the consolidation point, through which the equilibrium surface passes.

The equilibrium spiral can be completely defined by fixing one point and λ, but a number of questions arise:

(a) Does the coefficient of friction, μ, measured in chapter 3 equal the value of λ, and if it does not, how is a value of λ estimated?

(b) Given that the point of consolidation of the load is not defined, is there any other easily defined point that the spiral can pass through?

If the spiral passes through the measured shoulder point e, and $\mu=\lambda$ the spiral does not give a realistic interpretation of the equilibrium surface seen in the load, as shown in Figure 5.3. If the value of λ is increased above that of μ, then the spiral becomes more realistic. Even so, from observation of the cinematographic films it is probable that the spiral does not pass through the shoulder point for a number of reasons.

(a) Balls in the vicinity of the load shoulder continue moving upwards, but no longer move in circular paths about the mill centre. This implies that the balls are no longer predominantly under the influence of the radial force and have therefore passed through the equilibrium surface. This is shown in Figure 5.1, where ball positions have been taken frame-by-frame from the cinematographic film.

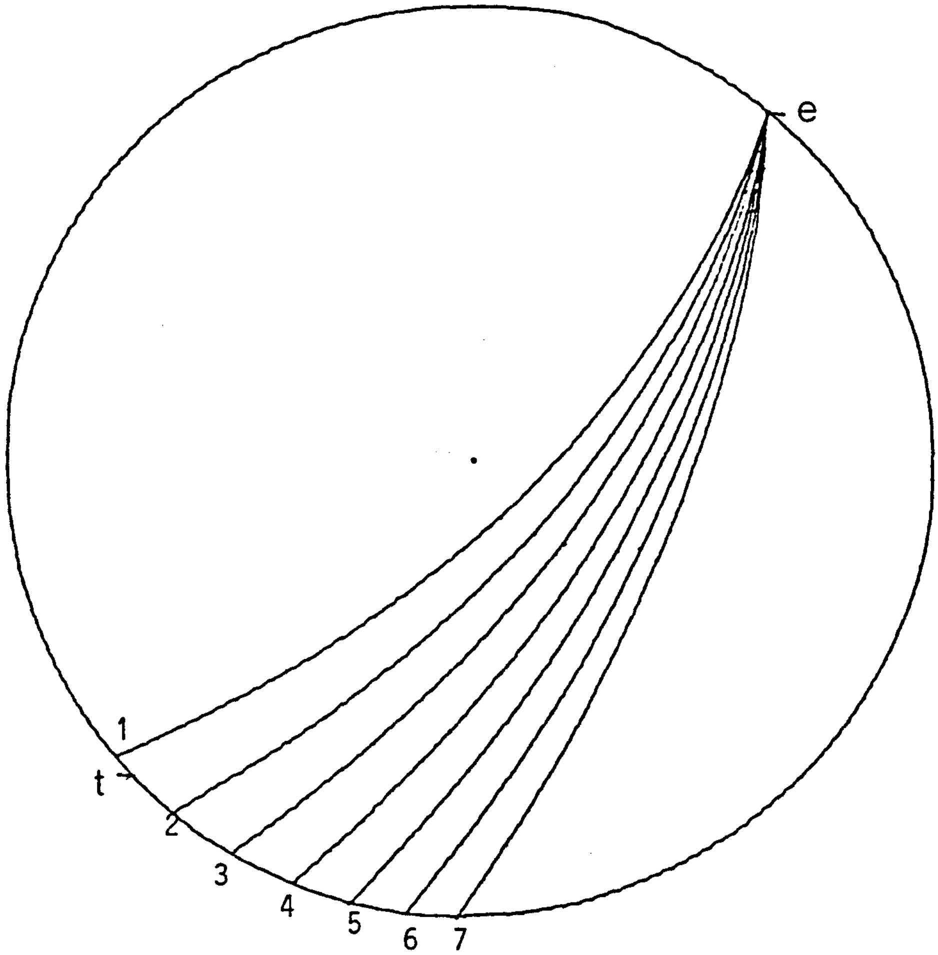

No.	λ	α°	j
1	0,89	41,8	0,466
2	1,0	45,0	0,417
3	1,1	47,7	0,373
4	1,2	50,2	0,334
5	1,3	52,4	0,299
6	1,4	54,5	0,268
7	1,5	56,3	0,242

Conditions: $J = 0,4$ $\phi = 0,75$ $C_v = 46,0$

$t = 0,374$ $e = 0,891$

$\alpha = \tan^{-1} \lambda$

Figure 5.3 The equilibrium surface, assuming that it passes through the measured shoulder point, for various values of λ

(b) When the cinematographic films are observed, balls in the vicinity of the load shoulder can be seen to be moving relative to each other, whilst still having an upward motion. This is further evidence that the balls in this region have passed through the equilibrium surface.

The treatment of Davis, as discussed in chapter 2, suggested that any particle that lies below the Davis circle cannot enter into free flight. The comparisons of the measured shoulder points and the Davis points made in chapter 4 showed that the load leaves the shell some way past the Davis point, as long as there is little or no slip. It can therefore be reasonable to assume (as a first approximation) that the equilibrium surface passes through the point of intersection between the Davis circle and the mill (i.e. s=d). This point of intersection is dependent on the mill speed and is given by:

$$d = \frac{1}{2\pi} \left(1{,}5\pi + \sin^{-1}\phi^2\right) \qquad (5.3)$$

where d is expressed as a fraction of one revolution, with the 12 o'clock position being zero. The position of the spiral under this condition is shown in Figure 5.4, and it can be seen that when $\mu=\lambda$ the position of the equilibrium surface is not unreasonable. Spirals are also shown for values of λ greater than μ and it can be seen that less material is contained below the equilibrium surface as λ is increased.

The centre of motion of the rising balls having circular paths

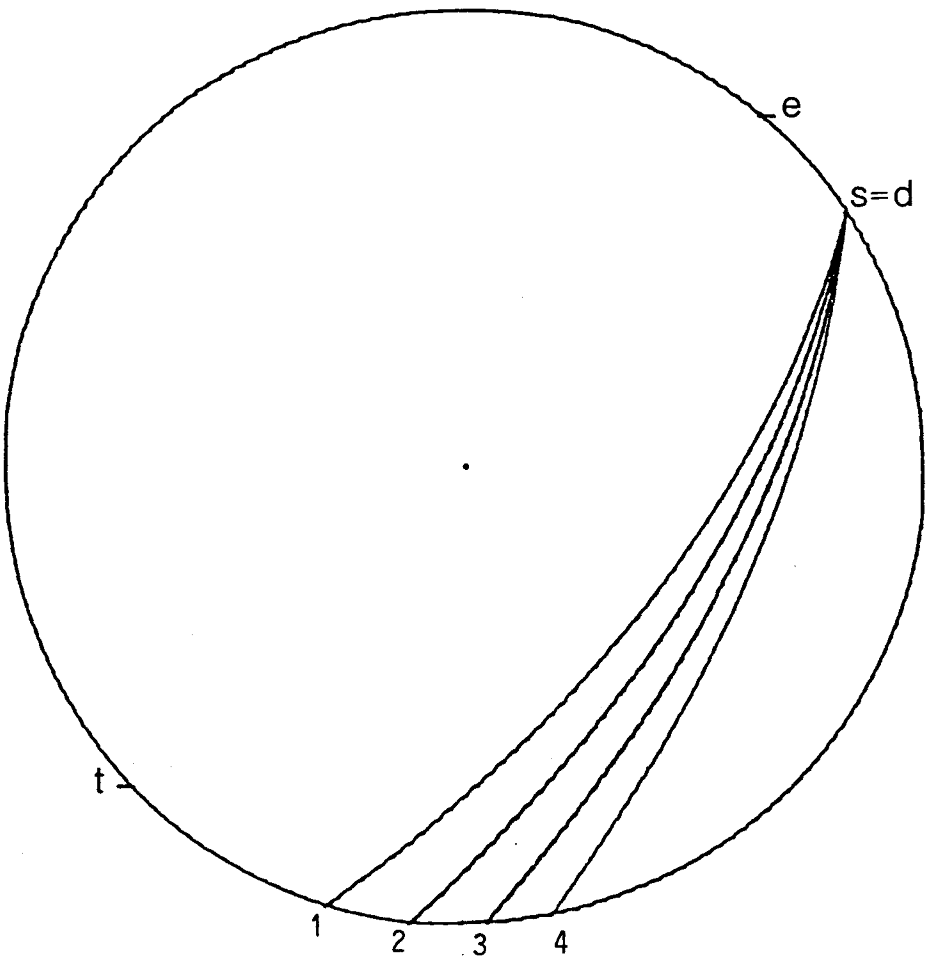

No.	λ	α°	j
1	0,89	41,8	0,231
2	1,0	45,0	0,185
3	1,1	47,7	0,155
4	1,2	50,2	0,129

Conditions: J = 0,4 ϕ = 0,75 C_v = 46,0
t = 0,374 s = d = 0,845
e = 0,891

Figure 5.4 The equilibrium surface, assuming that it passes through the Davis point, for various values of λ about the mill centre, c, lies on the equilibrium surface, and is found as the point where the spiral that describes the surface is tangential to the circumference of a circle concentric with the mill axis, as shown in Figure 5.5.

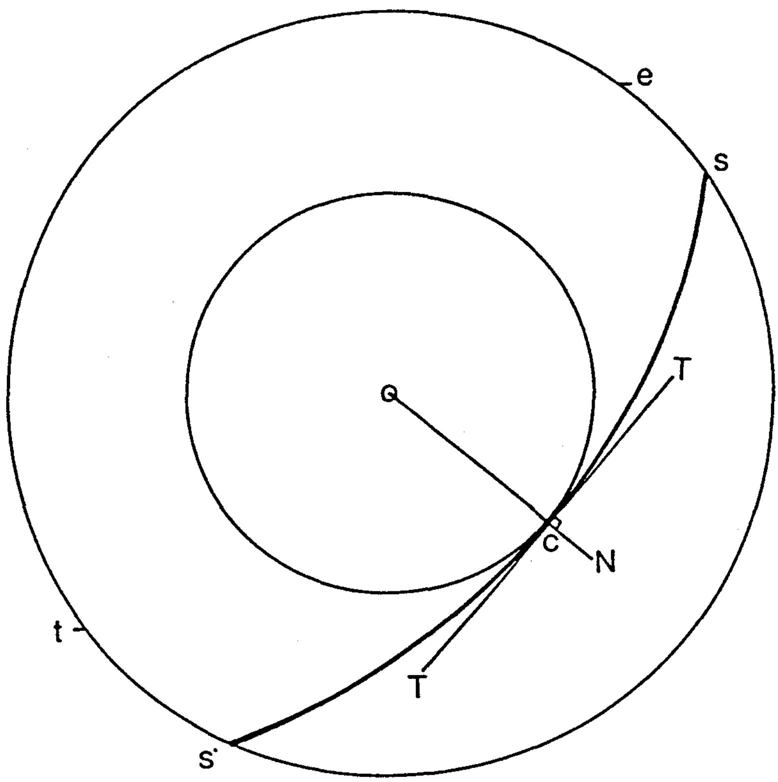

Figure 5.5 The position of the centre of motion of the load

5.2.2. Region 2

In this region balls move from the equilibrium surface to a surface from which the balls commence parabolic paths or downward rolling under the influence of gravity. In this region the load still has an upward motion, but the balls are not necessarily moving in circular paths. There is also relative movement between the balls, and there is an indication that the velocity of the balls decreases in this region.

This region has a triangular shaped cross-section, with the vertices being given by the intersection of the equilibrium surface and the mill, s, the shoulder point, e, and the point on the equilibrium surface which is the centre of motion, c.

Although the balls in region 2 have passed through the equilibrium surface, a number of effects can prevent them from falling under the influence of gravity:

(a) Inter-ball interference will cause a crowding effect that will prevent balls from falling. A ball will not fall if it is being supported by other balls below or to the side of it.

(b) Adhesion effects due to the pulp viscosity cause the load to form a loosely cohesive mass, and also promote some sticking to the mill liners.

At lower rotational speeds the crowding effect is predominant, as the load shoulder lies lower and the load is in a cascading condition. The crowding effect appears to reduce as the mill speed increases, and this is indicated in Figures 4.6 and 4.7, where the difference between the shoulder point and the Davis point becomes less as the speed increases.

The shape of the projection surface, from which the balls in the load commence their motion under the influence of gravity is difficult to define. It passes through the shoulder point and the point locating the centre of motion lying on the equilibrium spiral. It is likely that this surface has a curved shape, but will be taken here as a straight line between the aforementioned points.

5.2.3 Region 3

In this region the balls are being acted upon by gravity and have a net motion downwards. The type of motion depends on the position of a ball as it passes through the projection surface, the mill speed and, to some extent, the filling.

Balls that pass through the projection surface close to the centre of motion of the rising balls have a forced rolling action, due to the presence of other balls above bearing down on them. These balls can be characterized by the fact that they do not enter the turbulent region of the toe, but re-enter the consolidated mass of rising balls.

At the upper end of the projection surface, close to the liner, the balls have either a rolling or parabolic path, depending on the mill speed. At low speeds the balls roll down on the surface of the load, as the speed increases the paths become parabolic. As the speed increases further the packing of the balls in this region becomes more dilated, and the proportion of balls having parabolic, free-flight trajectories increases.

Balls that pass through the projection surface in the vinicity of its mid-point will probably have hindered parabolic paths at higher speeds, or rolling paths at lower speeds. A hindered parabolic path will occur when a ball is in contact with other balls for some or all of the time.

Previous considerations (10, 11, 12, 14) of the parabolic trajectory followed by a ball in free flight have assumed that the velocity at the commencement of the trajectory is tangential to the mill shell. It is of interest to examine this assumption for dry conditions using a frame-by-frame analysis of the cinematographic film. By plotting the position in each frame of a ball that is in free flight, and expressing the co-ordinates with the mill axis as the origin, the free flight path can be examined. The equation of a parabolic path under gravitational force only is given by:

$$y = y_o + (x_o - x)\cot\beta - \frac{g(x_o - x)^2}{2v_r \sin^2\beta} \qquad (5.4)$$

where x_o and y_o are the co-ordinates of the point where the parabolic path commenced, v_r is the velocity which is tangential to the parabola at the point of commencement, and β is the angle made by v_r with horizontal. If v_r is tangential to the mill shell then $\beta = \cot\ (y_o/x_c)$.

The parabolic path is composed of vertical and horizontal velocity components, the vertical component changes with time due to gravitational acceleration, and the horizontal component remains constant if there is no external influence. The equations of motion describing these components as a function of time (T) are given by:

$$\text{vertical,}\quad y(T) = y_o + v_y T - \frac{g}{2}T^2 \qquad (5.5)$$

$$\text{horizontal,}\quad x(T) = x_o + v_x T \qquad (5.6)$$

The observed path of a ball for dry conditions at J = 0,3, ϕ = 0,7 is shown in Figure 5.6, and the positions shown were fitted to equations 5.5 and 5.6 by a least squares regression fitting routine. The following empirical expressions were calculated.

$$x(\varepsilon) = 0{,}199 - 0{,}020\ \varepsilon \qquad (5.7)$$

$$y(\varepsilon) = 0{,}163 + 0{,}018\varepsilon - 0{,}00322\varepsilon^2 \qquad (5.8)$$

The symbol ε is the film speed in frames per second. The value of β as calculated from cot(0,163/0,199) is 39,3°, and the measured value (from Figure 5.6) is 40,5°. This indicates that, for dry conditions, the initial velocity is tangential to the mill shell.

The film speed can also be verified from the last term of equation 5.8 which is equal to $\frac{1}{2}gT^2$, therefore,

$$0{,}00322\varepsilon^2 = \tfrac{1}{2}g \qquad (5.9)$$

from which ε is 39 frames per second.

It is not possible to verify whether the velocity is tangential to the mill shell when a viscous fluid is in the mill, as the glycerine caused balls to stick to the transparent end-plate.

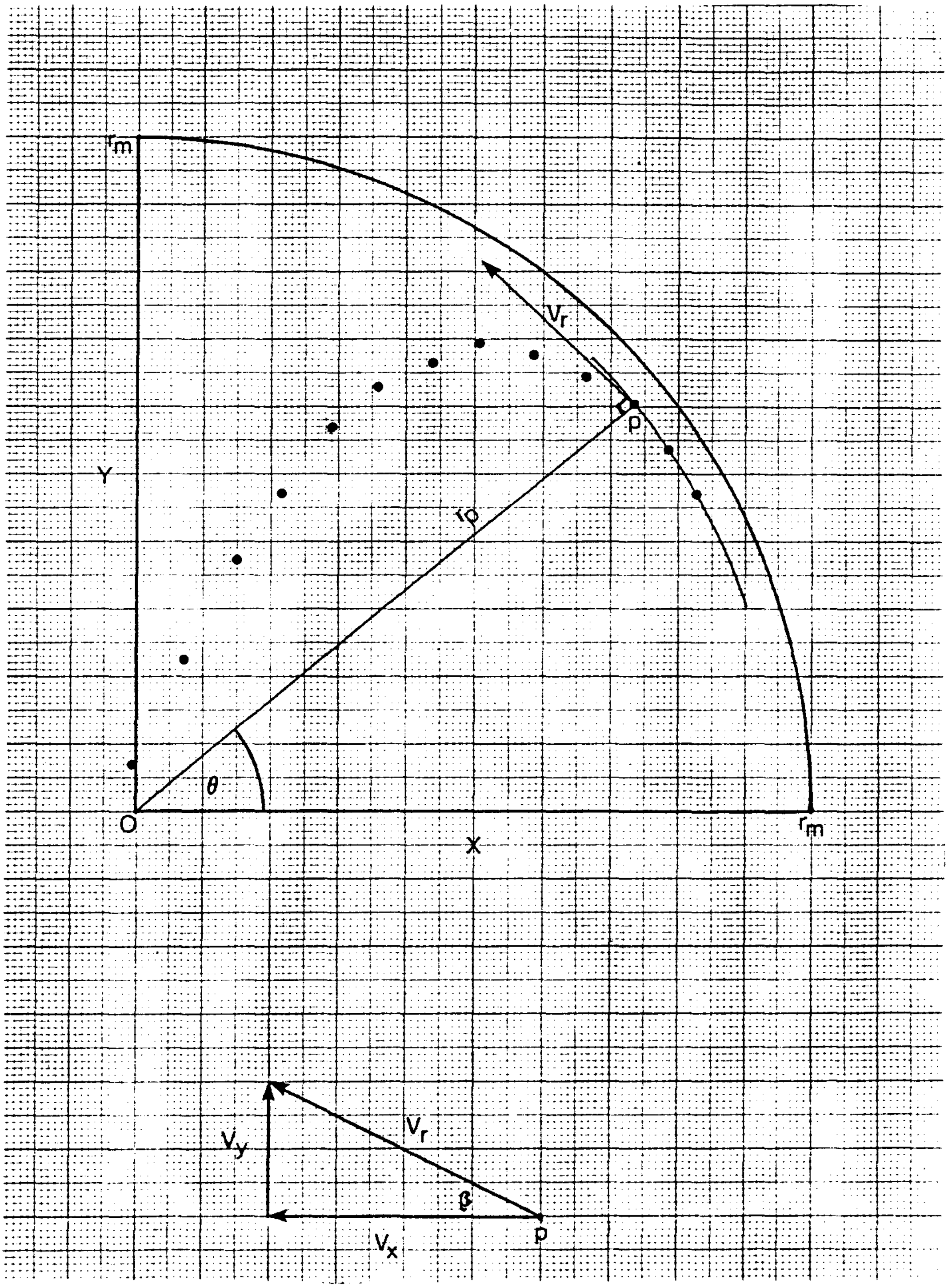

Figure 5.6 The measured parabolic path of a ball for dry conditions

5.2.4 Region 4

This is the toe region and the balls here have a random and turbulent motion. It is bounded on one side by the equilibrium surface, and on the other by the liner. Its upper surface is not easy to define and probably diffuses into the falling balls of region 3. Barth(11) shows this upper surface being curved, but this is based on the balls terminating their parabolic paths at the same radius that they commenced, which is improbable for a large number of balls.

As the balls in this region have a random motion it should not include the balls that are close to the centre of motion and this region does not therefore extend to the centre of motion. The upper boundary of the toe region will thus be given as a horizontal line that extends from the measured toe point to the equilibrium surface.

5.3 Prediction of the load regions using data from the conductivity probe

Using the criteria discussed in the previous section a computer programme was developed which generates the various regions of the load. The toe and shoulder positions measured by the conductivity probe for the steel media-sand pulp system are used in the programme. A listing of the programme is given in Appendix E. The programme also calculates the volume of the load lying below the equilibrium surface, j, expressed as a fraction of the mill volume.

Examples of the load configuration and the positions of the various regions are shown in Figures 5.7 to 5.9 at various speeds between 50 and 95 per cent of critical, for the conditions J = 0,4 Cv = 46,0, J = 0,5 Cv = 46,0 and J = 0,4 Cv = 52,2. At fillings of 30 per cent of the mill volume, slip is occurring and the angular speed of the mill does not represent that of the load. If the slip is known or estimated then the corrected speed can be used in the calculations.

A number of points are apparent from Figures 5.7 to 5.9 that require further discussion.

(a) At the lower mill speeds (50 and 60 per cent of critical) the parabolic trajectory of the outer ball does not define the upper surface of the load. At these speeds the outer layers of balls are rolling down on top of other balls, and are not in free flight.

(b) As the mill speed is increased, the amount of materil lying below the equilibrium surface increases (as indicated by j). This is to be expected as an increase in speed results in an increase in the centrifugal force, whereas the gravitational force remains constant. This increase in the volume of consolidated material is accompanied by a decrease in the amount present in the toe area, until the toe area almost disappears at the higher (90 per cent critical) speeds, where the outer balls are almost centrifuging. At the higher mill speeds the equilibrium spiral no longer gives a realistic

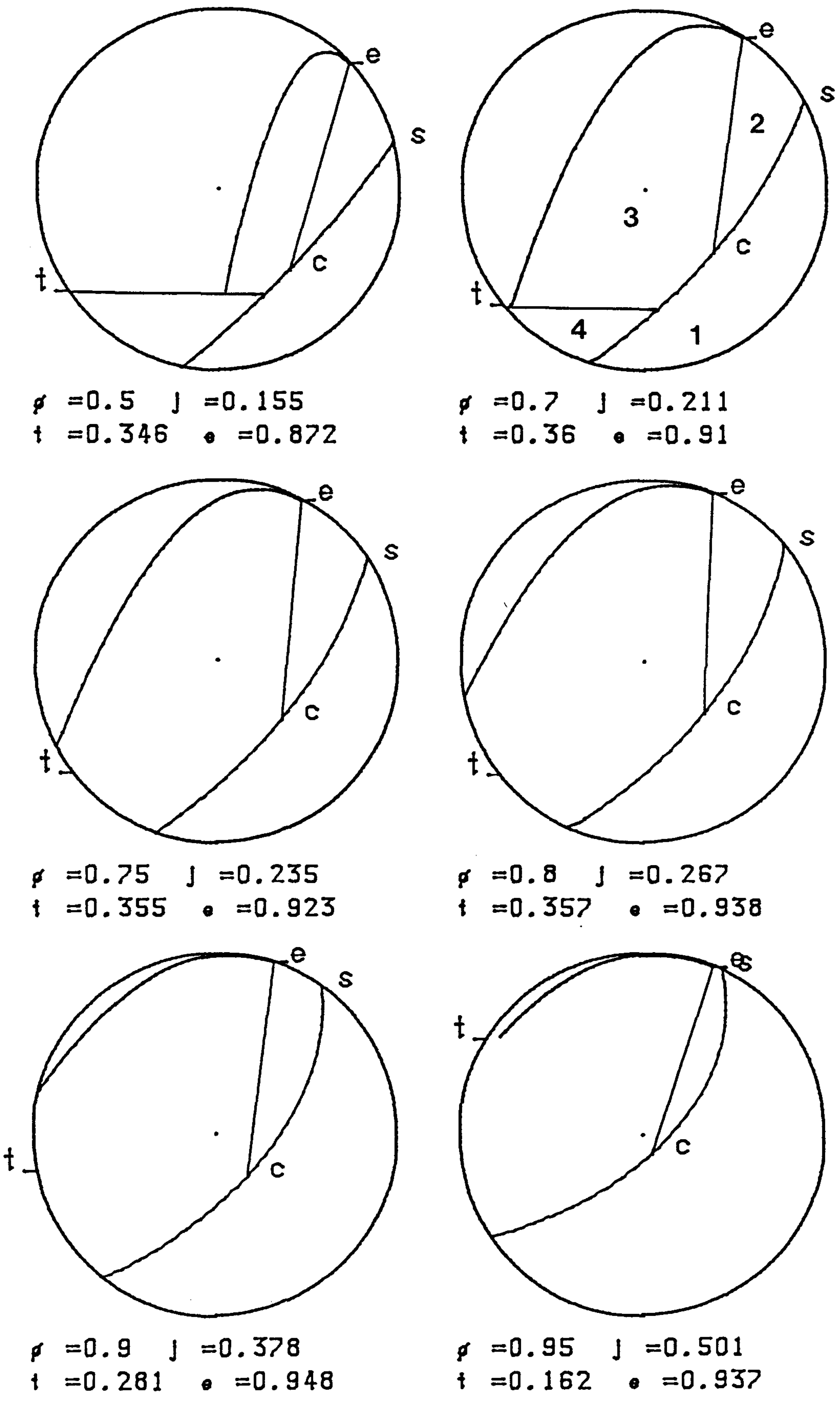

Figure 5.7 Predicted load regions for the conditions J = 0,4, C_v = 46,0

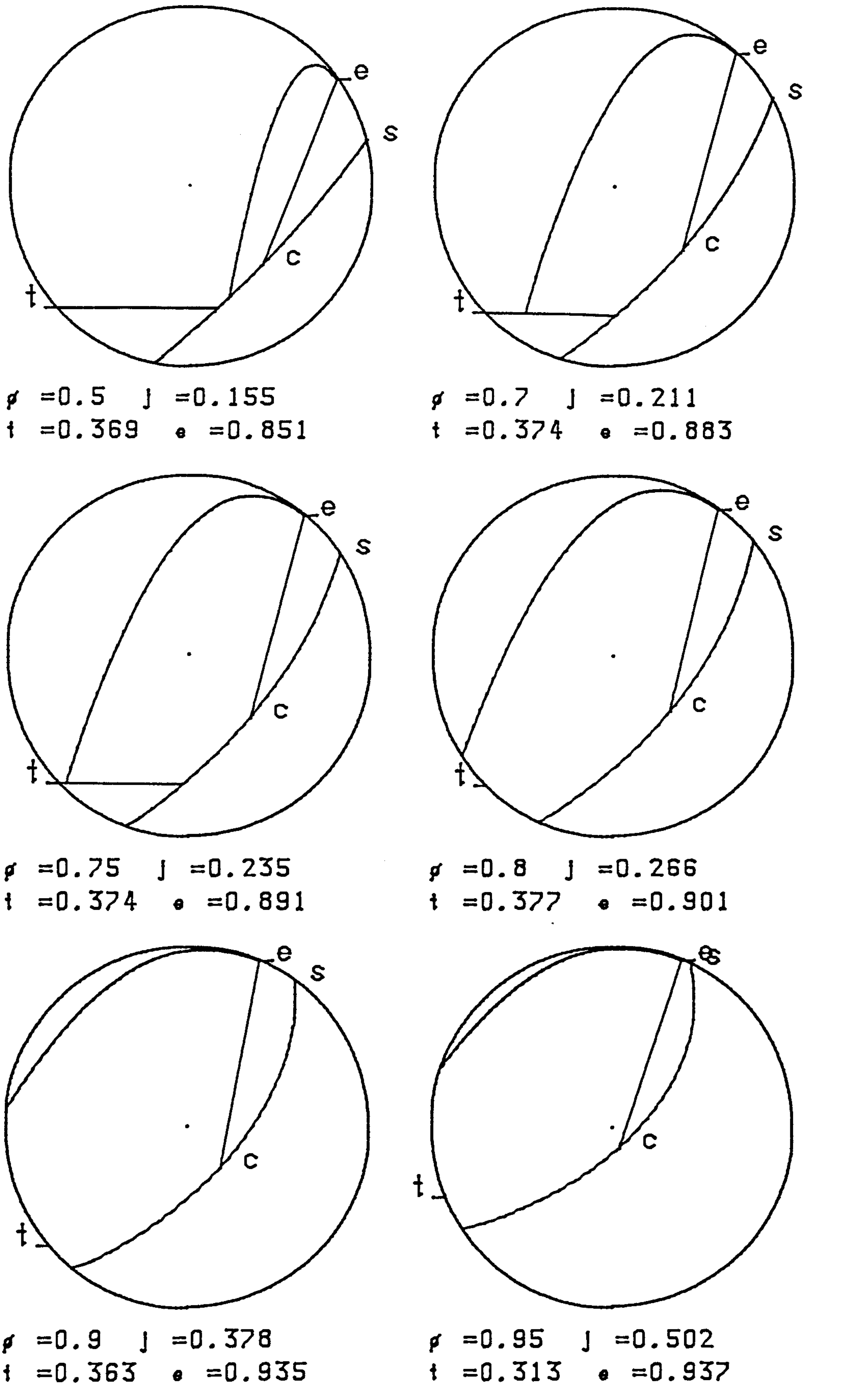

Figure 5.8 Predicted load regions for the conditions J = 0,5; C_v = 46,0

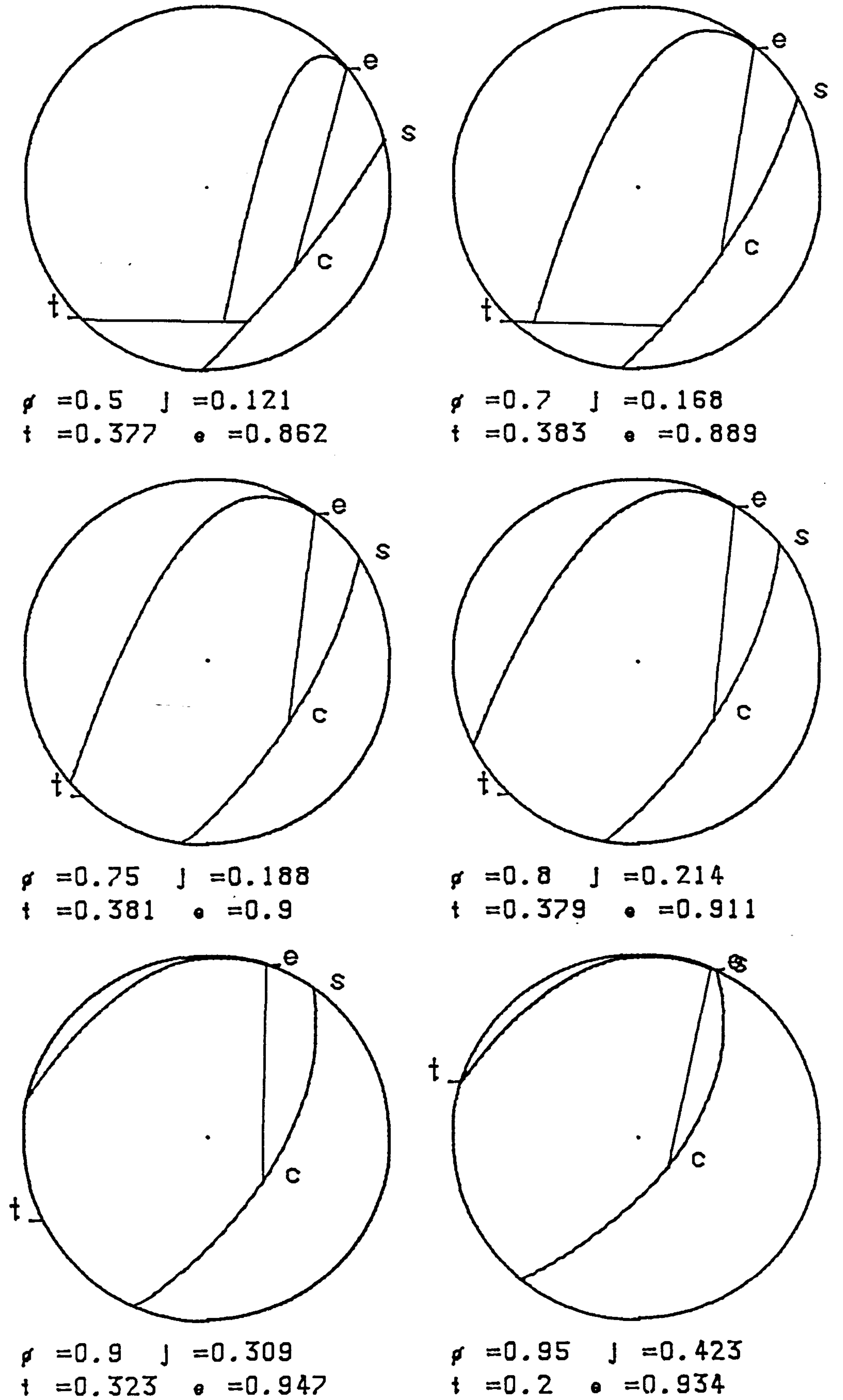

Figure 5.9 Predicted load regions for the conditions J = 0,4; C_v = 52,2

interpretation, as the volume below it becomes greater than that of the load; but it does indicate that a large proportion of the load is locked into the mill rotation, and that the load is therefore close to centrifuging. As the speed increases the centre of motion of the balls lying below the equilibrium surface moves towards the centre of the mill, this is reasonable, as under centrifuging conditions the centre of motion would be at the mill centre.

(c) The effect of an increase in filling upon the response of this treatment can be seen by comparing Figures 5.7 and 5.8. The value of j is not changed because the Davis point is not affected by the filling, and the value of λ is constant because the pulp solids contents are the same. The volumes of material contained in regions 2 and 4 are increased because the value of t decreases, and that of e increases.

(d) As the pulp solids content increases, the static angle of repose and therefore λ increases. This results in the value of j decreasing, as seen by a comparison of Figures 5.7 and 5.9. The volume of material in regions 2 and 4 is increased.

(e) At the higher mill speeds the parabolic paths of the outer balls terminate at positions higher up the liners than the measured toe position, this is possibly due to two reasons. Firstly, the threshold level of the probe output conditioning circuit was set so that the *en-masse* toe was measured, and that initial small peaks were ignored. These initial peaks were caused by individual ball impacts either from the termination of trajectories of individual balls, or from balls landing in the toe and rebounding onto the liner. Secondly, it is possible that in passing through region 2 the velocity of the balls decreases, and as a result commence their parabolic paths with velocities less than that of the mill shell. Evidence for this is shown in frame-by-frame analysis of individual balls, such as Figure 5.1, where the spacing of the ball centres becomes closer in region 2, indicating a reduction in velocity.

This reduction in velocity may be due to the area of the projection surface being greater than that of the equilibrium surface between the centre of motion and the mill shell. To maintain the same volumetric flow through the larger area the velocity has to decrease. An analogy to this is fluid flowing through an expanding pipe. For this reasoning to be valid, the bulk density of the material has to remain constant; examination of photographs of ceramic balls and glycerine media show that the bulk density of the balls in regions 1 and 2 is the same. The inter-ball movement seen in region 2 may also be indicative of a reduction in velocity, the balls are repacking themselves as they slow down so that the same bulk density is maintained.

As the form of the projection surface has not been defined here an allowance for any reduction in velocity has not been made in the computer programme. If an allowance is to be made, the velocity reduction is given by the ratio of the lengths of the equilibrium surface (between the centre of motion and the mill) and the projection surface (i.e. cs/ce). The length cs can be found by performing a line integration along the spiral between the points c and s, which yields:

$$cs = \frac{\sqrt{(1 + \lambda^2)}}{\lambda} \; k_s (e^{\lambda(\pi - \psi_c)} - e^{\lambda(\pi - \psi_s)}) \qquad (5.10)$$

The method proposed here, whilst still not being a complete definition of the regions within the load is an improvement upon the previous assumptions that the load is given by a straight line drawn between the toe and shoulder. It is hoped that this will form the basis of a complete definition of the load behaviour, from which a more realistic estimation of mill power may ultimately be made.

6. COMPARISON OF EQUATIONS PREDICTING MILL POWER

The derivation of a number of equations that predict mill power have been discussed in chapter 2. The major difference between them is the the way in which they assume that energy transfer into the load is achieved, although their final forms tend to be similar. A summary of the equations converted to S.I. units and common parameters is given below.

Hogg & Fuerstenau	$P = 3,627\ \rho_b\ \phi L D^{2,5} \mathrm{Sin}^3\ \theta \sin\alpha$	(2.11)
Rowland, (Bond)	$P = 12,262\ \rho_b \phi L D^{2,3} J(1-0,937J)(1-\frac{0,1}{2^{9-10\phi}})$	(2.14)
Arbiter & Harris	$P = 1,880\ mg\phi\ D^{0,5}(1-J)\sin\alpha$	(2.17a)
Arbiter & Harris	$P = 9,690\rho_b \phi L D^{2,5} J(1-J)$	(2.19)

These equations have been used to calculate the power for the conditions $J = 0,4$, $C_v = 46,0$, at the various mill speeds. The calculated powers are shown compared to the measured power (calculated from the torque and rotational speed) in Figure 6.1; the parameters α and θ used in equations 2.11 and 2.17a are given in Table 6.1. The values of α and θ are calculated from the measured values of t and e, as shown in Figure 6.2.

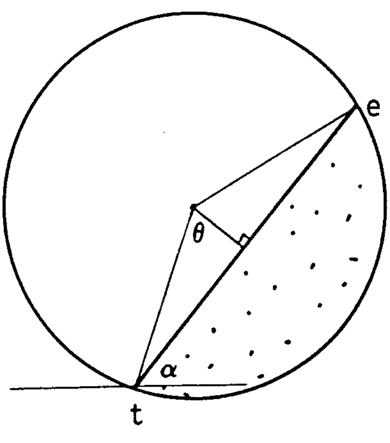

Figure 6.2 Determination of α and θ from load position data

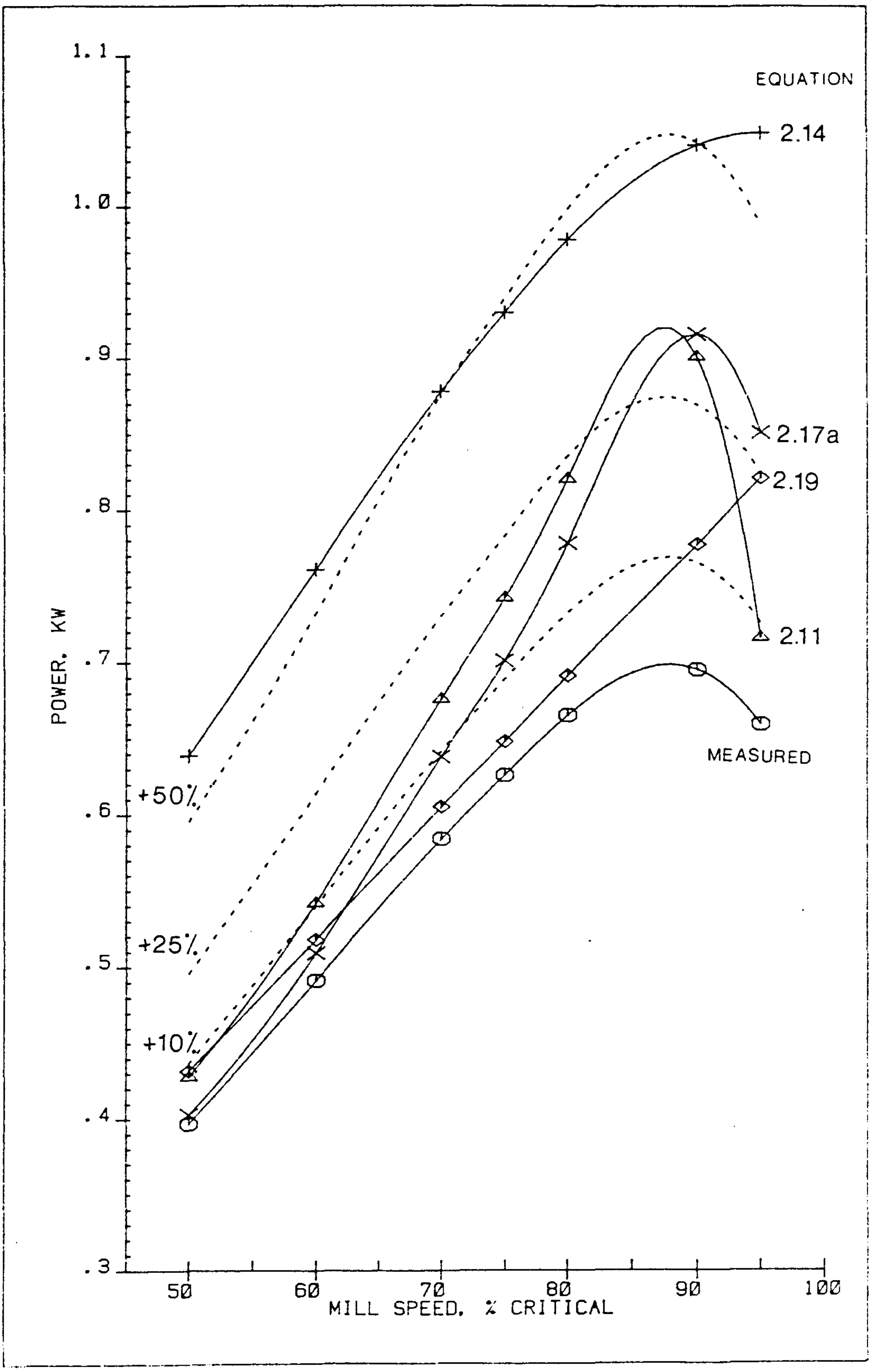

Figure 6.1 Comparison of predicted and measured power for various equations

TABLE 6.1 Parameters defining load position for equations 2.11 and 2.17a

Mill speed % critical	α^{o}	θ^{o}
50	39,5	87,7
60	42,1	88,7
70	46,0	91,6
75	47,6	93,1
80	50,2	94,3
90	53,5	103,0
95	45,0	112,3

It is evident from Figure 6.1 that all the equations overestimate the power to certain degrees. Also shown in Figure 6.1 are contours which represent 110, 125 and 150 per cent of the measured power value at any given speed.

Equation 2.14, which is the Allis-Chalmers design equation predicts powers that are approximately 50 per cent greater than the measured power. This excess is inherent in the equation constant, which probably includes a deliberate overestimation as a safety factor. It is interesting that this equation predicts a maximum power will occur at J = 0,53. This equation is claimed by Kjos (44) to predict the power of individual mills with an accuracy of 2 per cent (at a 75 per cent confidence level).

Equations 2.11 and 2.17a use measurements of the load position, and both become increasingly inaccurate as mill speed increases. Equation 2.19 uses a constant value, determined from a large number of industrial mills, for the angle of repose of the load, and for speeds up to 80 per cent critical predicts the mill power within 10 per cent. This equation, while only recently proposed (9,22,35) is a torque-arm model. It does not allow for energy recovery at higher speeds, and also predicts a maximum power occurring at J = 0,5.

The equation can be modified to give a more accurate prediction of power, the results from the steel-sand pulp tests for conditions J = 0,4, C_v = 46,0 will be used as an example.

The equation can be rewritten as follows.

$$P = 9{,}69\rho_b \phi L D^{2,5}\ J(1-1{,}06J)f(\phi) \qquad (6.1)$$

This ensures that the power is a maximum at J = 0,47, and f(ϕ) is a speed dependant function that is used to modify the power depending on the load motion. The modifying function can be derived from the torque curve, and when the torque is at a maximum, maximum energy is being transferred to the charge. The torque curve has been shown to be influenced by filling and pulp solids content, and allowance would need to be made for these when deriving the power modification function for specific conditions of filling and pulp solids content.

The values of f(ϕ) can be determined at the various speeds by dividing the torque at a given speed by the maximum torque, as shown in Table 6.2. The power calculated from equation 6.1 and the measured power are also shown in Table 6.2 and it can be seen that the power is accurately predicted by equation 6.1 over the entire range of speeds.

TABLE 6.2 Calculation of $f(\phi)$ and comparison of calculated and measured power

Mill speed % critical	Torque T kg.m	$f(\phi)$ T/T_{max}*	Power, kW	
			Calculated (eq. 6.1)	Measured
50	13,47	0,950	0,393	0,397
60	13,91	0,981	0,487	0,491
70	14,16	0,999	0,579	0,584
75	14,18	1,000	0,621	0,626
80	14,13	0,997	0,660	0,665
90	13,12	0,925	0,689	0,695
95	11,79	0,832	0,654	0,659

Conditions: Steel media, $J = 0,4$, $C_v = 46,0$

*T_{max} = 14,18 kg.m

For an industrial mill, the torque curve cannot be determined, but based upon the filling and pulp solids content, an estimation of the values of $f(\phi)$ can be made from the torque curves that have been determined for the steel media-sand pulp system.

7. CONCLUSIONS AND RECOMMENDATIONS FOR FUTURE RESEARCH

The results from this investigation show that the dynamic motion of the loading within a wet grinding mill is complex and is influenced by the mill speed, mill filling, pulp rheology and the static angle of repose of the load. A change in one of these variables will affect the torque required to turn the mill, and hence the power drawn, by changing the load motion within the mill. The effect of independently changing these variables has been shown and knowledge of these effects is useful when it is attempted to optimize the operation of existing milling installations, where the mill speed cannot be changed, by variation of the mill filling or the pulp solids content. The effect of increasing the filling will depend upon the mill speed and pulp solids content. At low speeds (< 75% critical) increasing the filling will increase the power. At higher speeds the power will be decreased as the filling increases, due to energy recovery. An increase in the pulp solids content tends to decrease the torque, with the decrease becoming greater at higher mill speeds and larger load fillings. This is because the increased adhesion effect of the more viscous pulps and the greater friction due to the increased number of particles causes the shoulder of the load to rise further up the mill, which causes the balls to impact further towards the opposite side of the mill, thus increasing the energy recovery from the falling balls. Therefore the optimization of pulp solids content will involve a compromise between: (a) the content that produces the rheology that corresponds to maximum grinding rate at acceptable power and (b) the solids content that gives maximum pulp flow through the mill.

At conditions where the load is not impacting onto the mill shell the mill filling can be defined by the position of the toe. This finding is of importance for the design of control strategies for autogenous (either pebble or run-of-mine) grinding circuits where the toe position can be measured using a conductivity, impact or pressure sensing probe, the technology of which has been developed and tested. Knowledge of the load volume would make the control strategies simpler and more effective and would enable them to control the feedrate to maintain the filling corresponding to maximum power draw. Generally, mill conditions are such that the load is not impacting onto the mill shell as this results in increased liner wear. Future work planned by the Council for Mineral Technology will examine the load motion in a run-of-mine mill at Deelkraal gold mine using a conductivity probe that is presently being installed and tested. The results from this future investigation will provide comparisons for the results presented in this dissertation.

An examination of the literature has shown that the equations which have been derived to predict power are based on simple assumptions about the configuration of the load, even though there have been attempts to calculate this configuration that date back to the 1930's. A mathematical treatment has been developed to predict the load configuration which is based upon the measured and observed motion within a wet mill. Although this treatment is still a simplification of the complex motion, it is based upon reality rather than ideal theoretical considerations of a dry mill with no pulp or powder present and is therefore more applicable. It is intended that this treatment should provide the basis for a method to predict mill power, based on knowledge of the load motion, which takes into account as many design variables as possible. Before this prediction of power can be made, research will have to be conducted in the following areas:

(a) Characterization of energy recovery from the falling balls as indicated by a reduction in torque; none of the power prediction models allow for this energy recovery. Results from this study show that under certain conditions energy from the falling balls is recovered and assists the mill to rotate. This energy recovery exists even at conditions where the load is not observed to be impacting onto the mill liners.

(b) Examination of the adhesion effects of rock pulps of differing viscosity, and the influence that this has on the parabolic trajectory of a falling particle. It is not possible to examine this effect in this study as the trajectories of the balls are affected because the glycerine was causing them to stick to the end plate. One way to overcome this would be to use rods in place of balls, due to the increased mass of the rods their adhesion to the end plate would be negligible.

The aim of this study would be to examine how the angle of the velocity resultant is affected by the pulp viscosity, it would also be interesting to examine in detail the movement of the falling rods within the load, and to define regions of free and hindered parabolic paths, and of a forced rolling motion.

Modifications of a recently published equation to predict mill power, which uses the torque-arm concept, results in a more accurate prediction of power over the speed range of 50 to 95 per cent critical. The equation was modified to allow for maximum power occurring at a filling of 47 per cent, and also to allow for energy recovery at higher speeds by using the profile of the torque curve.

APPENDIX A

Pulp Rheology Data

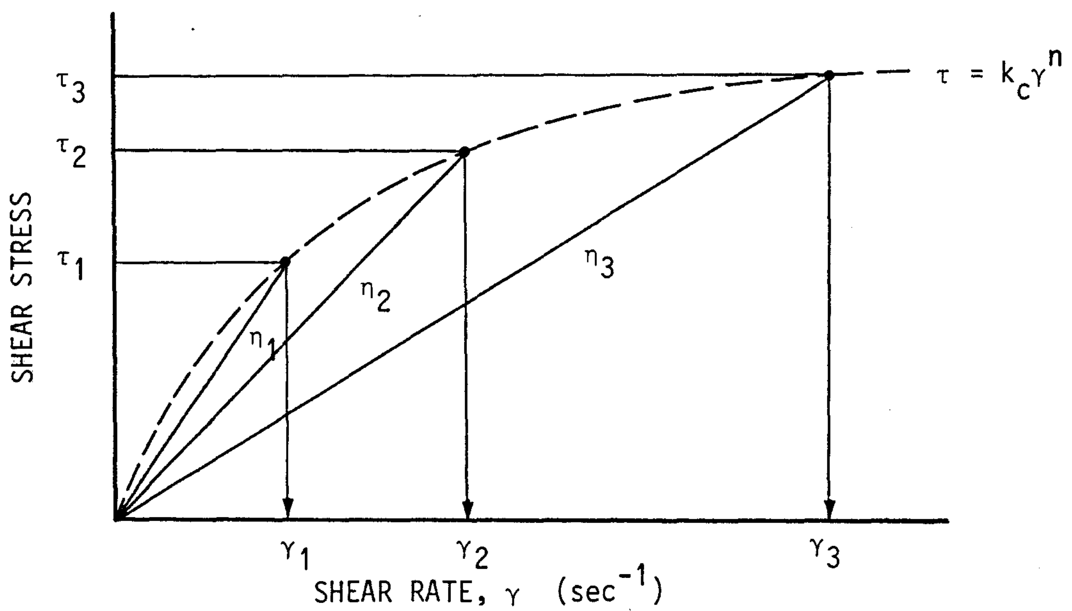

Figure A.1 Generation of the rate-stress curve, where viscosity and stress are known

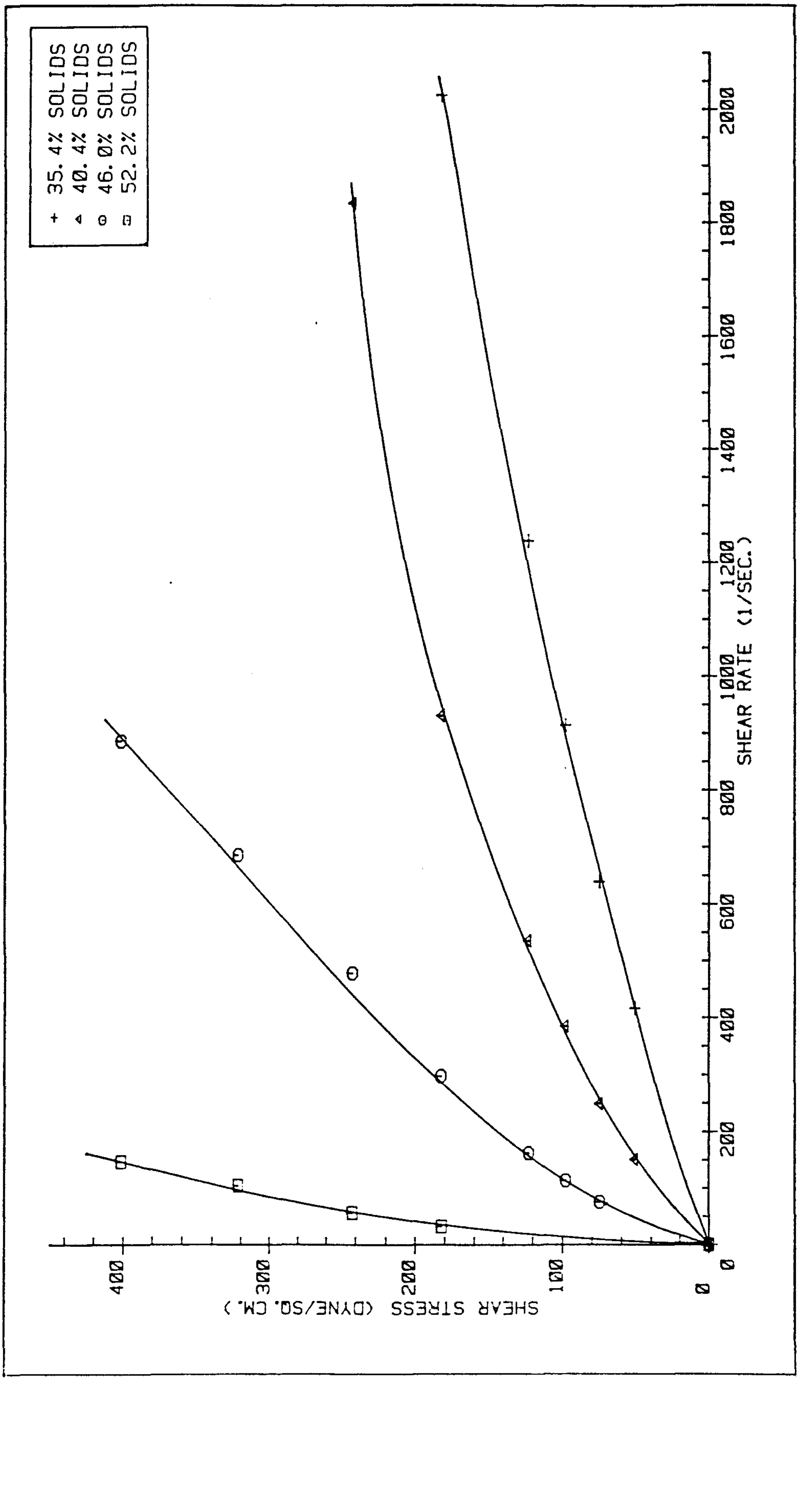

Figure A.2 Rate-stress diagram for pebble mill discharge pulps at various solids contents

Table A.1 Calibration equations for the Stormer viscometer

Driving mass (g)	Calibration equation
12	η = 1,557 t - 15,84
18	= 2,310 t - 18,22
24	= 3,200 t - 20,60
30	= 4,029 t - 22,99
45	= 6,233 t - 28,94
60	= 8,293 t - 34,89
80	=11,577 t - 42,83
100	=15,013 t - 50,77

η = viscosity, cP

t = time (s) for 100 revolutions of the spindle

Table A.2 Size distribution of East Driefontein pebble mill discharge

Size interval micron	Percent finer	Cumulative percent finer
1 100	13,5	97,0
300	11,3	83,5
212	15,4	72,2
150	18,7	56,8
106	9,2	38,1
75	6,9	28,9
53	3,4	22,0
38	18,6	18,6

Schumann slope = 0,78

Table A.3 Rheological data for pebble mill discharge

Volume percent solids	Shear stress $dyne/cm^2$ τ	Apparent viscosity poise η	Shear rate sec^{-1} $\gamma = (\frac{\tau}{\eta})$
35,4	50,9	0,122	417,2
	74,8	0,117	639,3
	97,8	0,107	914,0
	122,6	0,099	1238,4
	182,3	0,090	2024,4
40,4	50,9	0,338	150,6
	74,8	0,301	248,5
	97,8	0,254	385,0
	122,6	0,229	535,4
	182,3	0,196	930,1
	242,1	0,158	1832,1
46,0	74,8	1,004	74,5
	97,8	0,868	112,7
	122,6	0,758	161,7
	182,3	0,613	297,4
	242,1	0,507	477,5
	321,7	0,469	685,9
	401,4	0,453	886,1
52,2	182,3	5,690	32,0
	242,1	4,306	56,2
	321,7	3,096	103,9
	401,4	2,741	146,4

Table A.4 Values of n and k_c for pebble mill discharge pulps of various solids contents

Volume percent solids	Flow index n	Consistency index k_c
35,4	0,819	0,358
40,4	0,684	1,658
46,0	0,676	3,923
52,2	0,509	31,074

Table A.5 Viscosity (at 100 sec^{-1}) of pebble mill discharge pulps of varying solids content

Volume percent solids	Viscosity at $\gamma = 100\ sec^{-1}$ cP
35,4	15,6
40,4	38,7
46,0	89,6
52,2	325,4

APPENDIX B

Results for the steel-sand system

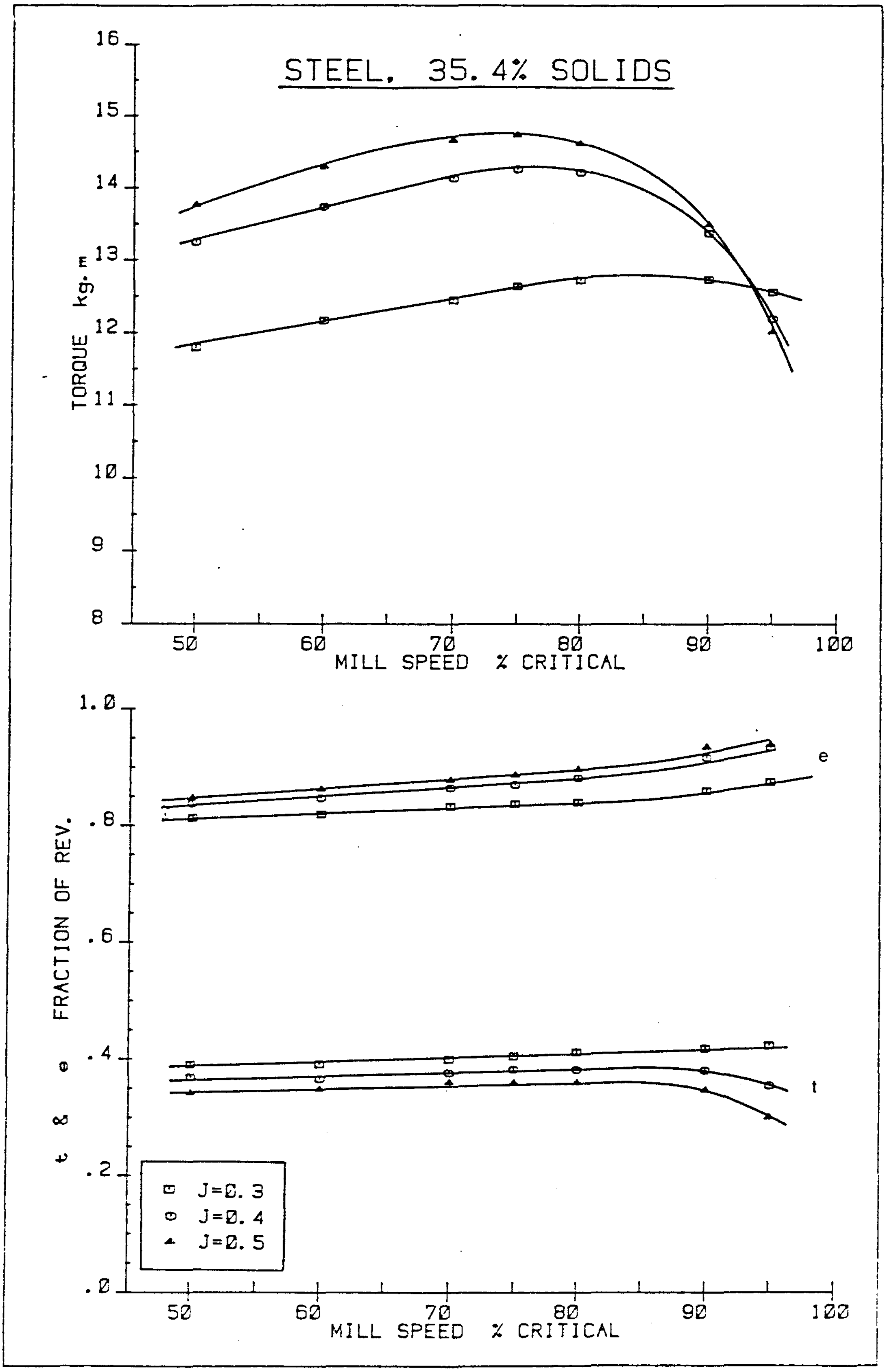

Figure B.1 Torque and load position for steel media, C_v = 35,4

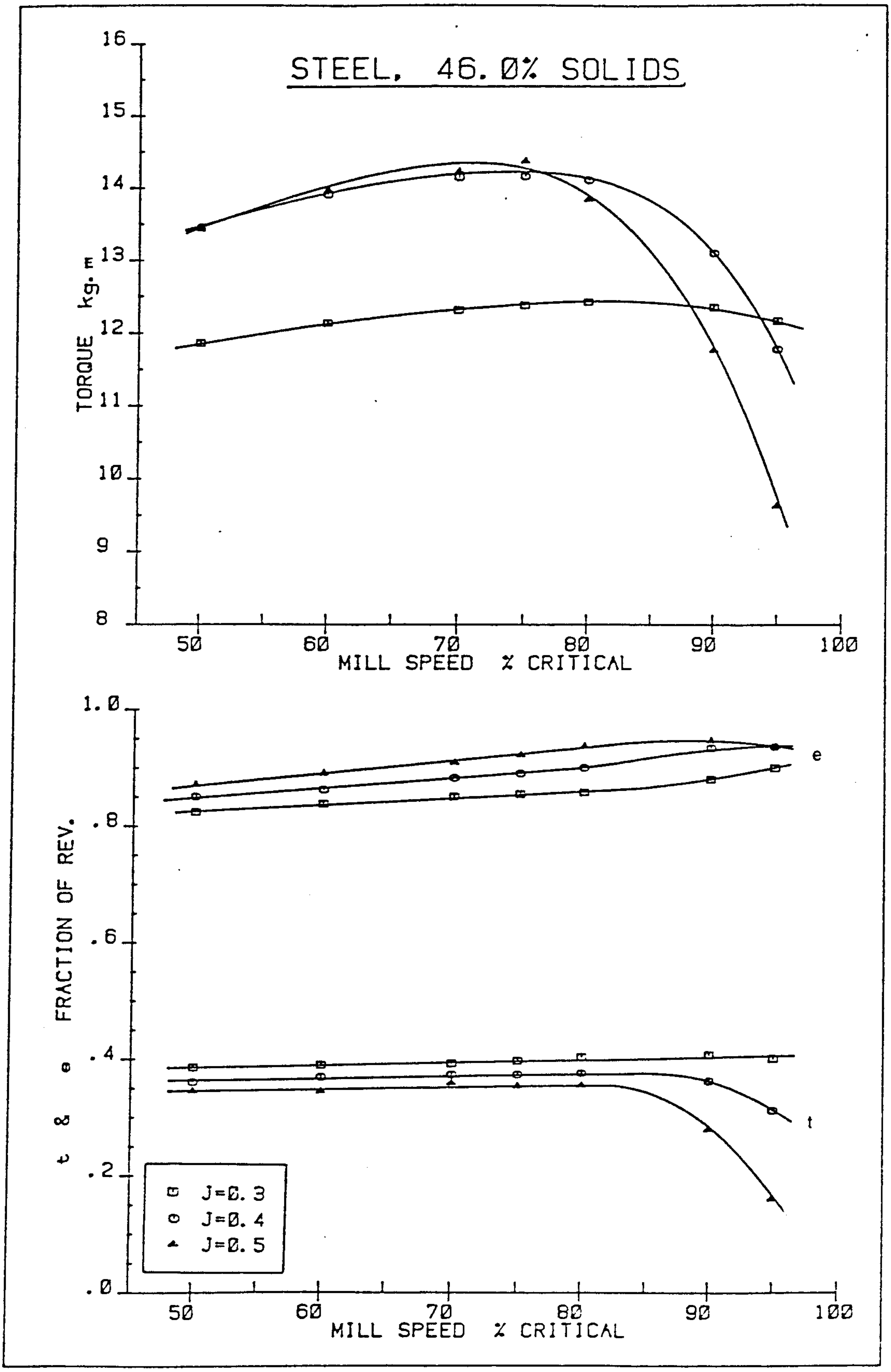

Figure B.2 Torque and load position for steel media, C_v = 46,0

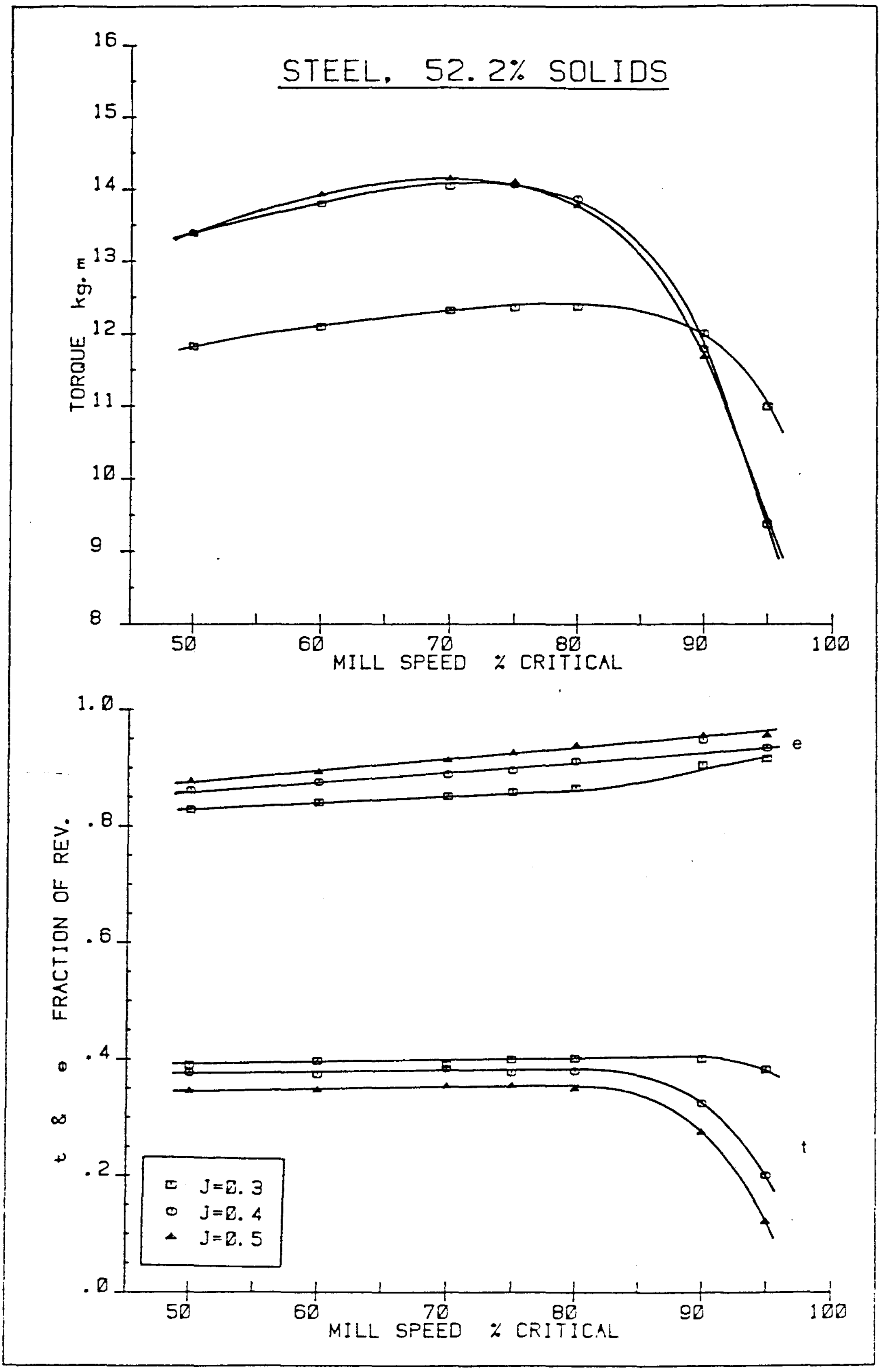

Figure B.3 Torque and load position for steel media, C_v = 52,2

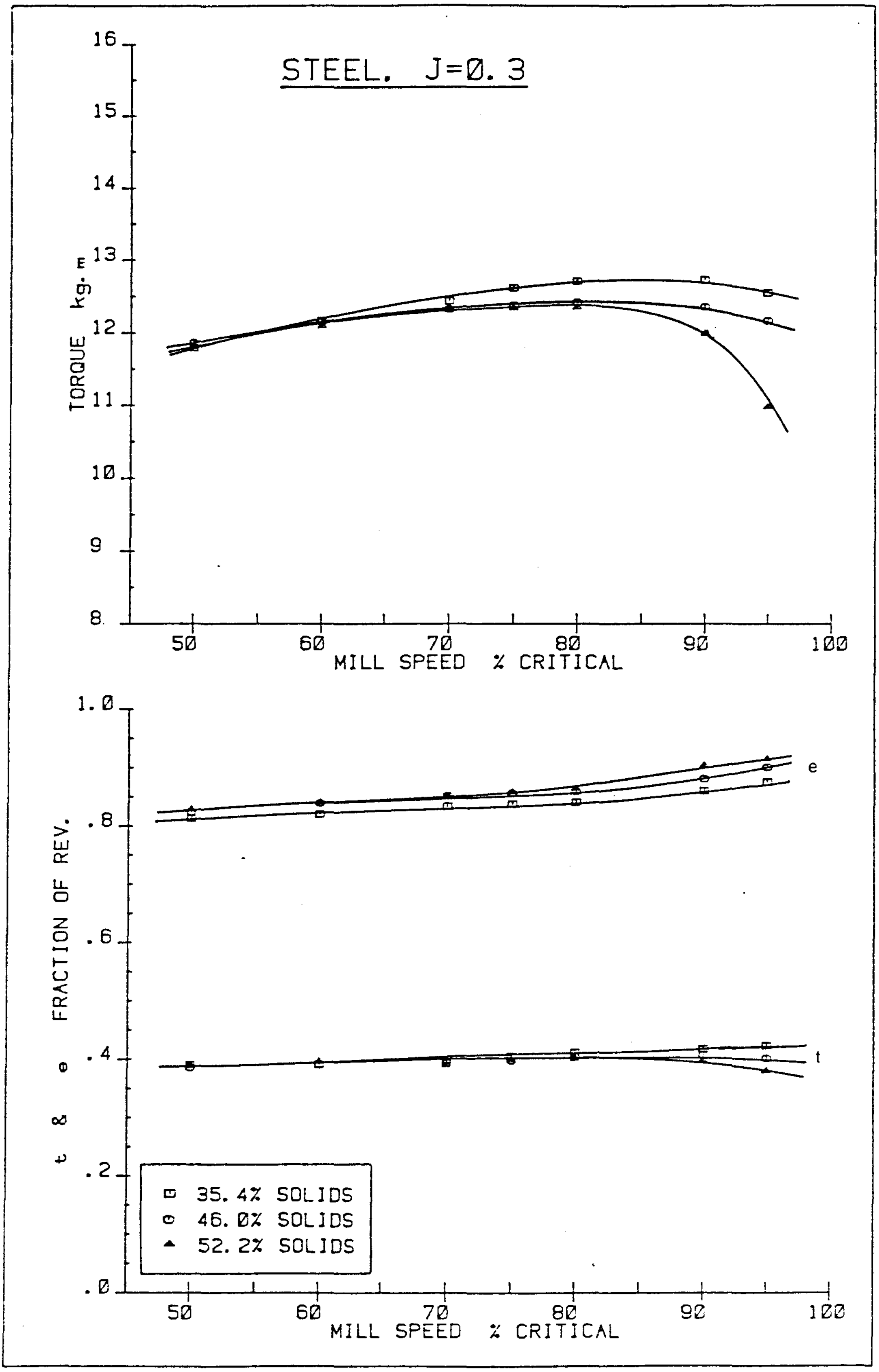

Figure B.4 Torque and load position for steel media, J = 0,3

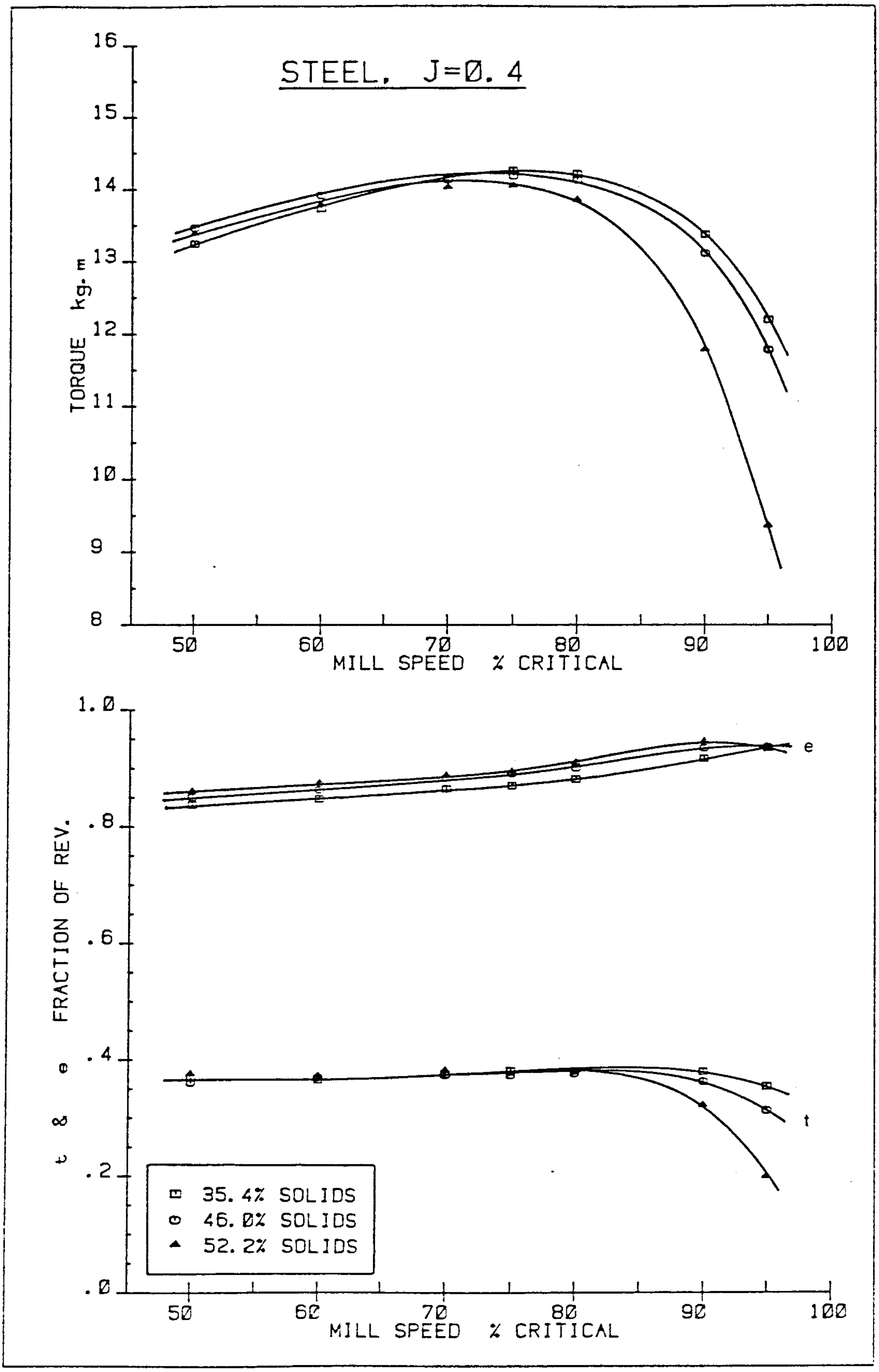

Figure B.5 Torque and load position for steel media, J = 0,4

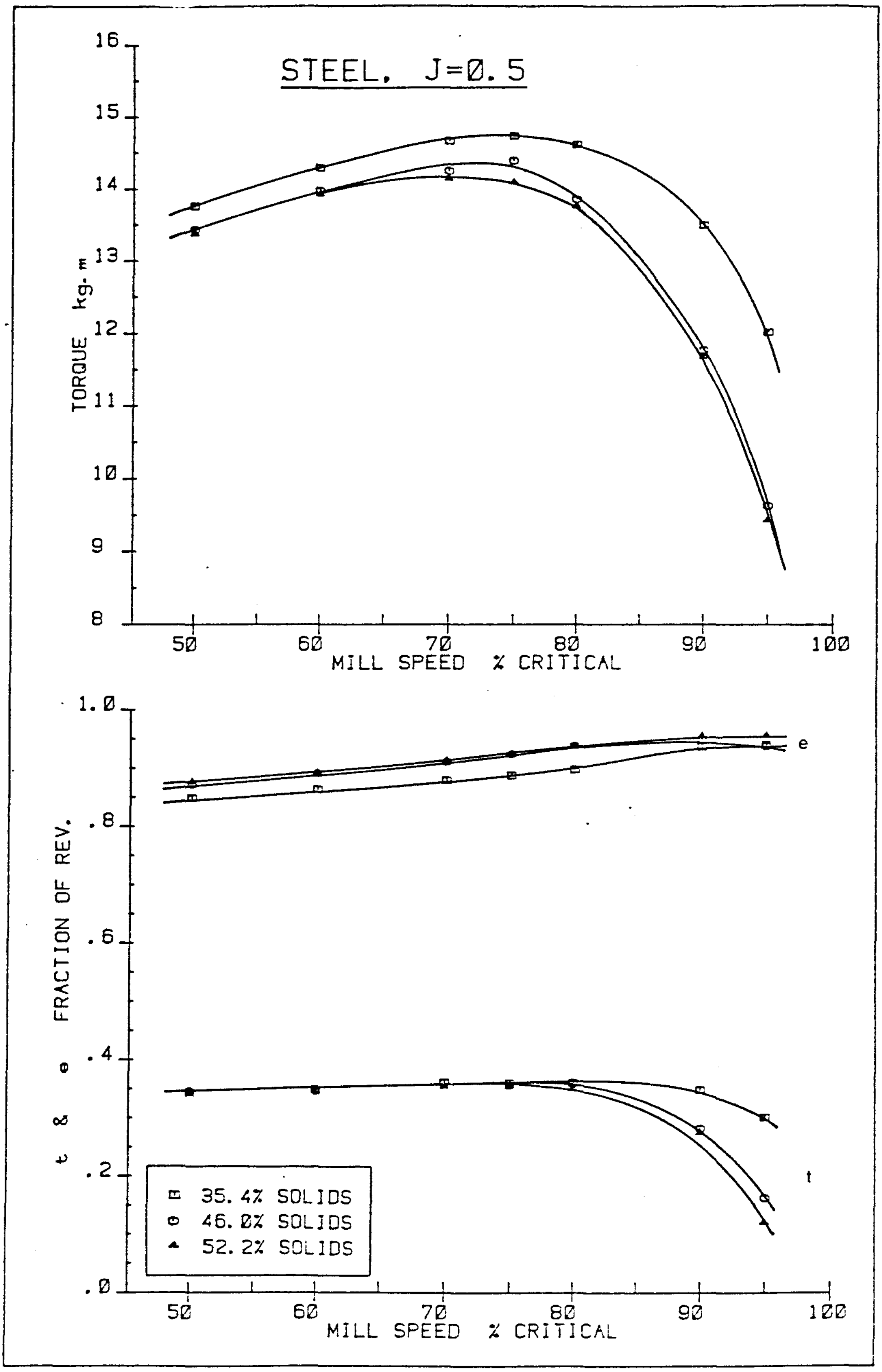

Figure B.6 Torque and load position for steel media, J = 0,5

SPEED %CRIT	TORQUE KG.M	****LOAD t	POSITION u	**** e
50	11.796	.391	.422	.813
60	12.169	.392	.428	.82
70	12.449	.399	.434	.833
75	12.635	.405	.432	.837
80	12.727	.417	.428	.845
90	12.748	.418	.442	.86
95	12.57	.423	.453	.876

TABLE B.1 J=0.3 Cv=35.4

SPEED %CRIT	TORQUE KG.M	****LOAD t	POSITION u	**** e
50	13.242	.369	.469	.838
60	13.736	.366	.482	.848
70	14.127	.376	.489	.865
75	14.252	.382	.488	.87
80	14.211	.382	.5	.882
90	13.383	.38	.537	.917
95	12.201	.355	.58	.935

TABLE B.2 J=0.4 Cv=35.4

SPEED %CRIT	TORQUE KG.M	****LOAD t	POSITION u	**** e
50	13.758	.343	.506	.849
60	14.289	.349	.514	.863
70	14.656	.361	.518	.879
75	14.722	.359	.528	.887
80	14.611	.36	.537	.897
90	13.507	.347	.589	.936
95	12.031	.301	.639	.94

TABLE B.3 J=0.5 Cv=35.4

SPEED %CRIT	TORQUE KG.M	****LOAD t	POSITION u	**** e
50	11.86	.386	.439	.825
60	12.147	.391	.448	.839
70	12.328	.393	.458	.851
75	12.398	.398	.458	.856
80	12.439	.405	.454	.863
90	12.37	.408	.473	.881
95	12.18	.402	.499	.901

TABLE B.4 J=0.3 Cv=46.0

SPEED %CRIT	TORQUE KG.M	****LOAD t	POSITION u	**** e
50	13.465	.369	.49	.851
60	13.912	.37	.493	.863
70	14.16	.374	.509	.883
75	14.175	.374	.517	.891
80	14.127	.377	.524	.901
90	13.116	.363	.572	.935
95	11.791	.313	.624	.937

TABLE B.5 J=0.4 Cv=46.0

SPEED %CRIT	TORQUE KG.M	****LOAD t	POSITION u	**** e
50	13.432	.346	.526	.872
60	13.974	.346	.545	.891
70	14.246	.36	.55	.91
75	14.385	.355	.568	.923
80	13.861	.357	.581	.938
90	11.785	.281	.667	.948
95	9.631	.162	.775	.937

TABLE B.6 J=0.5 Cv=46.0

SPEED %CRIT	TORQUE KG.M	****LOAD t	POSITION u	**** e
50	11.823	.39	.439	.829
60	12.099	.397	.443	.84
70	12.32	.39	.461	.851
75	12.352	.399	.459	.858
80	12.371	.401	.464	.865
90	12.009	.399	.505	.904
95	11	.381	.535	.916

TABLE B.7 J=0.3 Cv=52.2

SPEED %CRIT	TORQUE KG.M	****LOAD t	POSITION u	**** e
50	13.389	.377	.485	.862
60	13.793	.374	.502	.876
70	14.026	.383	.506	.889
75	14.051	.381	.519	.9
80	13.861	.379	.532	.911
90	11.8	.323	.624	.947
95	9.374	.2	.734	.934

TABLE B.8 J=0.4 Cv=52.2

SPEED %CRIT	TORQUE KG.M	****LOAD t	POSITION u	**** e
50	13.377	.346	.531	.877
60	13.923	.348	.545	.893
70	14.142	.354	.559	.913
75	14.095	.355	.571	.926
80	13.768	.349	.589	.938
90	11.697	.274	.681	.955
95	9.443	.121	.835	.956

TABLE B.9 J=0.5 Cv=52.2

APPENDIX C

Results for the ceramic-glycerine system

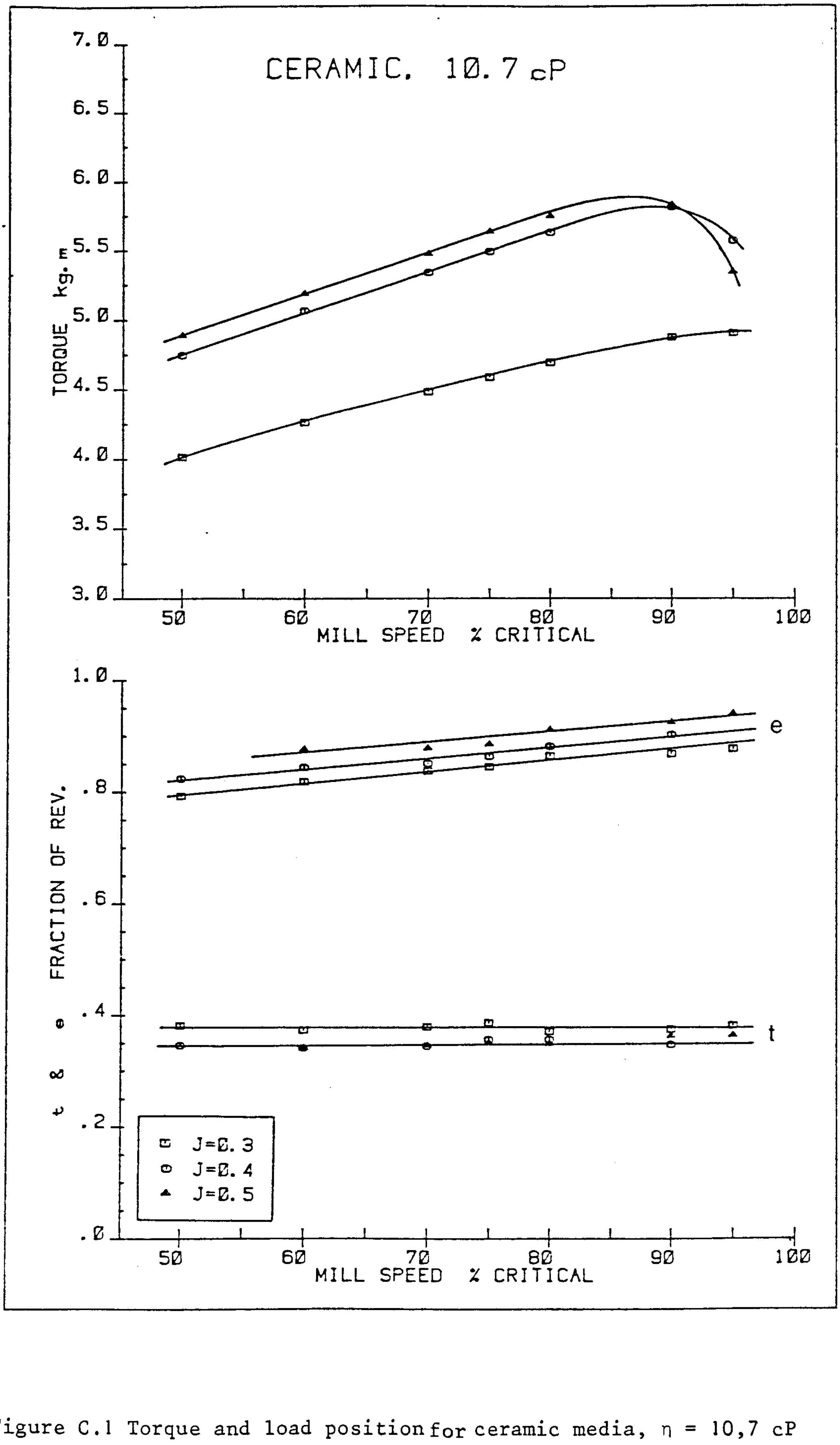

Figure C.1 Torque and load position for ceramic media, η = 10,7 cP

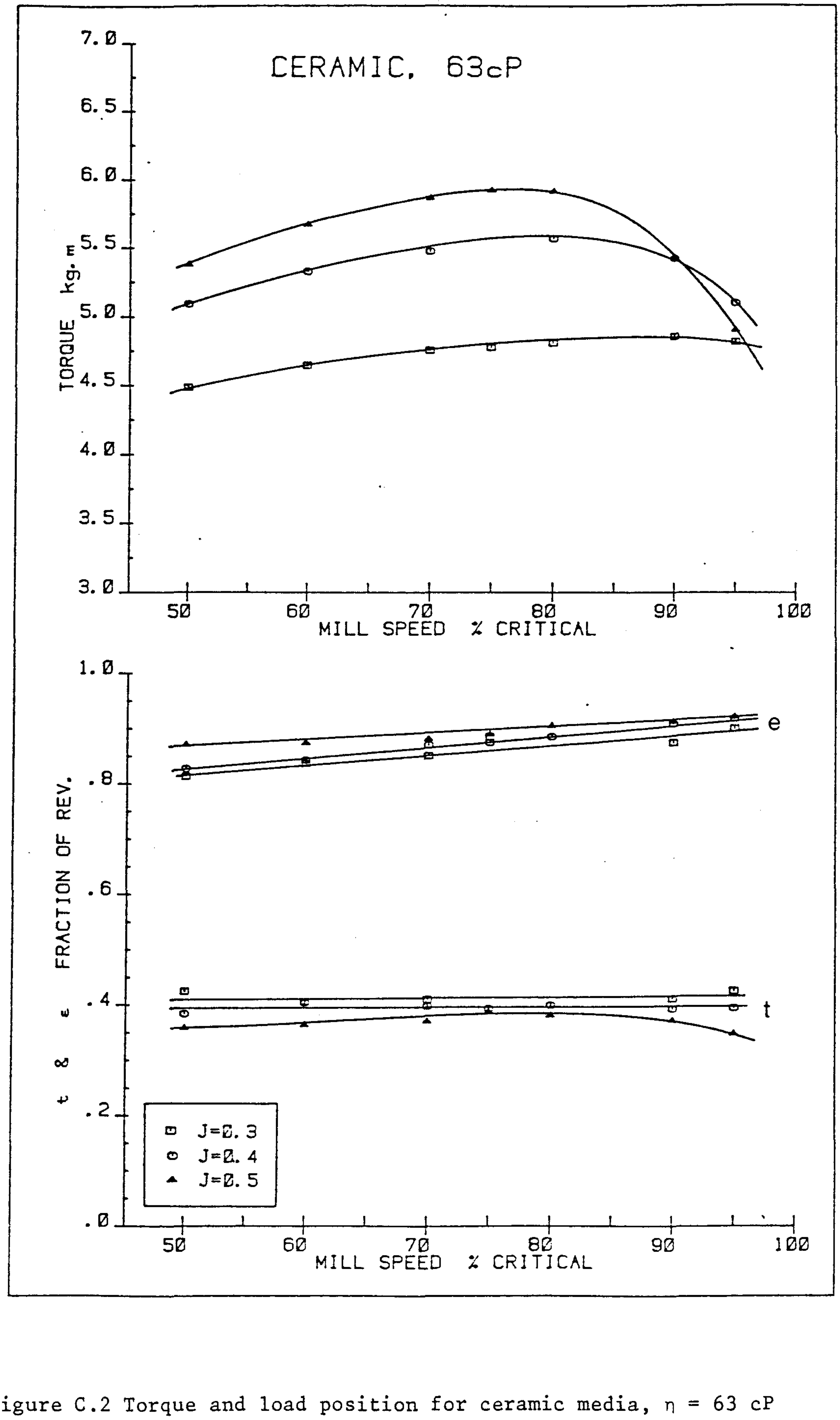

Figure C.2 Torque and load position for ceramic media, η = 63 cP

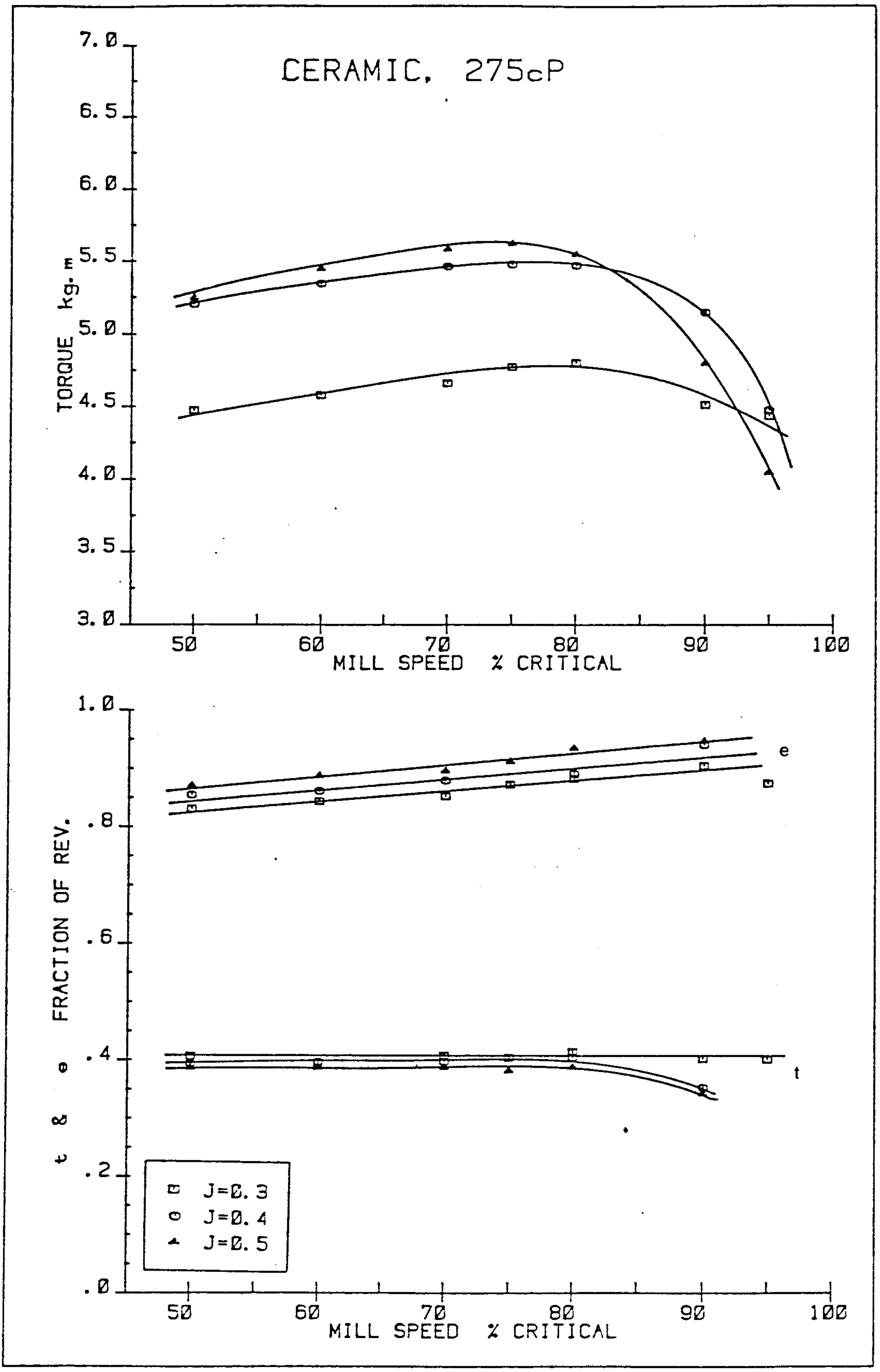

Figure C.3 Torque and load position for ceramic media, η = 275 cP

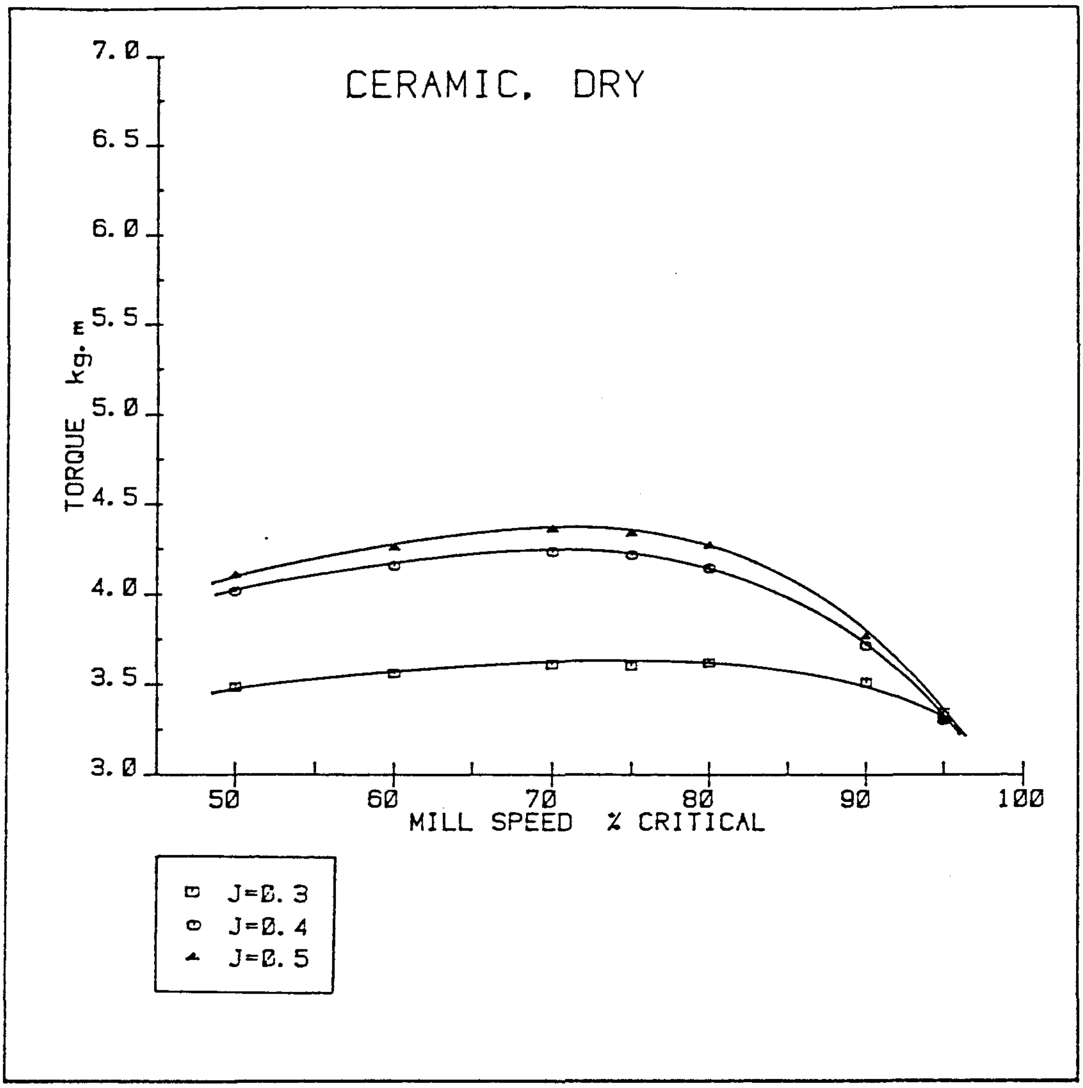

Figure C.4 Torque for ceramic media, dry conditions

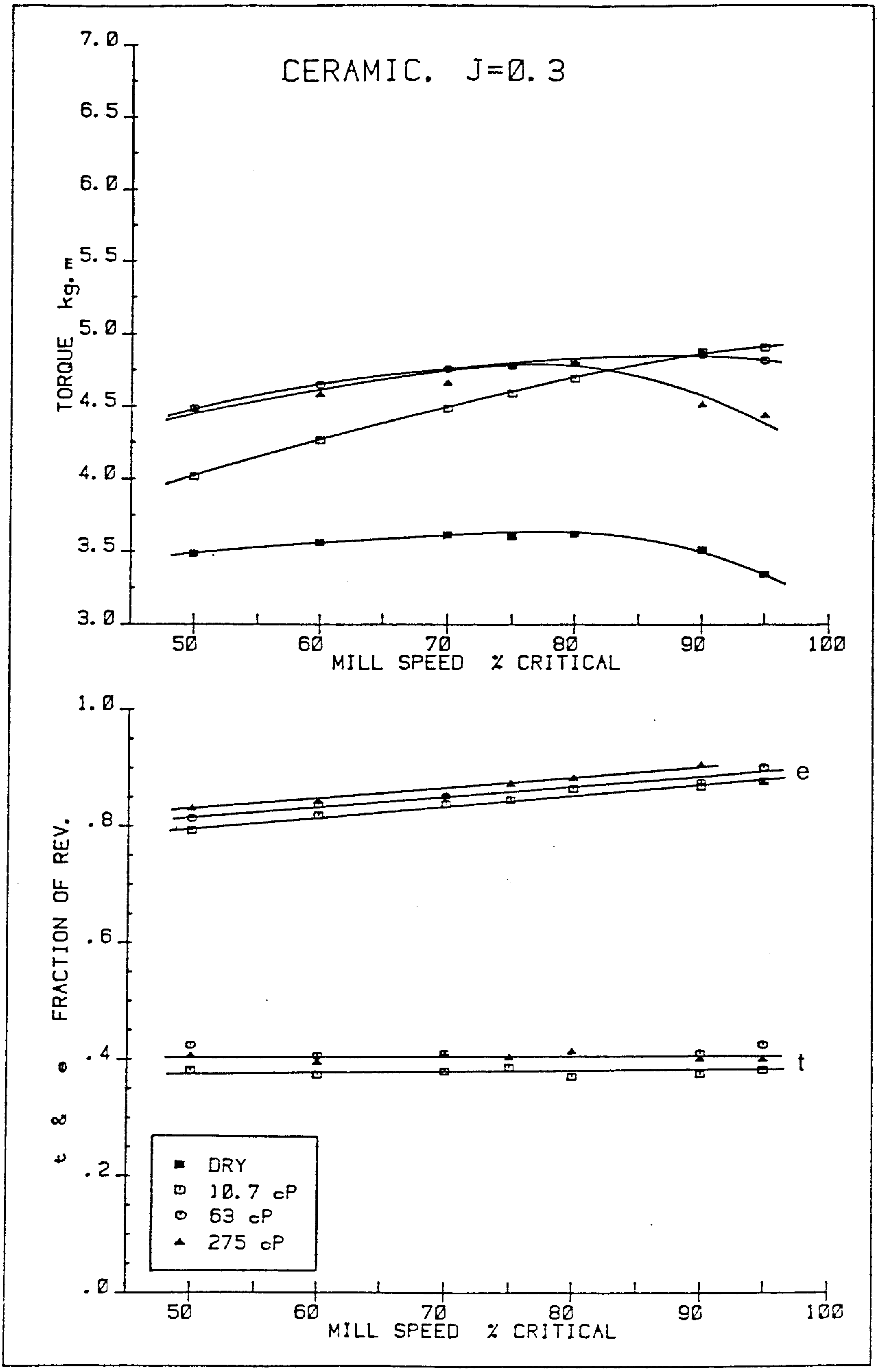

Figure C.5 Torque and load position for ceramic media, J = 0,3

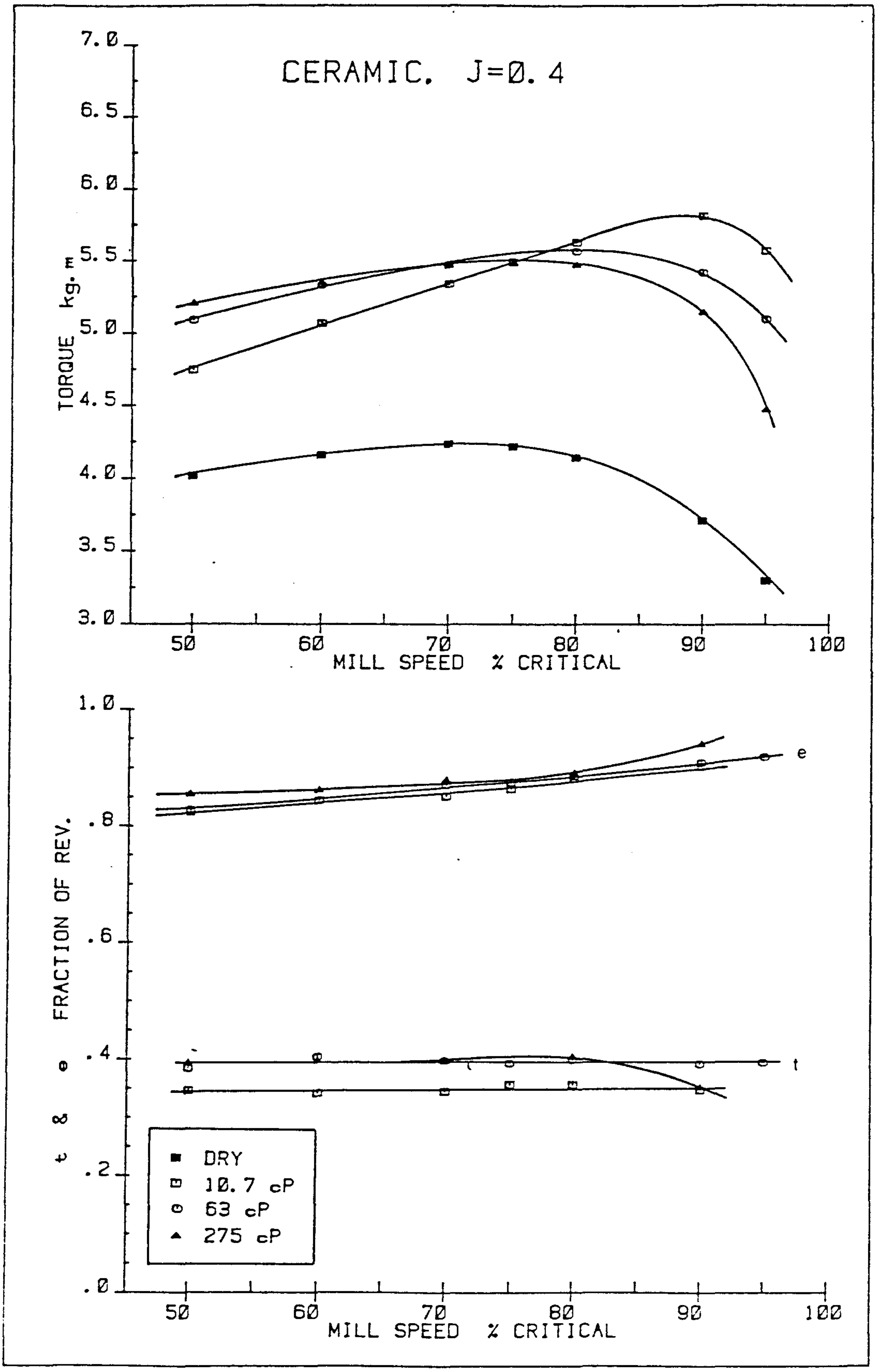

Figure C.6 Torque and load position for ceramic media, J = 0,4

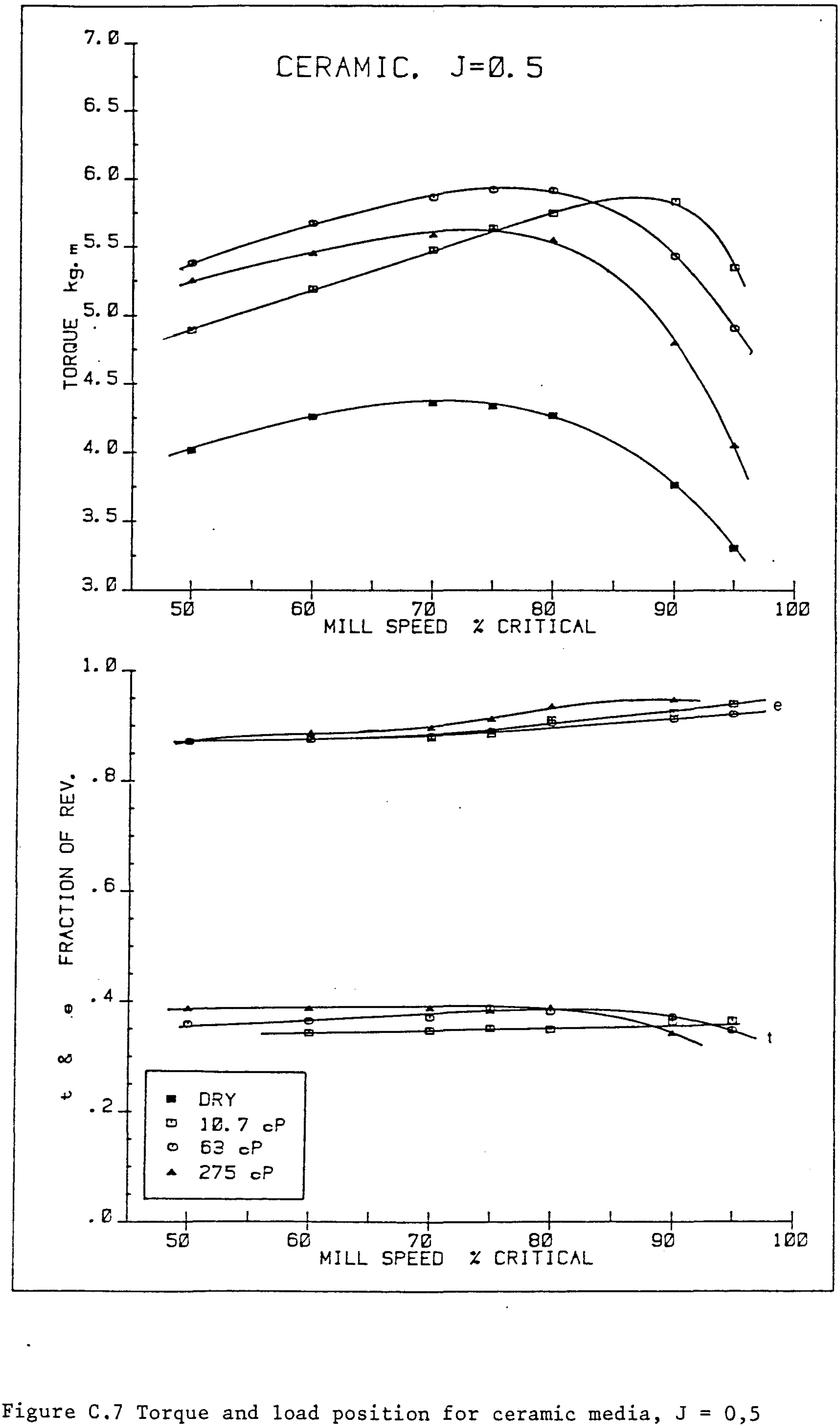

Figure C.7 Torque and load position for ceramic media, J = 0,5

SPEED %CRIT	TORQUE KG.M	****LOAD POSITION**** t	u	e	TEMP. ´C
50	4.015	.382	.411	.793	25.5
60	4.264	.374	.445	.819	26.2
70	4.481	.379	.458	.837	27.3
75	4.585	.386	.459	.845	28.6
80	4.692	.371	.493	.864	29.6
90	4.88	.375	.493	.868	31.1
95	4.911	.382	.495	.877	31.8

TABLE C.1 J=0.3, 10.7cP 24.7

SPEED %CRIT	TORQUE KG.M	****LOAD POSITION**** t	u	e	TEMP. ´C
50	4.747	.346	.478	.824	26.9
60	5.065	.342	.502	.844	27.4
70	5.339	.345	.506	.851	27.9
75	5.49	.356	.507	.863	28.6
80	5.63	.356	.525	.881	29.5
90	5.818	.347	.555	.902	30.1
95	5.575	.382	.495	.877	31.8

TABLE C.2 J=0.4, 10.7cP 26.7

SPEED %CRIT	TORQUE KG.M	****LOAD POSITION**** t	u	e	TEMP. ´C
50	4.891	.346	.478	.824	27.9
60	5.189	.343	.534	.877	28.3
70	5.475	.347	.532	.879	28.8
75	5.636	.351	.535	.886	29.5
80	5.749	.349	.562	.911	30.1
90	5.84	.363	.562	.925	31.3
95	5.353	.365	.575	.94	31.7

TABLE C.3 J=0.5, 10.7cP 26.7

SPEED %CRIT	TORQUE KG.M	***FRACTION OF REV.** t	u	e	TEMP. ´C
50	4.485	.425	.389	.814	27.1
60	4.645	.406	.431	.837	27.7
70	4.753	.41	.441	.851	28.6
75	4.774	.351	.535	.886	29.5
80	4.808	.39	.472	.862	30
90	4.857	.41	.465	.875	30.9
95	4.819	.425	.475	.9	31.2

TABLE C.4 J=0.3, 63cP 26.7

SPEED %CRIT	TORQUE KG.M	****LOAD POSITION**** t	u	e	TEMP. ´C
50	5.092	.385	.443	.828	24.6
60	5.327	.404	.439	.843	25.7
70	5.474	.398	.472	.87	27
75	5.522	.393	.482	.875	28.4
80	5.568	.399	.487	.886	29.5
90	5.428	.392	.517	.909	30.6
95	5.103	.394	.525	.919	31

TABLE C.5 J=0.4, 63cP 23.7

SPEED %CRIT	TORQUE KG.M	****LOAD POSITION**** t	u	e	TEMP. ´C
50	5.379	.359	.513	.872	23.8
60	5.671	.365	.51	.875	24.8
70	5.861	.371	.511	.882	25.6
75	5.918	.388	.502	.89	26.9
80	5.915	.382	.524	.906	28
90	5.439	.372	.541	.913	29.1
95	4.907	.348	.574	.922	30.2

TABLE C.6 J=0.5, 63cP 23

SPEED %CRIT	TORQUE KG.M	***LOAD POSITION**** t	u	e	TEMP. 'C
50	4.472	.407	.424	.831	25.5
60	4.578	.395	.448	.843	25.7
70	4.657	.407	.445	.852	26.5
75	4.771	.403	.469	.872	26.8
80	4.799	.413	.469	.882	27.7
90	4.513	.401	.503	.904	28.5
95	4.439	.4	.474	.874	29.1

TABLE C.7 J=0.3, 275cP 24.5

SPEED %CRIT	*****TORQUE KG.M***** J=0.3	J=0.4	J=0.5
50	3.485	4.018	4.105
60	3.563	4.16	4.259
70	3.611	4.234	4.363
75	3.603	4.216	4.337
80	3.62	4.142	4.268
90	3.512	3.716	3.767
95	3.342	3.299	3.307

TABLE C.10 DRY

SPEED %CRIT	TORQUE KG.M	****LOAD POSITION**** t	u	e	TEMP. 'C
50	5.205	.394	.461	.855	27.3
60	5.347	.397	.464	.861	28
70	5.463	.396	.483	.879	26.0
75	5.479	.403	.469	.872	27.7
80	5.472	.404	.487	.891	28.4
90	5.154	.352	.588	.94	29.5
95	4.48	.4	.474	.874	30.2

TABLE C.8 J=0.4, 275cP 26.8

SPEED %CRIT	TORQUE KG.M	****LOAD POSITION**** t	u	e	TEMP. 'C
50	5.251	.387	.484	.871	27.1
60	5.447	.387	.5	.887	27.8
70	5.582	.387	.509	.896	28.5
75	5.623	.382	.53	.912	28.6
80	5.55	.388	.547	.935	29.3
90	4.803	.342	.605	.947	30.1
95	4.052	.4	.474	.874	30.4

TABLE C.9 J=0.5, 275CP 26.8

APPENDIX D

RESULTS FOR THE STEEL-GLYCERINE SYSTEM

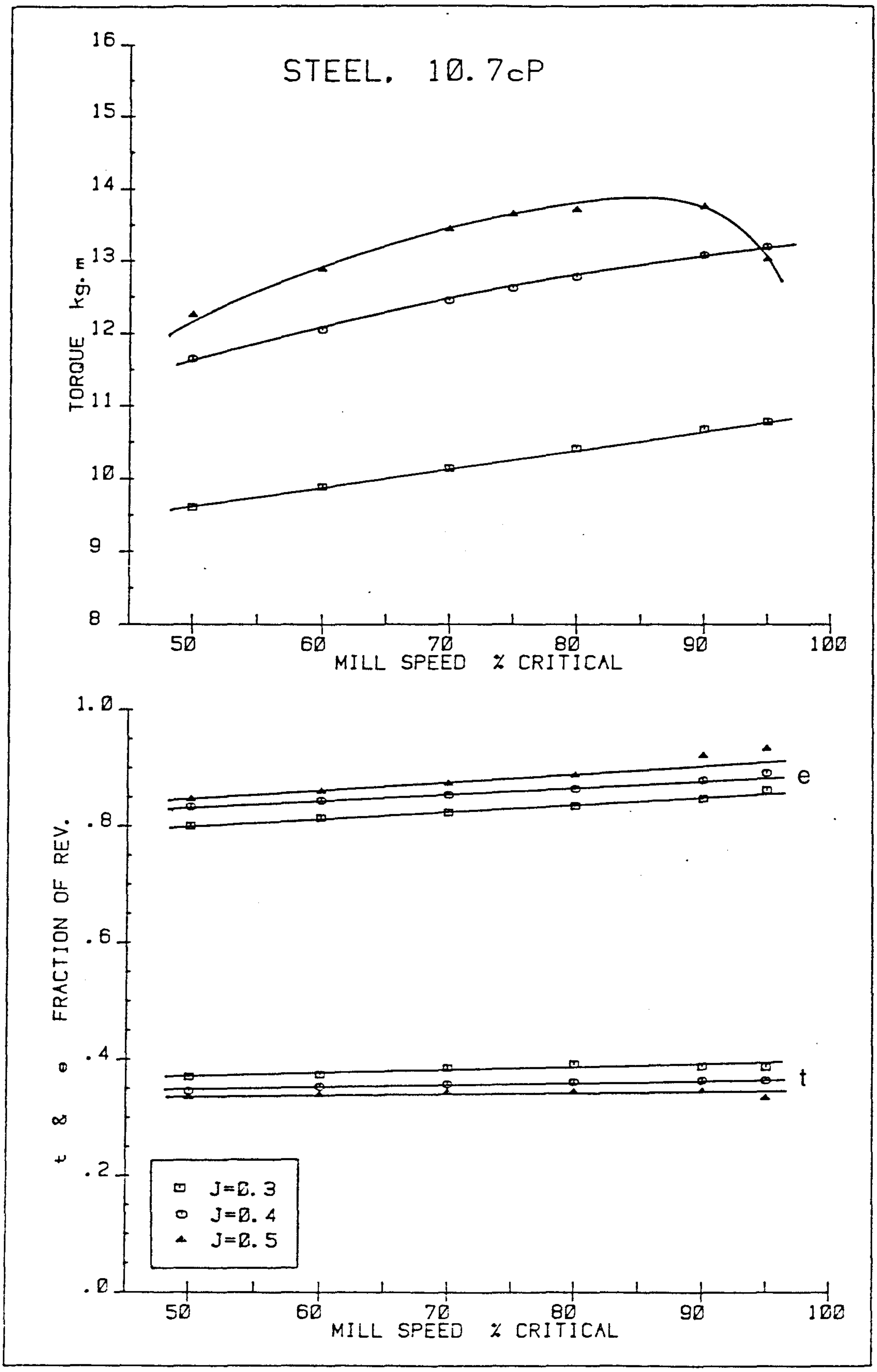

Figure D.1 Torque and load position for steel media, η = 10,7 cP

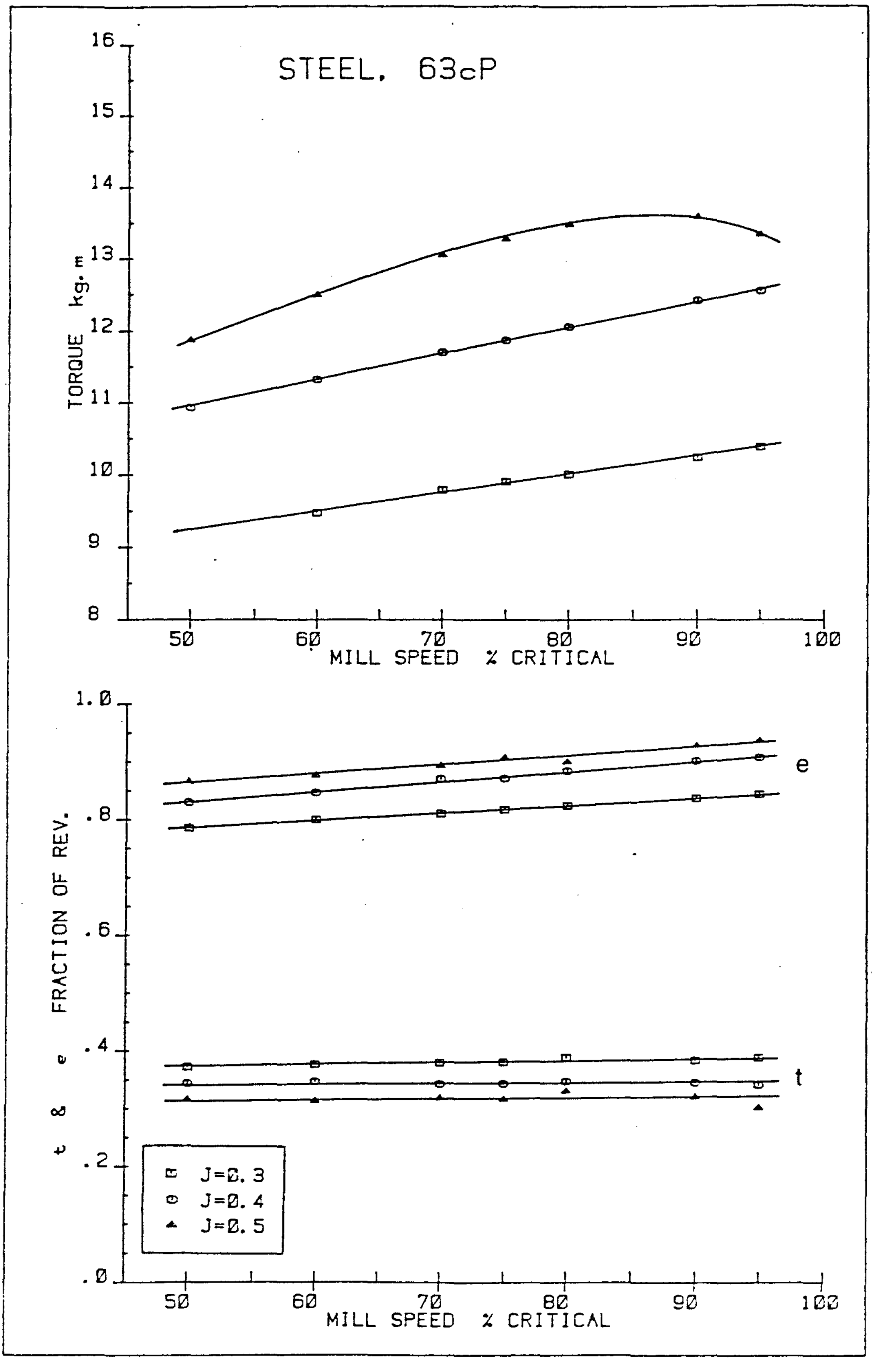

Figure D.2 Torque and load position for steel media, η = 63 cP

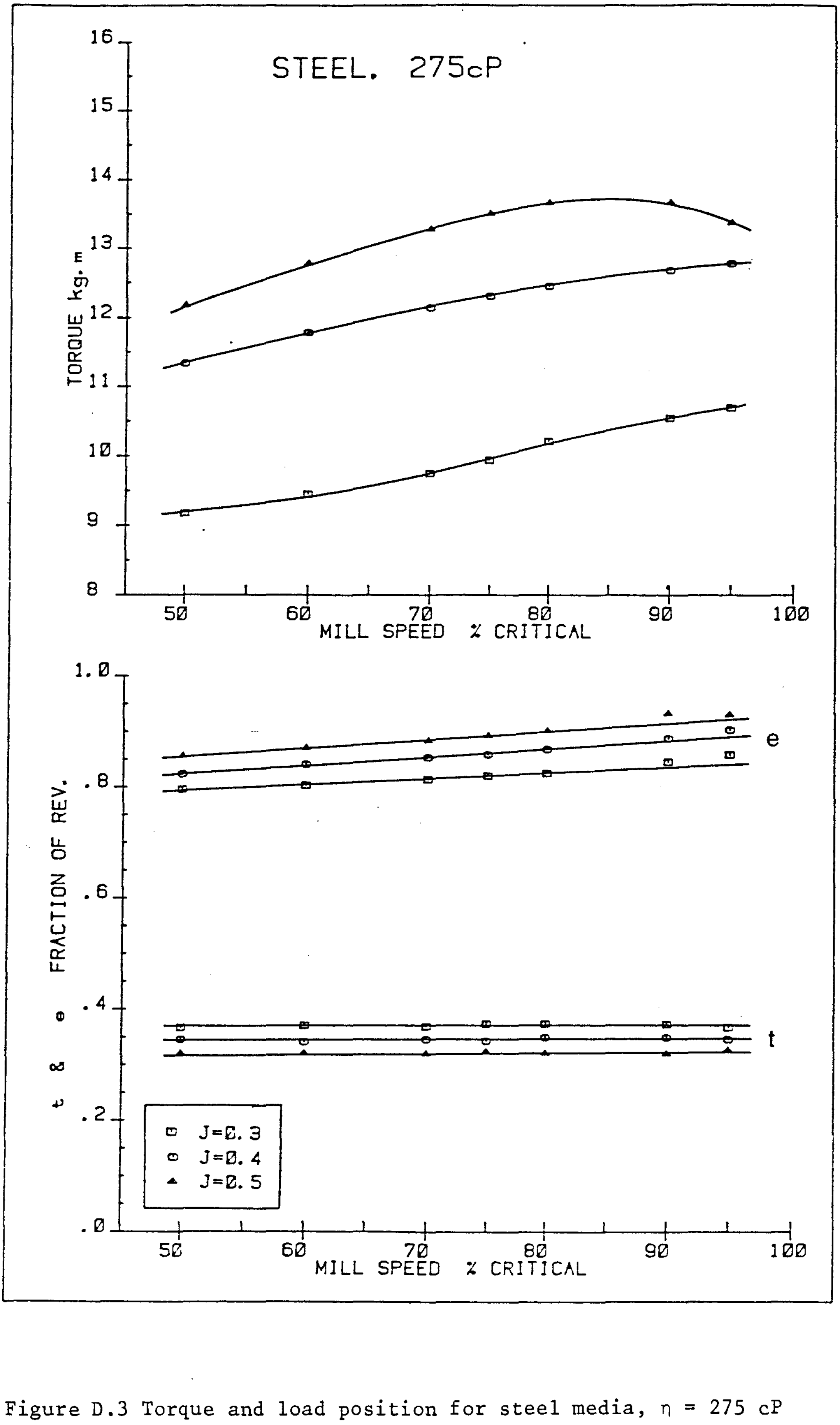

Figure D.3 Torque and load position for steel media, η = 275 cP

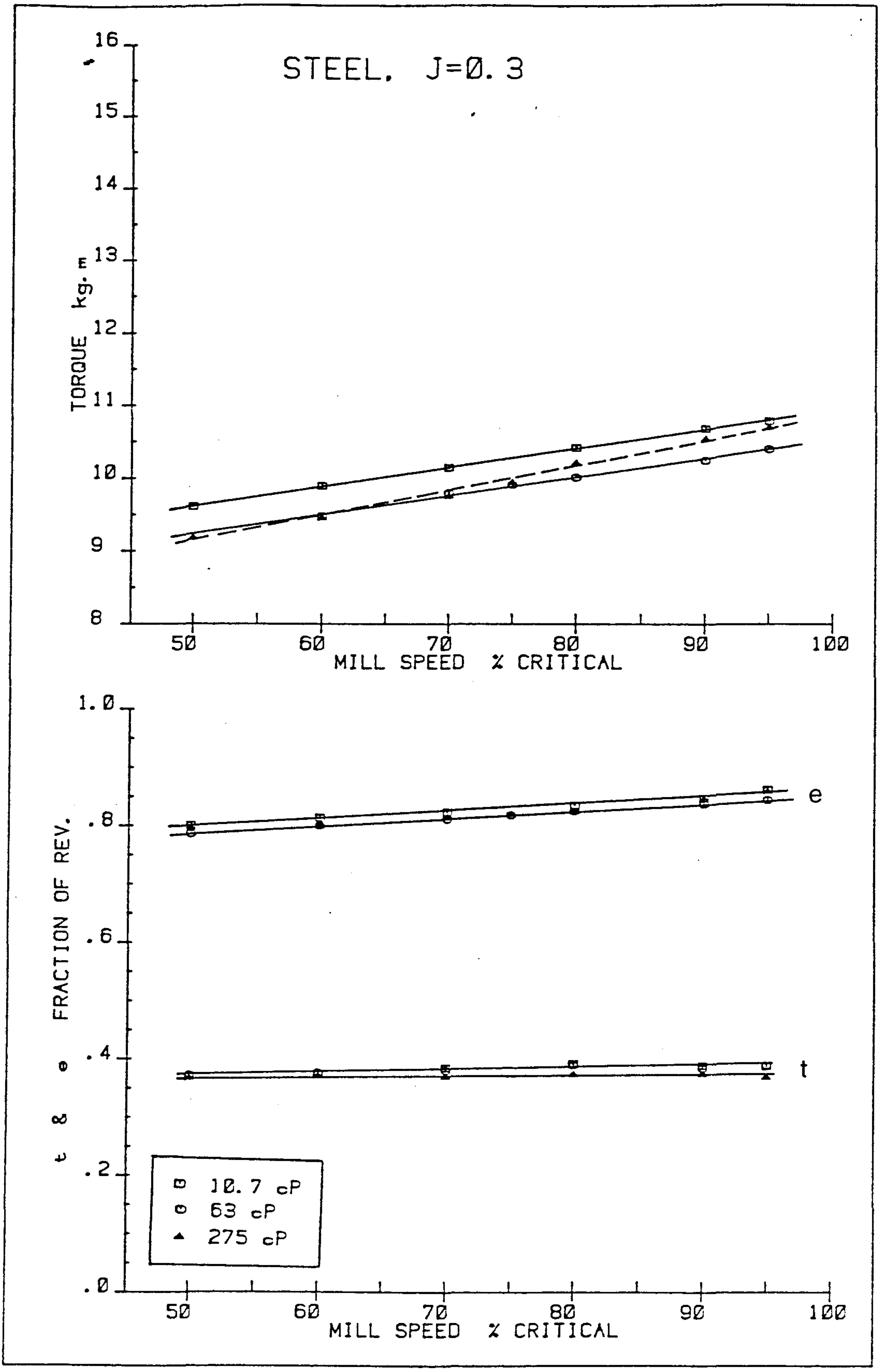

Figure D.4 Torque and load position for steel media, J = 0,3

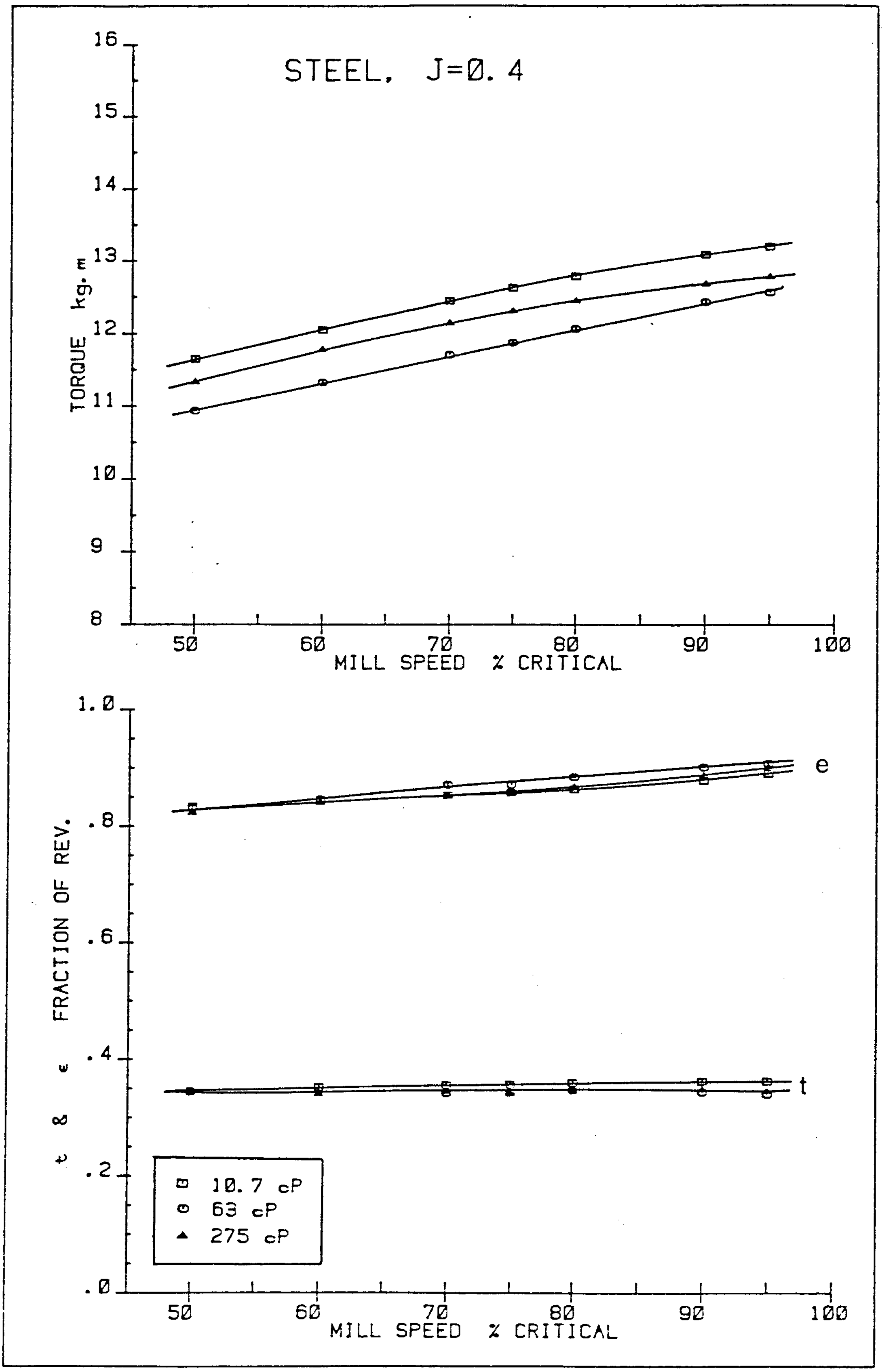

Figure D.5 Torque and load position for steel media, J = 0,4

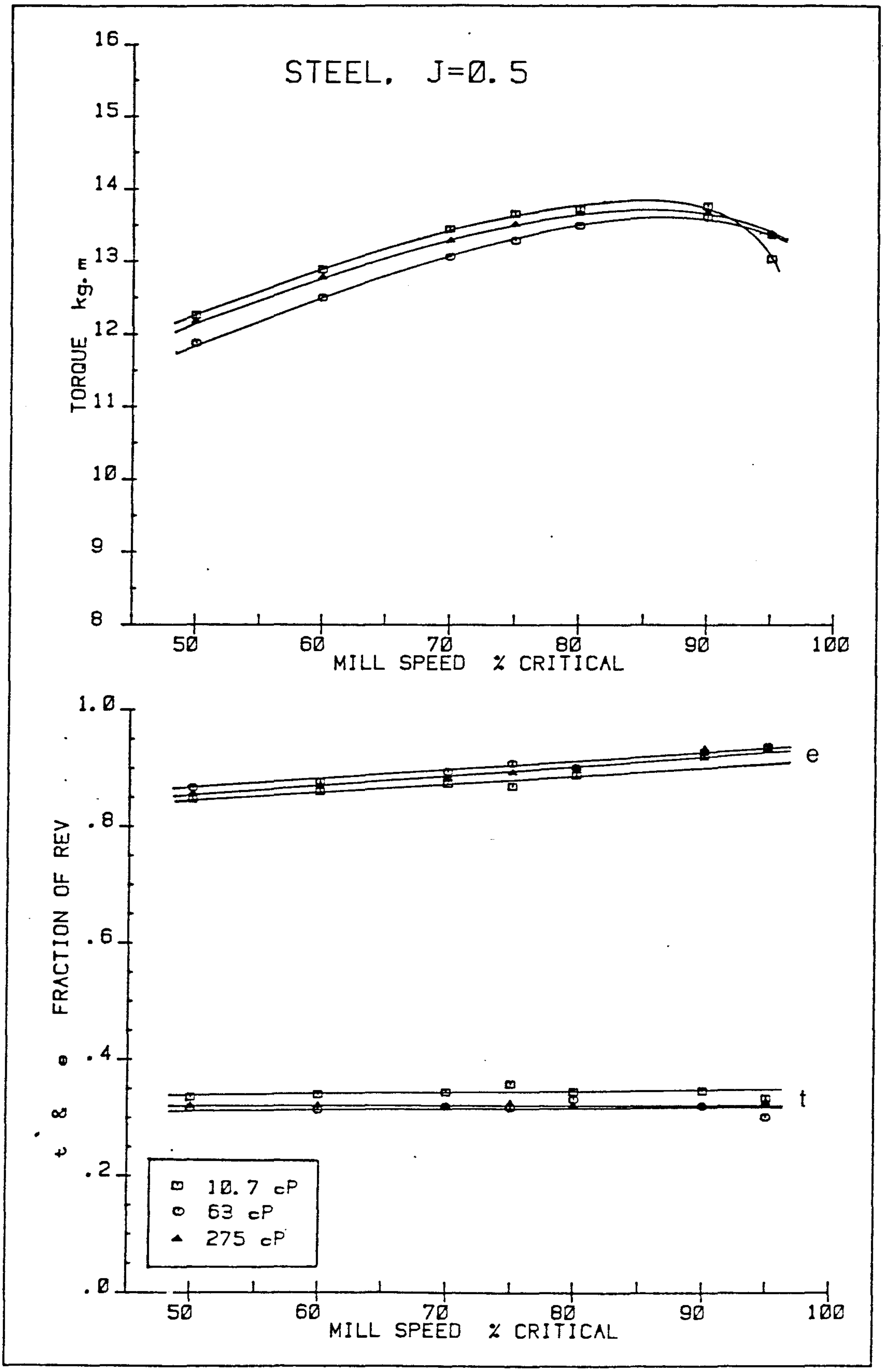

Figure D.6 Torque and load position for steel media, J = 0,5

SPEED %CRIT	TORQUE KG.M	****LOAD t	POSITION u	**** e
50	9.611	.371	.43	.801
60	9.894	.374	.44	.814
70	10.142	.385	.438	.823
75	-	-	-	-
80	10.421	.392	.443	.835
90	10.689	.388	.459	.847
95	10.791	.386	.476	.862

TABLE D.1 J=0.3, 10.7cP

SPEED %CRIT	TORQUE KG.M	****LOAD t	POSITION u	**** e
50	11.652	.346	.488	.834
60	12.055	.353	.491	.844
70	12.454	.357	.496	.853
75	12.634	.358	.5	.858
80	12.793	.361	.503	.864
90	13.087	.363	.516	.879
95	13.199	.363	.528	.891

TABLE D.2 J=0.4, 10.7cP

SPEED %CRIT	TORQUE KG.M	****LOAD t	POSITION u	**** e
50	12.263	.336	.511	.847
60	12.893	.34	.52	.86
70	13.439	.344	.529	.873
75	13.651	.358	.511	.869
80	13.721	.337	.543	.88
90	13.759	.346	.575	.921
95	13.031	.334	.599	.933

TABLE D.3 J=0.5, 10.7cP

SPEED %CRIT	TORQUE KG.M	****LOAD t	POSITION u	**** e
50	9.627	.373	.413	.786
60	9.480	.377	.423	.8
70	9.792	.38	.431	.811
75	9.909	.381	.437	.818
80	10.016	.389	.436	.825
90	10.251	.383	.454	.837
95	10.401	.388	.456	.844

TABLE D.4 J=0.3, 63cP

SPEED C	TORQUE KG.M	****LOAD t	POSITION u	**** e
50	10.937	.345	.486	.831
60	11.327	.347	.5	.847
70	11.701	.343	.528	.871
75	11.874	.344	.528	.872
80	12.068	.348	.537	.885
90	12.436	.345	.557	.902
95	12.571	.341	.567	.908

TABLE D.5 J=0.4, 63cP

SPEED %CRIT	TORQUE KG.M	****LOAD t	POSITION u	**** e
50	11.881	.317	.55	.867
60	12.502	.314	.563	.877
70	13.059	.319	.575	.894
75	13.286	.317	.591	.908
80	13.491	.332	.569	.901
90	13.606	.32	.609	.929
95	13.356	.302	.635	.937

TABLE D.6 J=0.5, 63cP

SPEED	TORQUE	****LOAD	POSITION****	
%CRIT	KG.M	t	u	e
50	9.18	.368	.428	.796
60	9.45	.371	.432	.803
70	9.75	.369	.445	.814
75	9.942	.374	.446	.82
80	10.215	.374	.451	.825
90	10.554	.373	.473	.846
95	10.7	.368	.491	.859

TABLE D.7 J=0.3, 275cP

SPEED	TORQUE	****LOAD	POSITION****	
%CRIT	KG.M	t	u	e
50	11.336	.346	.478	.824
60	11.785	.342	.499	.841
70	12.145	.346	.507	.853
75	12.314	.343	.516	.859
80	12.455	.349	.519	.868
90	12.69	.349	.539	.888
95	12.786	.346	.557	.903

TABLE D.8 J=0.4, 275cP

SPEED	TORQUE	****LOAD	POSITION****	
%CRIT	KG.M	t	u	e
50	12.181	.322	.535	.857
60	12.786	.322	.549	.871
70	13.285	.321	.563	.884
75	13.514	.325	.568	.893
80	13.668	.322	.58	.902
90	13.675	.321	.612	.933
95	13.38	.327	.604	.931

TABLE D.9 J=0.5, 275cP

SPEED	TORQUE	****LOAD	POSITION****	
%CRIT	KG.M	t	u	e
50	11.965	.366	.466	.832
60	12.47	.374	.468	.842
70	12.858	.378	.477	.855
75	13.028	.385	.478	.863
80	13.106	.384	.488	.872
90	12.51	.382	.527	.909
95	11.22	.361	.567	.928

TABLE D.10 J=0.4, 10.7 cP+2KG SAND

APPENDIX E

Listing of the computer programme

```
10  REM   CONSTRUCTION OF THEORETICAL SHAPE OF MILL LOAD
20  REM  BY K.S.LIDDELL,NOV 1985.
30  REM  ON APPLE 2E, WATANABE 4675 PLOTTER
40  REM  DEFINITION OF TERMS
50 RM = .2725: REM     RM=MILL RADIUS=.2725M.
60 RM = .2725
70 NC = 57.3: REM   NC=CRITICAL SPEED=57.3 RPM
80  REM FC=FRACTION OF CRITICAL SPEED
90  REM RD=DAVIS CIRCLE RADIUS
100  REM   RO=OPERATING RPM
110 PI = 3.1415927
120  DIM R(110): DIM X(110): DIM Y(110): DIM YC(110)
130  DIM H(110): DIM A(110): DIM C(110)
140  HOME :R1 = 500:X0 = 1100:Y0 = 1500: REM    MILL PLOTTING CO-ORDS & RADIUS
150  INPUT "DO YOU WISH A SUMMARY OF THE PROGRAM    INFORMATION ? (Y/N) ";Q$: IF
 Q$ = "Y" THEN  GOSUB 1560
160  INPUT "FRACTION OF CRITICAL SPEED? ";FC
170  INPUT "PULP SOLIDS CONTENT (BY VOL.)? ";PS
180  INPUT "MILL FILLING? ";J
190  INPUT "TOE & SHOULDER POSITIONS?";TF,TE
200  REM ASSIGN COEFF. OF FRICTION DEPENDING ON Cv
210  IF PS = 35.4 THEN LA = .756
220  IF PS = 46 THEN LA = .866
230  IF PS = 52.2 THEN LA = .99
240 RO = NC * FC:RD = 447.348 / (RO ^ 2)
250 GA = TE * 2 * PI
260 TGA = TF * 2 * PI
270  INPUT "DRAW MILL?";Q$
280  IF Q$ = "N" THEN  GOTO 390
290  PR# 5
300  PRINT "S5"
310  PRINT "M";X0;",";Y0: PRINT "N1"
320  PRINT "M";X0;",";Y0 - R1
330 ZZ = 200
340  FOR N = (ZZ * .75) TO  - (ZZ * .25) STEP  - 1
350 P =  INT (R1 *  COS (N * 2 * PI / ZZ)) + X0
360 Q =  INT (R1 *  SIN (N * 2 * PI / ZZ)) + Y0
370  PRINT "D";P;",";Q
380  NEXT N
390  REM  DRAW DAVIS CIRCLE
400 R2 = (RD * R1) / RM
410  REM CALC. INTERSECT OF MILL & D.C.
420 YDM = ((RM ^ 2) / (2 * RD)):XDM = ( SQR ((RM ^ 2) - (YDM ^ 2)))
430 Y1 = (Y0 - R2): REM   CENTRE OF D.C.
440  INPUT "DRAW D.C.?";Q2$: IF Q2$ = "N" GOTO 510
450  PR# 5: FOR N = 100 TO  - 100 STEP  - 1
460 P =  INT (R2 *  COS (N * 2 * PI / 400)) + X0 + 1
470 Q =  INT (R2 *  SIN (N * 2 * PI / 400)) + Y1 + 1
480  IF Q <  =  INT (Y0 - (YDM * R1 / RM)) THEN  GOTO 510
490  PRINT P","Q
500  NEXT N
510  PR# 5: REM    CALC TOE & SHOULDER CO-ORDS
520 XT =  - (RM *  COS (TGA - (PI / 2))):PT = X0 + (XT * R1 / RM)
530 YT =  - (RM *  SIN (TGA - (PI / 2))):QT = Y0 + (YT * R1 / RM)
540 XE =  - (RM *  COS (GA - (PI / 2))):PE = X0 + (XE * R1 / RM)
550 YE =  - (RM *  SIN (GA - (PI / 2))):QE = Y0 + (YE * R1 / RM)
560  REM  PLOT TOE & SHOULDER POINTS
```

```
570  PRINT "M"; INT (PT - 20);","; INT (QT): PRINT "D"; INT (PT);","; INT (QT)
580  PRINT "M"; INT (PT - 50);","; INT (QT): PRINT "Pt"
590  PR# 5: PRINT "M"; INT (PE + 20);","; INT (QE): PRINT "D"; INT (PE);","; INT
 (QE)
600  PRINT "M"; INT (PE + 30);","; INT (QE): PRINT "Pe"
610  REM  CALC DISTANCE (L) & ANGLE(T) OF TOE TO SPIRAL POLE
620 RT =  SQR (((2 * RD - YT) ^ 2) + (XT ^ 2))
630 TT = (1.5 * PI) +  ATN (XT / ((2 * RD) - YT))
640 S = (1.5 * PI +  ATN (YD / XD)) / (2 * PI): REM  INTERSCEC OF SPIRAL & MILL
CIRCLE
650 BE = 2 * PI * S - 1.5 * PI
660  REM   CALC DISTANCE (L) & ANGLE(T) OF POINT S TO SPIRAL POLE
670 XS = XD:YS = YD
680 RS =  SQR (((2 * RD - YS) ^ 2) + (XS ^ 2))
690 TS = (1.5 * PI) +  ATN (XS / ((2 * RD) - YS))
700  REM CALC SP. CONST USING POINT S
710 CO =  EXP ( LOG (RS) - ((PI - TS) * LA))
720  PR# 5: PRINT "M"; INT (X0 + (XS * R1 / RM));","; INT (Y0 + (YS * R1 / RM))
730  REM  FIND OTHER INTERSECT OF SP. & MILL CIRCLE
740  FOR T = (TS + ((TT - TS) * .70)) TO 1 STEP .001
750 R = CO *  EXP ((PI - T) * LA): REM  SP. EQUATION
760 X = R *  COS (T)
770 Y = (R *  SIN (T)) + (2 * RD)
780  IF  SQR (X ^ 2 + Y ^ 2) >  = RM THEN  GOTO 800
790  NEXT T
800 TZ = T: REM  ANGLE OF OTHER INTERSECT
810  REM  DRAW SPIRAL
820  FOR T = TS TO TZ STEP (TZ - TS) / 30
830 R = CO *  EXP ((PI - T) * LA)
840 X = R *  COS (T)
850 Y = (R *  SIN (T)) + (2 * RD)
860 P =  INT (X0 + X * R1 / RM):Q =  INT (Y0 + Y * R1 / RM)
870  PRINT "D";P;",";Q: NEXT T
880 U = 0
890  REM  FIND c
900  FOR T = TS TO TZ STEP (TT - TS) / 60
910 U = U + 1
920 R = CO *  EXP (LA * (PI - T))
930 A = R *  COS (T):X = A
940 B = R *  SIN (T):Y = B + (2 * RD)
950 C(U) =  SQR (X ^ 2 + Y ^ 2): IF U = 1 GOTO 970
960  IF C(U) >  = C(U - 1) GOTO 980
970  NEXT T
980 XM = X:YM = Y: REM CO-ORDS OF c
990 P =  INT (X0 + XM * R1 / RM):Q =  INT (Y0 + YM * R1 / RM)
1000  PR# 5: PRINT "M"; INT (P + 40);","; INT (Q): PRINT "Pc": PRINT "M"; INT (P
);","; INT (Q)
1010  GOSUB 1400: REM  SUBR. TO CALC AREA BELOW SP.
1020  REM   CALC AREA BELOW SP. AS FRAC OF MILL VOL
1030 JS = AA / (RM ^ 2 * PI):JS =  INT ((JS * 1000) + .5) / 1000
1040  REM CALC ANGLE BETWEEN c & SP. POLE
1050 TM = 1.5 * PI +  ATN (XM / ((RD * 2) - YM))
1100 AL =  ATN (YE / XE): REM  INITIAL ANGLE OF PROJECTION
1110  REM  CALC VEL. RESULTANT & CO-ORDS
1120 VR = (2 * PI * FC * (RM - RB) * NC) / 60
1130 XB = RM *  COS (AL):YB = RM *  SIN (AL)
1140  PRINT "D"; INT (PE);","; INT (QE)
1150  PR# 5: REM  DRAW PARA PATH
1160  FOR XP = (XB - .01) TO  - 1 STEP  - .01
1170 YP = YB + ((XB - XP) /  TAN (AL)) - (9.81 * ((XB - XP) ^ 2) / (2 * (VR ^ 2)
```

```
 * ( SIN (AL) ^ 2)))
1180 P = X0 + XP * R1 / RM:Q = Y0 + YP * R1 / RM
1190  IF  SQR ((P - X0) ^ 2 + (Q - Y0) ^ 2) > R1 GOTO 1220
1200  PRINT "D"; INT (P);","; INT (Q)
1210  NEXT XP
1220  FOR XP = (XP + .01) TO  - 1 STEP  - .0005
1230 YP = YB + ((XB - XP) /  TAN (AL)) - (9.81 * ((XB - XP) ^ 2) / (2 * (VR ^ 2)
 * ( SIN (AL) ^ 2)))
1240 P = X0 + XP * R1 / RM:Q = Y0 + YP * R1 / RM
1250  IF YP =  < YT GOTO 1280
1260  IF  SQR ((P - X0) ^ 2 + (Q - Y0) ^ 2) >  = R1 GOTO 1280
1270  NEXT XP
1280  PRINT "D"; INT (P);","; INT (Q)
1290  PR# 5: PRINT "M";30 +  INT (XS * R1 / RM + X0);","; INT (YS * R1 / RM + Y0
): PRINT "Ps"
1300  PRINT "M";X0 - 600;",";Y0 - 700
1310  PRINT "Po =";FC: PRINT "P  J =";J: PRINT "P  j =";JS: PRINT "P Cv =";PS
1320  PRINT "M";X0 - 600;",";Y0 - 709
1330  PRINT "P/"
1340  PRINT "M";X0 - 600;",";Y0 - 800
1350  PRINT "Pt =";TF: PRINT "P  e =";TE: PRINT "P  s ="; INT ((S * 1000) + .5)
/ 1000
1360  PRINT "H": PRINT "MORE?": INPUT Q$
1370  IF Q$ = "N" THEN  END
1380  GOTO 140
1390  END
1400 TI = (TE - TZ) / 100:N = 0:AS = 0
1410 TI = (TS - TZ) / 100:N = 0:AS = 0
1420  FOR T = TZ TO TS STEP TI
1430 N = N + 1
1440 R(N) = CO *  EXP ((PI - T) * LA)
1450 X(N) = R(N) *  COS (T)
1460 Y(N) = (R(N) *  SIN (T)) + (2 * RD)
1470 YC(N) =  -  SQR (RM ^ 2 - X(N) ^ 2)
1480 H(N) =  - (YC(N) - Y(N))
1490  IF N = 1 THEN 1510
1500 A(N) = ((H(N) + H(N - 1)) / 2) * (X(N) - X(N - 1))
1510 AS = AS + A(N)
1520  NEXT T
1530 AR = (RM ^ 2 / 2) * ((2 *  ATN (YS / XS)) -  SIN (( ATN (YS / XS) * 2)))
1540 AA = AS + AR: PRINT AS,AR,AA
1550  RETURN
1560  HOME : PRINT "THIS PROGRAM GENERATES VARIOUS AREAS    WITHIN THE LOAD OF A
 MILL.THE DERIVATION IS DISCUSSED IN DETAIL IN CHAPTER 5.   THE PROGRAM PROMPTS
FOR TEST DETAILS    SUCH AS:
1570  PRINT "      *MILL SPEED                             *FILLING(THIS IS NOT
USED IN            THE CALCULATONS)                        *PULP SOLIDS CONTENT(
ONLY 35.4          46.0, 52.2 % TO BE USED)                *TOE & SHOULDER POINT
S
1580  PRINT : PRINT "THE PROGRAM PERFORMS THE FOLLOWING STEPS 1) CALCS. THE DAVI
S CIRCLE RADIUS       2) DRAWS THE MILL CIRCLE (OPTIONAL)      3) DRAWS THE DAVIS
 CIRCLE FROM THE MILL    CENTRE TO SHELL (DAVIS POINT)
1590  PRINT " 4) PLOTS THE TOE & SHOULDER POINTS       5) DRAWS TOE EQM. SURFACE
THRO' THE          DAVIS POINT (SEE NOTE 1)
             Hit any key for next page
1600  GET Q
1610  HOME : PRINT " 6) FINDS THE CENTRE OF BALL CIRCULATION     THE POINT LIES O
N THE EQM. SURF. AND      IS TANGENTIAL TO A CIRCLE CONCENTRIC     WITH THE MILL
                    7) CALCS. THE AREA BOUNDED BY THE EQM.
1620  PRINT "     SURF. & MILL BY A TRAPEZIUM SUM            METHOD
1630  PRINT "     8) THE PARABOLIC PATH IS DRAWN FOR A        PARTICLE IN CONTACT
WITH THE MILL        LINER (SEE NOTE 3)
1640  PRINT : PRINT : PRINT "Hit any key for notes": GET Q
1650  HOME : PRINT "NOTES"
1660  PRINT "1) THE EQM. SURF. IS POSITONED TO PASS      THRO' THE DAVIS POINT BE
CAUSE ITS        POSITON CANNOT BE PREDICITED WITH       CONFIDENCE. REFER TO CH.
5 FOR MORE       DETAILS
1670  PRINT "2) AT HIGHER MILL SPEEDS THE VOLUME         BELOW THE EQM SURF CAN B
ECOME LARGER     THAN THE LOAD VOLUME. THIS IMPLIES THAT THE LOAD IS STARTING TO
CENTRIFUGE.
1690  PRINT "    NOT DEFINE THE UPPER SURFACE OF THE      LOAD, BECAUSE THE BALL A
RE ROLLING       DOWN THE UPPER SURFACE OF THE LOAD.
                 Hit any key to return"
1700  GET Q: HOME : RETURN
```

REFERENCES

1. Stairmand, C.J. The energy efficiency of milling processes. A review of some fundamental investigations and their application to mill design, *Europaischen Symposions Zerkleinern*, vol. 4, no. 1, 1975, pp. 1-15.

2. Hartley, J.N., Prisbrey, K.A. and Wick, O.J. Chemical additives for ore grinding: How effective are they?, *E/MJ Second Operating Handbook of Mineral Processing*, Thomas (ed), McGraw-Hill, New York, pp. 371-377.

3. Austin, L.G. A review of grinding as a rate process, *Powder Technology*, vol. 5, 1971/72, pp. 1-17.

4. Herbst, J.A. and Fuerstenou, D.W. Scale-up procedure for continuous grinding mill design using population balance models, *International Journal of Mineral Processing*, vol. 7, 1980, pp. 1-31.

5. Klimpel, R.R. and Austin, L.G. The back-calculation of specific rates of breakage from continuous mill data, *Powder Technology*, vol. 38, 1984, pp. 77-91.

6. Bond, F.C. Confirmation of the Third Theory, *A.I.M.E. Transactions*, vol. 217, 1960, pp. 139-153.

7. Austin, L.G. Concepts in Process Design of Mills, Gaudin Lecture, *Mining Engineering*, June 1984, pp. 628-635.

8. Burns, R.S. and Erskine, J.G. Experience with large diameter ball mills at Bougainville Copper Ltd., *Mineral and Metallurgical Processing*, May 1984, pp. 15-28.

9. Arbiter, N. and Harris, C.C. Scale-up and dynamics of large grinding mills - A case study, *Design and Installation of Comminution Circuits*, Mular and Jergensen (eds), AIME, 1982, Chapter 26, pp. 491-508.

10. Davis, E.W. Fine crushing in ball mills, *A.I.M.E. Transactions*, vol. 61, 1919, pp. 250-296.

11. Barth, W. Power consumption in tube mills, *Forschung in Ingenieurwesen*, vol. 1, no. 9, 1930, pp. 321-328.

12. Rose, H. and Sullivan, R. *Ball, Tube and Rod Mills*, Chemical Publishing Co., New York, 1958.

13. Hinsley and Fobelets, Work discussed by Rose and Sullivan in 12.

14. Vermeulen, L.A., Ohlson de Fine, M.J. and Schakowski, F. Physical information from the inside of a rotary mill, *Journal of the S.A.I.M.M.*, vol. 84, no. 8, 1984, pp. 247-253.

15. Guerro, P.K. and Arbiter, N. Tumbling mill power at cataracting speeds, *A.I.M.E. Transactions*, vol. 217, 1960, pp. 73-75.

16. Hogg, R. and Fuerstenou, D.W. Power relationships for tumbling mills, *S.M.E.-A.I.M.E. Transactions*, vol. 252, 1972, pp. 418-423.

17. Bond, F.C. *Crushing and Grinding Calculations*, Allis-Chalmers Publication 07R9235C.

18. Rowland, C.A. and Kjos, D.M. Plant Design Considerations for Rod and Ball Mill Grinding Circuits, Chapter 12, *Minerals Processing Plant Design*, Mular and Bhappu (eds), AIME, 1978.

19. Rose, H.E. and Evans, D.E. The dynamics of the ball mill. Part I: Power requirements based on the ball and shell system, *Proceedings of the Inst. of Mechanical Engineers*, vol. 170, 1956, pp. 773-783.

20. Austin, L.G. Understanding ball mill sizing, *Ind. Eng. Chem. Process Des. and Develop.*, vol. 12, no. 2, 1973, pp. 121-129.

21. Harris, C.C., Schnock, E.M. and Arbiter, N. Grinding mill power consumption, *Mineral Processing and Technology Review*, vol. 1, 1985, pp. 297-345.

22. Arbiter, N. and Harris, C.C. Scale-up problems with large ball mills, *Minerals and Metallurgical Processing*, May 1984, pp. 4-10.

23. Pauw, O.G. *Control of a Pebble Mill Using a Multivariable Peak-seeking Controller*, MSc Dissertation, University of the Witwatersrand, 1984.

24. Bird, R., Stewart, W. and Lightfoot, E. *Transport Phenomena*, Wiley, 1960, pp. 48-59.

25. Cheng, D.C.H. Viscosity-concentration equations and flow curves for suspensions, *Chemistry and Industry*, 17 May 1980, pp. 403-406.

26. Levy, C.D. *A Rheological Investigation of Three South African Gold Mine Pulps*, MSc Thesis, University of Cape Town, 1974.

27. Meloy, T.P. and Crabtree, D. Surface tension and viscosity in wet grinding, *Euopischen Symposions Zerkleinern*, vol. 1, 1967, paper C1, pp. 405-426.

28. Hockings, W.A., Volin, M.E. and Mular, A.L. Effect of suspending fluid viscosity on batch mill grinding, *A.I.M.E.-S.M.E. Transactions*, vol. 232, 1965, pp. 59-62.

29. Yen, W.T. and Salman, T. Pulp density of the ball mill and grindability, *Canadian Mining Journal*, November 1969, pp. 63-66.

30. Tucker, P. Rheological factors that affect the wet grinding of ores, *I.M.M. Transactions*, vol. 91, Sept. 1982, pp. C117-C122.

31. Tucker, P. The influence of pulp density on the selective grinding of ores, *International Journal of Mineral Processing*, vol. 12, 1982, pp. 273.284.

32. Tangsathitkulchai, C. and Austin, L.G. The effect of slurry density on breakage parameters of quartz, coal and copper ore in a laboratory ball mill, *Powder Technology*, vol. 42, 1985, pp. 287-296.

33. Klimpel, R.R. Slurry rheology influence on the performance of mineral/coal grinding circuits, *Mining Engineering*, part 1 - Dec. 1982, pp. 1665-1668; part 2 - Jan. 1983, pp. 21-26.

34. Klimpel, R.R. Laboratory studies of the grinding and rheology of coal-water slurries, *Powder Technology*, vol. 32, 1982, pp. 267-277.

35. Klimpel, R.R. and Austin, L.G. Chemical additives for wet grinding of minerals, *Powder Technology*, vol. 31, 1982, pp. 239-253.

36. Klimpel, R.R. and Manfroy, W. Computer analysis of viscosity effects on selection for breakage and breakage distribution parameters in the wet grinding of ores, *Proceedings of the 14th Symposium of Application of Computer Methods in the Mineral Industry*, Ramani (ed), AIME, New York, 1977, Chapter 16, pp. 197-206.

37. Klimpel, R.R. The influence of a chemical dispersant on the sizing performance of a 24-in. hydrocyclone, *Powder Technology*, vol. 31, 1982, pp. 255-262.

38. Harris, C.C. and Arbiter, N. Grinding mill operation and scale-up: Theory and Equations, *Mineral Processing and Technology Review*, vol. 1, 1985, pp. 249-263.

39. Moys, M.H. The measurement of parameters describing the dynamic behaviour of the load in a grinding mill, *Mintek 50 Proceedings*, Sandton, 1984, paper A2/3.

40. Shoji, K. et al. Further studies of ball and powder filling effects in ball milling, *Powder Technology*, vol. 31, 1982, pp. 121-126.

41. Van der Walt, P.J. and Fourie, A.M. Determination of the viscosity of unstable industrial suspensions with the aid of a Stormer viscometer, *Journal of the S.A.I.M.M.*, July 1957, pp. 709-723.

42. Manz, R. Experimental investigation into the slip of the charge of grinding medium in ball mills, *Europaischen Symposions Zerkleinen*, Cannes, Oct. 1971, pp. 721-749.

43. Vermeulen, L.A. *Private Communication*, Randburg, 1985.

44. Kjos, D.M. *Grinding Circuits: Current Status and Projected Future Development*, Allis-Chalmers Publication 22P10735.